UNIVERSITY OF CALIFORNIA

Santa Barbara

Assessing the Impacts of Engineered Nanomaterials (ENMs) on Crop Plant Growth Using Targeted Proteomics and Targeted Metabolomics Approaches

A dissertation submitted in partial satisfaction of the

requirements for the degree Doctor of Philosophy

in Environmental Science and Management

by

Weiwei Li

Committee in charge:

Professor Arturo Keller, Chair

Professor Patricia Holden

Professor Kathy Foltz

March 2024

The dissertation of Weiwei Li is approved.

Patricia Holden

Kathy Foltz

Arturo Keller, Committee Chair

March 2024

Assessing the Impacts of Engineered Nanomaterials (ENMs) on Crop Plant Growth Using Targeted Proteomics and Targeted Metabolomics Approaches

by

Weiwei Li

ACKNOWLEDGEMENTS

I extend my deepest gratitude to my advisor, Prof. Arturo Keller, for his unwavering support, invaluable guidance, and insightful feedback throughout the entire process of researching and writing this dissertation. His expertise and mentorship have been instrumental in shaping the direction of my work. I would like to thank the members of my dissertation committee, Prof. Patricia Holden and Prof. Kathy Foltz, for their constructive critiques and thoughtful suggestions, which greatly enriched the quality of this research. Each member's expertise in their respective fields provided diverse perspectives that enhanced the depth and breadth of my study.

My sincere appreciation goes to my lab mates at Keller lab, Yuxiong Huang, Qian Gao and Xiangning Huang, for their collaborative efforts, stimulating discussions, and shared enthusiasm. Their contributions have added a valuable dimension to the overall research.

Special thanks are due to my husband Hui Kang, my daughter Zoe Kang, my son Leo Kang, my parents and sisters, for their unwavering encouragement, understanding, and patience during this challenging academic journey. Their constant support provided the emotional foundation necessary for me to persevere.

Lastly, I extend my appreciation to all my friends and colleagues who offered encouragement and inspiration throughout this dissertation process. Your camaraderie made this academic endeavor more rewarding.

VITA OF WEIWEI LI

February 2024

EDUCATION

Ph.D., Environmental Science & Management — Mar 2024
Bren School of Environmental Science & Management, UC, Santa Barbara, CA

M.S., Public Health, Environmental Health — May 2012
Rollins School of Public Health, Emory University, Atlanta, GA

B.S., Chemistry and Biology — Jul 2010
Chemistry Department, Tsinghua University, Beijing, China

RESEARCH EXPERIENCE

Graduate Student Researcher — Mar 2020 - Current
Bren School of Environmental Science & Management, UC Santa Barbara, CA

Associate Specialist — Aug 2017 - Dec 2019
Bren School of Environmental Science & Management, UC Santa Barbara, CA

Research Fellow (ORISE) — Sep 2015 – Aug 2017
U.S. EPA National Exposure Research Laboratory, Research Triangle Park, NC

Student Services Contractor — Sep 2012 – Dec 2014
U.S. EPA National Exposure Research Laboratory, Research Triangle Park, NC

Graduate Student Researcher — May 2011 – May 2012
Rollins School of Public Health, Emory University, Atlanta, GA

PUBLICATIONS

- Santos, J. P.; **Li, W**.; Keller, A. A.; Slaveykova, V. I. Mercury Species Induce Metabolic Reprogramming in Freshwater Diatom *Cyclotella Meneghiniana*. *Journal of Hazardous Materials* **2024**, *465*, 133245.
- **Li, W**.; Keller, A. A. Assessing the Impacts of Cu and Mo Engineered Nanomaterials on Crop Plant Growth Using a Targeted Proteomics Approach. *ACS Agric. Sci. Technol.* **2024**, *4* (1), 103–117.
- **Li, W**.; Keller, A. A. Optimization of Targeted Plant Proteomics Using Liquid Chromatography with Tandem Mass Spectrometry (LC-MS/MS). *ACS Agric. Sci. Technol.* **2023**, *3* (5), 421–431.
- Desgens-Martin, V.; **Li, W**.; Medina, T.; Keller, A. A. Estimated Influent PFAS Loads to Wastewater Treatment Plants and Ambient Concentrations in Downstream Waterbodies: Case Study in Southern and Central California. *ACS EST Water* **2023**, *3* (8), 2219–2228.

- Liu, W.; Li, M.; **Li, W**.; Keller, A. A.; Slaveykova, V. I. Metabolic Alterations in Alga *Chlamydomonas Reinhardtii* Exposed to nTiO $_2$ Materials. *Environ. Sci.: Nano* **2022**, *9* (8), 2922–2938.
- Slaveykova, V. I.; Majumdar, S.; Regier, N.; **Li, W**.; Keller, A. A. Metabolomic Responses of Green Alga Chlamydomonas Reinhardtii Exposed to Sublethal Concentrations of Inorganic and Methylmercury. *Environ. Sci. Technol.* **2021**, *55* (6), 3876–3887.
- Liu, W.; Majumdar, S.; **Li, W**.; Keller, A. A.; Slaveykova, V. I. Impact of Silver Nanoparticles on the Biouptake, Physiological Responses and Metabolic Perturbations in Freshwater Alga Poterioochromonas Malhamensis. *Toxicology Letters* **2021**, *350*, S181.
- Huang, X.; Cervantes-Avilés, P.; **Li, W**.; Keller, A. A. Drilling into the Metabolomics to Enhance Insight on Corn and Wheat Responses to Molybdenum Trioxide Nanoparticles. *Environ. Sci. Technol.* **2021**, *55* (20), 13452–13464.
- Starr, J. M.; **Li, W**.; Graham, S. E.; Shen, H.; Waldron, F. Is Food Type Important for in Vitro Post Ingestion Bioaccessibility Models of Polychlorinated Biphenyls Sorbed to Soil? *Science of The Total Environment* **2020**, *704*, 135421.
- Liu, W.; Majumdar, S.; **Li, W**.; Keller, A. A.; Slaveykova, V. I. Metabolomics for Early Detection of Stress in Freshwater Alga Poterioochromonas Malhamensis Exposed to Silver Nanoparticles. *Sci Rep* **2020**, *10* (1), 20563.
- Vieira, P. A.; Shin, C. B.; Arroyo-Currás, N.; Ortega, G.; **Li, W**.; Keller, A. A.; Plaxco, K. W.; Kippin, T. E. Ultra-High-Precision, in-Vivo Pharmacokinetic Measurements Highlight the Need for and a Route Toward More Highly Personalized Medicine. *Frontiers in Molecular Biosciences* **2019**, *6*.
- Shen, H.; **Li, W**.; Graham, S. E.; Starr, J. M. The Role of Soil and House Dust Physicochemical Properties in Determining the Post Ingestion Bioaccessibility of Sorbed Polychlorinated Biphenyls. *Chemosphere* **2019**, *217*, 1–8.
- Starr, J. M.; Graham, S. E.; **Li, W**.; Gemma, A. A.; Morgan, M. K. Variability of Pyrethroid Concentrations on Hard Surface Kitchen Flooring in Occupied Housing. *Indoor Air* **2018**.
- Mailyan, A. K.; Chen, J. L.; **Li, W**.; Keller, A. A.; Sternisha, S. M.; Miller, B. G.; Zakarian, A. Short Total Synthesis of [15N5]-Cylindrospermopsins from 15NH4Cl Enables Precise Quantification of Freshwater Cyanobacterial Contamination. *J. Am. Chem. Soc.* **2018**, *140* (18), 6027–6032.
- Huang, Y[1].; **Li, W[1]**.; Minakova, A. S.; Anumol, T.; Keller, A. A. Quantitative Analysis of Changes in Amino Acids Levels for Cucumber (*Cucumis Sativus*) Exposed to Nano Copper. *NanoImpact* **2018**, *12*, 9–17.
- Starr, J. M.; **Li, W**.; Graham, S. E.; Bradham, K. D.; Stout II, D. M.; Williams, A.; Sylva, J. Using Paired Soil and House Dust Samples in an in Vitro Assay to Assess the Post Ingestion Bioaccessibility of Sorbed Fipronil. *Journal of Hazardous Materials* **2016**, *312*, 141–149.
- Shen, H.; Starr, J.; Han, J.; Zhang, L.; Lu, D.; Guan, R.; Xu, X.; Wang, X.; Li, J.; **Li, W**.; Zhang, Y.; Wu, Y. The Bioaccessibility of Polychlorinated Biphenyls (PCBs) and

Polychlorinated Dibenzo-*p*-Dioxins/Furans (PCDD/Fs) in Cooked Plant and Animal Origin Foods. *Environment International* **2016**, *94*, 33–42.

- **Li, W**.; Morgan, M. K.; Graham, S. E.; Starr, J. M. Measurement of Pyrethroids and Their Environmental Degradation Products in Fresh Fruits and Vegetables Using a Modification of the Quick Easy Cheap Effective Rugged Safe (QuEChERS) Method. *Talanta* **2016**, *151*, 42–50.
- Chen, M.-S.; Zhao, D.-S.; Yu, Y.-P.; **Li, W**.; Chen, Y.-X.; Zhao, Y.-F.; Li, Y.-M. Characterizing the Assembly Behaviors of Human Amylin: A Perspective Derived from C-Terminal Variants. *Chem. Commun.* **2013**, *49* (18), 1799–1801.

TALKS & SEMINARS

Poster Presentation, American Chemistry Society Spring 2022 National Meeting, San Diego, USA

HONORS & AWARDS

Bren School Graduate Fellowship, UCSB	2020 - 2023
Mentoring Fellowship - Bren Environmental Leadership Program	Summer 2023

FIELDS OF STUDY

Targeted Plant Proteomics, Targeted Plant Metabolomics, Nanotechnology, Liquid Chromatography with tandem mass spectrometry

Faculty Advisor: Prof. Arturo A. Keller

ABSTRACT

Assessing the Impacts of Engineered Nanomaterials (ENMs) on Crop Plant Growth Using Targeted Proteomics and Targeted Metabolomics Approaches

by

Weiwei Li

As the agricultural use of ENMs becomes more prevalent, the exposure of plants to these nanomaterials has emerged as a significant abiotic stress. Researchers have previously explored plant responses to ENMs through non-targeted proteomics studies, revealing qualitative insights into protein-level responses to abiotic stress. However, there remains a knowledge gap in understanding the molecular mechanisms underlying these responses. This study aims to bridge that gap by employing targeted proteomics, which involves the quantitative measurement of a specific set of ENM-responsive proteins. Unlike non-targeted approaches, targeted proteomics allows for high-quality quantification of pre-selected signature peptides associated with targeted proteins. This approach is valuable for hypothesis-driven experiments and provides detailed insights into the perturbations in biological pathways triggered by ENMs.

A key focus of the study was the optimization of targeted plant proteomics methods to ensure high reproducibility of results. By refining signature peptide selection, liquid chromatography with tandem mass spectrometry (LC-MS/MS) analytical methods, and

sample preparation, the study establishes a robust workflow for the specific quantification of ENMs-responsive proteins. The investigation then applied the optimized targeted proteomics approach to explore the responses of crop plants, specifically *Triticum aestivum* (wheat), to copper (Cu) based nano-pesticide ($Cu(OH)_2$-NP) and molybdenum (Mo) based nano-fertilizer (MoO_3-NP). The study measured protein and metabolite levels in different plant tissues exposed to these ENMs through root or leaf routes. Joint pathway analysis was employed to comprehensively understand the changes in both protein and metabolite levels, providing a holistic view of the molecular responses.

The study optimized targeted proteomics methods, revealing the phenol extraction method with fresh plant tissue and trypsin digestion as the best for sample preparation. Applying this approach to wheat exposed to ENMs, significant upregulation of 16 proteins associated with 11 metabolic pathways was observed for Mo exposure through root. Notably, a dose-dependent response of this treatment highlighted the delicate balance between nutrient stimulation and toxicity, as the high Mo dose led to robust protein upregulation (especially amino acid metabolism related proteins) but depressed physiological measurements (include biomass, length and color of plant tissue), while low doses showed no physiological depression but downregulation of proteins. Integration of targeted proteomics and metabolomics identified responsive metabolites and proteins for ENM treatments, with Cu effects prominent through leaf exposure and Mo effects through root exposure. A joint pathway analysis was conducted using MetaboAnalyst 6.0 to integrate information from various omics platforms to comprehensively understand biological pathways. It revealed 23 perturbed pathways, emphasizing the interconnectedness of metabolic and proteomic responses. Coordinated responses in protein and metabolite concentrations, particularly in

amino acids, demonstrated a dynamic proteomic-to-metabolic-to-proteomic relationship. Contrasting expression patterns in glutamate dehydrogenase highlighted dose-dependent regulatory trends influencing both proteins and metabolites following specific Mo exposure through roots.

Overall, this study contributes to advancing our understanding of plant responses to ENMs at the molecular level. By quantifying specific proteins and employing joint pathway analysis to integrate proteomics with metabolomics, the research sheds light on the intricate biological pathways affected by exposure to ENMs. The optimized targeted proteomics approach ensures the reliability and reproducibility of results, paving the way for further research in the field of nanomaterial impacts on plant biology and sustainable agriculture. The significance of our research lies in the potential for guiding agricultural practices and environmental safety protocols by providing a comprehensive understanding of how plants respond to exposure to ENMs. By taking into account ENM design, dose optimization, and exposure routes, this project aims to contribute to the advancement of sustainable agricultural practices, and facilitate the utilization of nanotechnology's benefits while mitigating potential risks to plants, ecosystems, and human health.

TABLE OF CONTENTS

I. Introduction

A. Background

Proteomics has emerged as a groundbreaking approach to gain insights into proteins serving as biomarkers for plant responses to both biotic and abiotic stresses.[1] Modern mass spectrometry (MS)-based proteomics technologies, encompassing non-targeted and targeted proteomics, have facilitated the identification and quantification of the plant proteome.[2] This has significantly contributed to our understanding of the molecular mechanisms underlying plant phenotypes. Non-targeted proteomics, a comprehensive analysis quantifying thousands of proteins, is commonly used in plant proteomics. However, it lacks accuracy and reproducibility due to the stochastic nature of full spectrum scans, resulting in missing values and low reproducibility.[2,3,4] In contrast, targeted proteomics, particularly using selected reaction monitoring (SRM), offers high sensitivity, accuracy, and reproducibility by analyzing pre-defined proteins.[5,6] This method has been recognized as the Method of the Year (2012) by Nature Methods.[7] Several studies have utilized targeted proteomics to determine allergen levels in plants and identify potential protein biomarkers for plant breeding.[8,9,10,11] Additionally, targeted proteomics has been employed to characterize specific plant biological processes at the proteome level.[12] Despite its potential, targeted proteomics in plant research requires optimization to ensure high reproducibility of results.

The exposure of crops to engineered nanomaterials (ENMs), such as nano-pesticides and nano-fertilizers, designed to enhance productivity has garnered attention.[13,14] The potential benefits include more targeted delivery of active ingredients and controlled release

mechanisms.[15] However, the physicochemical properties of ENMs raise concerns about their toxicity potential.[15,16] Understanding how ENMs interact with plants is crucial for balancing enhanced productivity with minimal negative impacts on the environment and human health. Thus, the application of proteomics in studying the effects of ENMs on crop plants is gaining significance. Previous non-targeted proteomics studies have provided insights into plant responses to ENMs related to abiotic stress. However, there is a need for targeted proteomics to quantitatively analyze specific proteins impacted by ENMs, addressing the limitations of qualitative results.[5,12,17] This study aims to optimize targeted proteomics for selected proteins related to the impact of ENMs on crop plant growth, using wheat as the model crop.

Omics technologies, including genomics, transcriptomics, proteomics, and metabolomics, play a pivotal role in unraveling the complex molecular responses of plants to various environmental stressors, including ENMs.[18] Integrating multi-omics datasets can provide comprehensive insights into the intricate regulatory networks within biological systems.[19,20] In contrast to the broad and comprehensive view provided by untargeted multi-omics approaches, targeted methods offer a more precise and focused analysis by concentrating on specific molecules or pathways of interest. While untargeted approaches have been commonly utilized in previous multi-omics investigations, they often face challenges related to accuracy and reproducibility.[21,22,23,5] Thus, in our study, we have chosen to employ our previously optimized targeted metabolomics and targeted proteomics approaches. By doing so, we aim to delve into the specific molecular responses of plants to ENMs. This enables us to zoom in on particular molecules or pathways of interest, thereby offering a more refined and detailed understanding of how plants react to exposure to ENMs.

B. Objectives and significance

This project focuses on *Triticum aestivum* (wheat), a pivotal crop plant due to its widespread cultivation and its response to treatments with two ENMs. Copper (Cu) based nano-pesticide ($Cu(OH)_2$-NP) and molybdenum (Mo) based nano-fertilizer (MoO_3-NP) are ENMs developed because of the essential roles Cu and Mo play in plant biology. Both Cu and Mo are crucial micronutrients vital for optimal plant growth and development. Cu aids in disease mitigation and enhances crop quality, while Mo facilitates the production of molybdoenzymes crucial for nitrogen fixation, amino acid, and protein biosynthesis in plants. Through targeted proteomics analysis of early-stage wheat grass, this project aims to investigate how these treatments influence plant responses. The objectives and significance of this research endeavor lie in elucidating the molecular mechanisms underlying the effects of Cu and Mo nanoparticles on wheat growth and, consequently, advancing sustainable agricultural practices. Specific objectives and significances for each chapter include:

Chapter II: Optimize targeted proteomics approaches using wheat grass

a. Signature peptide selection of target proteins: This step is crucial for identifying specific proteins affected by ENMs. It allows for a focused analysis, ensuring that the chosen peptides are indicative of the proteins of interest.

b. LC-MS/MS analysis method optimization: The optimization of analytical method enhances the sensitivity and accuracy of protein quantification. It ensures reliable results in detecting changes in protein expression under ENM exposure.

c. Sample preparation method optimization: The effectiveness of the sample preparation method is vital for obtaining high-quality proteomic data. The efficiency of TCA/acetone method, phenol method and TCA/acetone/phenol method coupled with 2 digestion methods,

including trypsin digestion and LysC/trypsin digestion method were compared, and the optimized method were selected and used in the future targeted proteomics analysis experiments.

Significance: Successful optimization of these methods ensures the reliability of subsequent proteomic analyses, laying the foundation for accurate identification and quantification of proteins.

Chapter III: Explore the responses of wheat plants in proteomic processes with exposure to nano-pesticides/nano-fertilizers

a. Up/downregulation of selected proteins: Identifying protein regulation provides insights into how ENMs impact specific cellular processes. This information contributes to understanding the molecular mechanisms behind the observed physiological measurements such as biomass, length, and color.

b. Pathway analysis of protein regulation: Examining protein regulation in the context of pathways offers a holistic view of the cellular response. Different aspects of ENMs exposure, including the type of ENMs, exposure approaches (root vs. leaf routes), and variations in tissue parts were considered.

Significance: This objective helps unravel the complex interplay of proteins in response to ENMs exposure, shedding light on the intricate defense responses and physiological changes in wheat plants.

Chapter IV: Integrate targeted proteomics with targeted metabolomics

a. Up/downregulation of selected metabolomics: Understanding how metabolites are regulated complements the proteomic analysis, providing a comprehensive view of the cellular response.

b. Joint pathway analysis of proteins/metabolites regulation: Integrating proteomic and metabolomic data enhances the understanding of coordinated cellular responses.

Significance: Integration of proteomic and metabolomic data offers a more comprehensive understanding of how ENMs influence biological pathways, providing a nuanced view of the plant's response.

In summary, these research objectives collectively aim to unravel the intricate molecular and biochemical responses of wheat plants to Cu and Mo-based nano-pesticides and nano-fertilizers, contributing valuable insights to agricultural and environmental sciences.

II. Optimization of targeted plant proteomics using liquid chromatography with tandem mass spectrometry (LC-MS/MS)

Material from:

Li, W.; Keller, A. A. Optimization of Targeted Plant Proteomics Using Liquid Chromatography with Tandem Mass Spectrometry (LC-MS/MS). *ACS Agric. Sci. Technol.* **2023**, *3* (5), 421–431.

Abstract This study was conducted to optimize a targeted plant proteomics approach, from signature peptide selection, LC-MS/MS analytical method development and optimization, to sample preparation method optimization. Three typical protein extraction and precipitation methods, including TCA/acetone method, phenol method and TCA/acetone/phenol method, and two digestion methods, including trypsin digestion and LysC/trypsin digestion were evaluated for selected proteins related to the impact of engineered nanomaterials (ENMs) on wheat (*Triticum aestivum*) plant growth. In addition, we compared two plant tissue homogenization methods: grinding freeze-dried tissue and fresh tissue into fine powder using mortar and pestle aided with liquid nitrogen. Wheat plants were grown under a 16 h photoperiod (light intensity 150 $\mu mol \cdot m^{-2} \cdot s^{-1}$) for 4 weeks at 22 °C with a relative humidity of 60% and were watered daily to maintain a 70-90% water content in the soil. Processed samples were analyzed with an optimized LC-MS/MS method. The concentration of selected signature peptides for the wheat proteins of interest indicated that the phenol extraction method using fresh plant tissue, coupled with trypsin digestion, was the best sample preparation method for the targeted proteomics study. Overall, the optimized approach

yielded the highest total peptide concentration (68,831 ng/g, 2.4 times the lowest concentration) as well as higher signature peptide concentrations for most peptides (19 out of 28). In addition, three of the signature peptides could only be detected using the optimized approach. This study provides a workflow for optimizing targeted proteomics studies.

A. Introduction

Plant proteomics is a novel approach to generate knowledge about the proteins as biomarkers of plant response to biotic and abiotic stresses.[1] Particularly, modern mass spectrometry (MS)–based proteomics technologies, including non-targeted proteomics and targeted proteomics have enabled identification and quantification of the plant proteome that helps to understand the molecular mechanisms underlying plant phenotypes.[2] Non-targeted proteomics is a discovery based comprehensive analysis that quantifies thousands of proteins detectable in samples, and is the most commonly used in plant proteomics. [2] It is generally performed using data dependent acquisition (DDA) with a quadrupole time-of-flight (Q-TOF) tandem mass spectrometer.[2,3] However, the approach lacks accuracy and reproducibility due to the characteristics of full spectrum scan. [3,4] The scans are performed over the full accessible mass range with the highest abundance ions selected as precursor ions for fragmentation. Since the selection of precursor ions is a stochastic process, DDA generates missing values and low reproducibility.[3,4] Although non-targeted proteomics allows for the comprehensive analysis of proteins, the accuracy remains limited due to the broad scale quantification.[3] Since more than 100,000 peptides may be identified, it is impossible to develop calibration curves coupled with internal standards for them. Thus, the results of non-targeted proteomics are semi-quantitative, reporting relative abundances rather than calibrated results.[24] In contrast, targeted proteomics employs selected reaction

monitoring (SRM) to analyze selected signature peptides in order to quantify the proteins of interest, leading to high sensitivity, accuracy, and reproducibility.[5,6] Only the selected peptide precursor ion (Q1) with certain fragment ions (Q3) will be detected, since only specific mass-to-charge ratios (m/z) of Q1 and Q3 will be filtered into the detector.[5,12,17] Calibration curves are developed for each peptide, with rigorous quality assurance. Therefore, targeted proteomics approaches can perform a specific, high-quality quantification of a limited set of pre-selected peptides for targeted proteins, useful for hypothesis driven experiments.[4,25,26] However, there is a need to optimize the methods used in targeted plant proteomics, to ensure high reproducibility of results.

Several studies have employed targeted proteomics to determine allergen levels in plants such as soybean[8], hazelnut[9], wheat[10], and maize[11]. Chawade et al. identified and analyzed potential protein biomarkers for potato plant breeding with targeted proteomics approaches, which leads to new possibilities of protein-based quantitation for understanding of molecular mechanisms at the post-transcriptional level.[27] Targeted proteomics were also used to characterize specific plant biological processes at the proteome level. Stecker et al. identified several regulatory proteins in *Arabidopsis* as specific targets for early events in dehydration responses, provided insights into plants biological processes involved in the osmotic stress response.[12] Different methods of sample preparation and analysis were employed in these studies, but there was no detailed evaluation and optimization of the various steps in the analytical method.

To exemplify the use of proteomics in plant studies, we considered the exposure of crops to engineered nanomaterials (ENMs). ENMs have been studied for use in agriculture, especially as nano-pesticides and nano-fertilizers to increase productivity.[13,14] With the

growing agricultural application of ENMs, exposure to ENMs as a trending abiotic stress has drawn the attention of researchers to plant proteomics studies. Previous non-targeted proteomics studies have revealed plant responses to ENMs related to abiotic stress at the protein level (Table S1). For example, several studies investigated the proteomic response of *Oryza sativa L*[28], *Triticum aestivum*[29] and *Glycine max*[30] after exposure to silver nanoparticles and identified responsive proteins that are involved in oxidative stress tolerance, electron transfer and signaling, transcription and protein degradation, and N-metabolism. The effects of cerium dioxide nanoparticles to *Phaseolus vulgaris* were also investigated with proteomic analysis and the responsive proteins involved in oxidative stress regulation, photosynthesis and protein biosynthesis and turnover were revealed.[31,32] However, these qualitative results cannot fill the knowledge gap of the mechanisms underlying the biological responses to ENMs at molecular level. By quantifying a specific set of ENMs responsive proteins with targeted proteomics, the changes of targeted proteins can provide clues about the perturbations in biological pathways triggered by ENMS[33], and hypotheses such as "the exposure of plants to metal-based ENMs triggers defense responses in plant cells through specific biological pathways and affect protein regulation" can be tested.

Developing robust and specific assays for targeted plant proteomics can be challenging. First, it's important to choose targeted proteins that are relevant to the research hypothesis. Next, the signature peptides unique to those proteins need to be selected. Then signature and isotopically-labeled peptides selected as internal standards need to be synthesized to prepare analytical standards for liquid chromatography with tandem mass spectrometry (LC-MS/MS) method development. Then an LC-MS/MS analytical method with high accuracy and sensitivity for the signature peptides and experimental design needs to be developed. Finally,

the biggest challenge is to optimize sample preparation methods to extract the proteins of interest from plant tissue, followed by proteolytic digestion and peptide purification to achieve samples suitable for LC-MS/MS analysis. After completing these steps, the acquired data can finally be interpreted to accept or reject the research hypothesis. Currently, there is no published study that evaluates and optimizes these critical steps in targeted plant proteomics from beginning to end.

In this study we optimized a targeted plant proteomics approach (Figure S1) for selected proteins related to the impact of ENMs on crop plant growth, using wheat as the crop of interest. First, signature peptides were selected and synthesized to order. Then the LC-MS/MS analytical method for the selected peptides was optimized. Next, we evaluated 3 typical protein extraction and precipitation methods and 2 proteolytic digestion methods, to develop the most effective sample preparation procedures for targeted plant proteomics. Finally, the finalized sample preparation method was used to process fresh and freeze-dried plant tissues to determine the best homogenization method. The optimized protocol for targeted proteomics in plant systems can serve as a template for food and plant researchers to perform targeted proteomics based on their specific research hypotheses.

B. Materials and Methods

1. Selection of signature peptides

For this study, 24 proteins were firstly selected as targets based on the reported importance for wheat growth and response to ENMs in previous non-targeted proteomics studies (Table S1). With the list of targeted proteins, signature peptides were selected based on a public wheat proteome database (wheatproteome.org) with the criteria discussed in

Section 3.1. By searching for proteins within metabolic pathways of interest for testing the hypothesis, a list of potential signature peptides was generated. The wheat proteome database provided information on relative peptide abundance, whether the peptide is MRM detectable, and the occurrence of this peptide sequence within the entire wheat proteome. If the peptide is only present in a particular protein, it is a signature peptide candidate. Considering the pathways and proteins identified in previous non-targeted studies, the peptides were filtered into a list of 28 signature peptides candidates (Table S1).

2. Materials

Triticum aestivum (wheat) seeds were purchased from Harmony Farms KS (Jennings, KS, USA). Sodium hypochlorite solution, Triton X-100, protease inhibitors cocktail, dithiothreitol (DTT), iodoacetamide (IAA), trypsin protease, trifluoroethanol (TFE), formic acid, ammonium acetate, trichloroacetic acid (TCA), dimethyl sulfoxide (DMSO), 0.5M pH 8.0 ethylenediaminetetra-acetic acid (EDTA), sucrose, HPLC grade water, acetone, Isopropyl alcohol (IPA) and methanol were obtained from Sigma Aldrich (St. Louis, MO, USA). Urea, ammonium bicarbonate and acetonitrile (ACN) were purchased from Spectrum Chemicals (New Brunswick, NJ, USA). Tris-buffered phenol solution, 1.5 M pH 8.8 Tris-HCl solution, LysC/trypsin protease mix, phenylmethanesulfonyl fluoride (PMSF), 2-mercaptoethanol (2-ME), sodium n-dodecyl sulfate (SDS), 5 mL and 15 mL Eppendorf centrifuge tube were purchased from Fisher Scientific (Waltham, MA, USA). C-18 cartridge (Waters Sep-Pak C18 1 cc, 50 mg sorbent) was purchased from Waters Corporation (Milford, MA, USA).

The analytical standards of the 28 selected peptides (Table S1) were purchased from GenScript (Piscataway NJ, USA). These standards were synthesized as ordered in white lyophilized powder phase with ≥95% HPLC purity. For each peptide, 1 mg/mL working

stock solution was prepared by dissolving the standard powder into HPLC grade water for water soluble peptides (IQNGGTEVVEAK, SVHEPMQTGLK, TAVAAVPYGGAK, LVGVSEETTTGVK, VAEGDAEDVDRAVVAAR, KALDYEELNENVK, SGDVYIPR, GMAVPDSSSPYGVR, GNATVPAMEMTK, EFAPSIPEK, FVIGGPHGDAGLTGR, AADNIPGNLYSVK, TVVSIPNGPSELAVK, TLGELPAGSVIGSASLRR, YIGSLVGDFHR, TALIDEIAK, VAPEVIAEYTVR, IGGLTLNELGR, TLAEEVNQAFR, IGLFGGAGVGK, VQLLEIAQVPDEHVNEFK, KPWNLSFSFGR and TWPEDVVPLQPVGR), or 50 % (v:v) ACN in HPLC grade water for non-water soluble peptides (ADGGLWLLVR, TAIAIDTILNQK, FASINVENVEDNRR, VAEFSFR and AAVIGDTIGDPLK). Peptide stock solutions were stored at - 20 °C. Isotopic labeled peptide standards were also purchased from GenScript (Piscataway NJ, USA) to use as internal standard for LC-MS/MS analysis and quantitation. The selected internal standards include SVHEPMQTGLK{Lys($^{13}C_6$,$^{15}N_2$)}, SGDVYIPR{Arg($^{13}C_6$,$^{15}N_4$)}, TALIDEIAK{Lys($^{13}C_6$,$^{15}N_2$)} and KPWNLSFSFGR{Arg($^{13}C_6$,$^{15}N_4$)}. A 1 mg/mL working stock solution for each internal standard was prepared in HPLC grade water and stored at - 20 °C.

3. LC-MS/MS analysis method

The working stock solution of 28 peptide standards and 4 isotopic labeled internal standards were diluted 100 times with water to reach a concentration of 10 µg/mL for compound optimization using an Agilent InfinityLab 1290 Infinity II Series liquid chromatography system coupled to an Agilent 6470 triple quadrupole mass spectrometer in positive ionization mode. Then a mixture of all 28 peptides and 4 internal standards was prepared in 30% ACN with 0.1% formic acid and 3% DMSO in water at 1000 ng/mL to

optimize the column and mobile phase to separate peaks of peptides with adequate abundance and sensitivity. An Agilent Polaris 3 C18-Ether column (150x3.0mm, p/n: A2021150X030) coupled with gradient mobile phase (A: Water + 0.1% (v:v) formic acid + 3% (v:v) DMSO; B: ACN + 0.1% (v:v) formic acid + 3% (v:v) DMSO) was selected as the optimal HPLC settings (Table S2). The flow rate was set to 0.4 mL/min with a column temperature of 25 °C and a 2 μL injection volume. Gradient mobile phase started at 5% B and gradually increased to 70% B in 10 mins, then decreased to 5% B to re-equilibrate the column. Source optimization was performed by the Agilent Source Optimizer to optimize MS settings (Table S2) including 340 °C gas temperature at a 12 L/min flow rate, 250 °C sheath gas temperature at a 9 L/min flow rate, nebulizer at 40 PSI, capillary voltage of 3,500 V, and nozzle voltage at 2,000 V. The total run time for each sample was 14 min. Needle wash with TFE was done between injections.

For each analyte, two pairs of transitions (m/z values associated to the precursor and fragment ions) with highest abundance and signal to noise (s/n) were selected for each compound as quantifier and qualifier. The limit of detection (LOD) of each peptide was calculated by diluting standards until the concentration that gives a signal/noise = 3. Method detection limit (MDL) was calculated based on sample extraction method. Since 200 mg plant tissue were extracted and reconstituted into 1 mL for instrument analysis, MDL (ng/g) = LOD (ng/mL)/0.2 (g/mL) = 5 × LOD (ng/g).

Calibration standards were prepared at 8 levels, including 1 ng/mL, 2.5 ng/mL, 5 ng/mL, 10 ng/mL, 25 ng/mL, 50 ng/mL, 75 ng/mL and 100 ng/mL. 50 ng/mL of internal standards were added into each level of calibration standards and plant samples to adjust for matrix effects during quantification.

4. Plant growth, harvest and homogenization

As one of the most important crop plants, wheat (*Triticum aestivum*) was selected as the model plant for this research. This project focused on early-stage wheat plants, since stressors at this stage may affect the formation of tillers that ensures the yield potential of wheat.[34] Wheat plants were grown for 4 weeks to harvest the early-stage plant tissue for the experiments.

Before germination, all wheat seeds were sterilized in 1% sodium hypochlorite solution for 10 min., followed by 5 rinses with NANOpure water. Then sterilized seeds were soaked in NANOpure water overnight before germination. Vermiculite was used as the growth matrix, since it helps to maintain good aeration while simultaneously retaining water and nutrients that eventually are released for plant adsorption. Vermiculite was saturated with 10% Hoagland solution and then transferred into plant pots up to 2.5 cm below the rim.[35] Then 80 soaked seeds were planted (4 seeds per pot) with tips facing up to ensure successful germination, then covered by vermiculite to fill the pot. Each pot was watered daily with 20 ml of 10% Hoagland water to maintain a 70-90% water content. Plants were grown under a 16 h photoperiod (light intensity 150 $\mu mol \cdot m^{-2} \cdot s^{-1}$) for 4 weeks at 22 °C with a relative humidity of 60%. Diluted 10% Hoagland solution was employed throughout the project to provide sufficient water and nutrients for plant growth.[35] The concentrated Hoagland solution was prepared in NANOpure water using 82.6 mg/L $Ca(NO_3)_2 \bullet 4H_2O$, 308.7 mg/L $CaCl_2 \bullet 2H_2O$, 233.23 mg/L $Mg(NO_3)2 \bullet 6H_2O$, 132 mg/L KH_2PO_4, 25.8 mg/L KNO_3, 1.43 mg/L H_3BO_3, 4.04 mg/L $Fe(NO_3)3 \bullet 9H_2O$ and 0.11 mg/L $Zn(NO_3)_2) \bullet 6H_2O$.[35]

After 28 days, the shoots of 80 wheat plants were harvested and divided into two parts, 40 plants in each group, to test different sample homogenization strategies. The first portion

was ground into a fine powder directly starting with fresh plant tissue frozen with liquid nitrogen, and then ground with ceramic mortar and pestle for homogenization. The second group was freeze-dried with lyophilizer (HRFDSSS Freeze Dryer, Harvest Right) and then finely ground into powder using mortar and pestle with liquid nitrogen aided for homogenization. The two groups of homogenized plant tissue samples were stored at -80°C until further processing and analysis.

5. Sample preparation and protein digestion

To extract targeted peptides from plant samples, plant tissues were processed through protein extraction and precipitation, proteolytic digestion, and peptide purification. The general workflow starts with protein extraction from plant tissues using an extraction buffer, followed by protein precipitation to remove biological interferences from pigments, carbohydrates, nucleic acids, and other biomolecules, using organic solvents such as acetone and methanol. Then, protein pellets are solubilized with a urea solution, and processed through proteolytic digestion to cleave proteins into MRM detectable peptide sequences. Finally, the digested peptides are purified via solid-phase extraction (SPE) before LC-MS/MS analysis.

To optimize the protein extraction and precipitation method, the most popular approaches including TCA/acetone method[36,37], phenol method[38], and TCA/acetone/phenol method[39] were compared in this study (Figure 1). In addition, two digestion methods, including trypsin digestion and LysC/trypsin digestion, were also compared. Homogenized fresh shoot tissues were used for these method comparisons. Full details of these methods are in the Supporting Information.

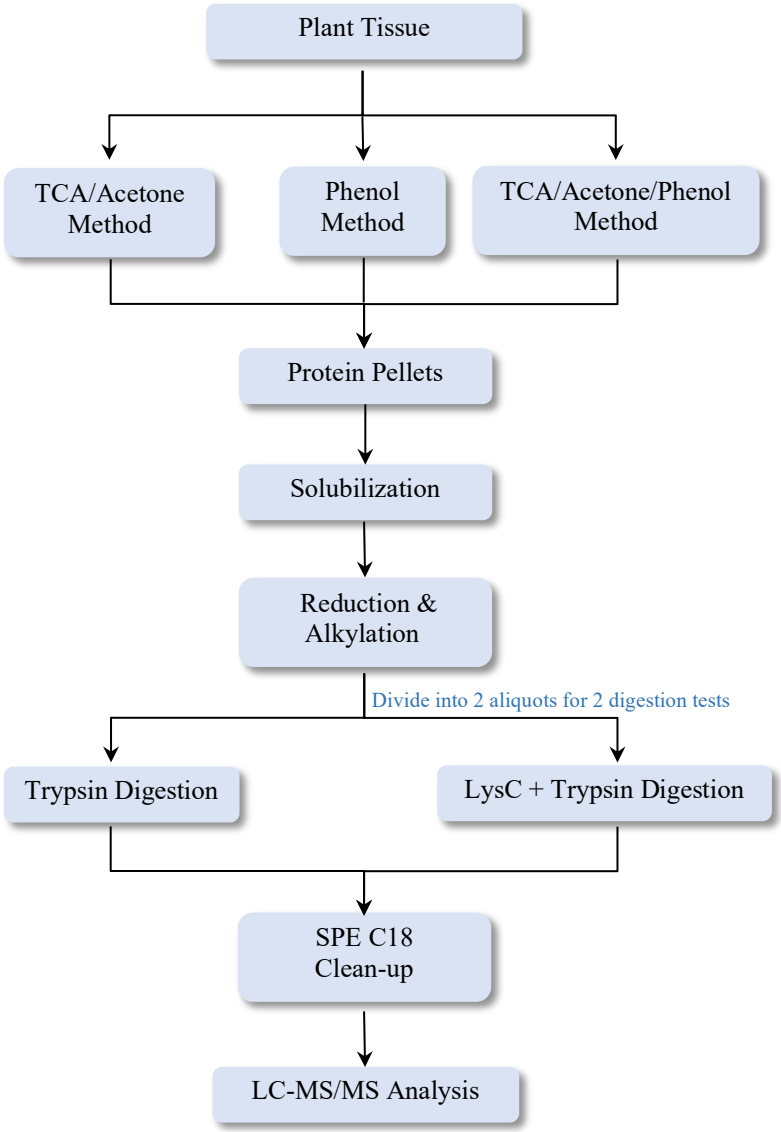

Figure 1. Flowchart of method comparisons of 3 protein extraction and precipitation methods, with 2 protein digestion methods.

5.1 Protein extraction/precipitation

Two hundred mg of plant sample was weighed out into 5 mL centrifuge tube and processed with 3 methods of protein extraction and precipitation, including A: TCA/acetone method, B: phenol method and C: TCA/acetone/phenol method, to achieve protein pellets (Figure 2). Full details of these 3 methods are in the Supporting Information. Procedures were modified from previous studies and are discussed in Section 3.2.1.

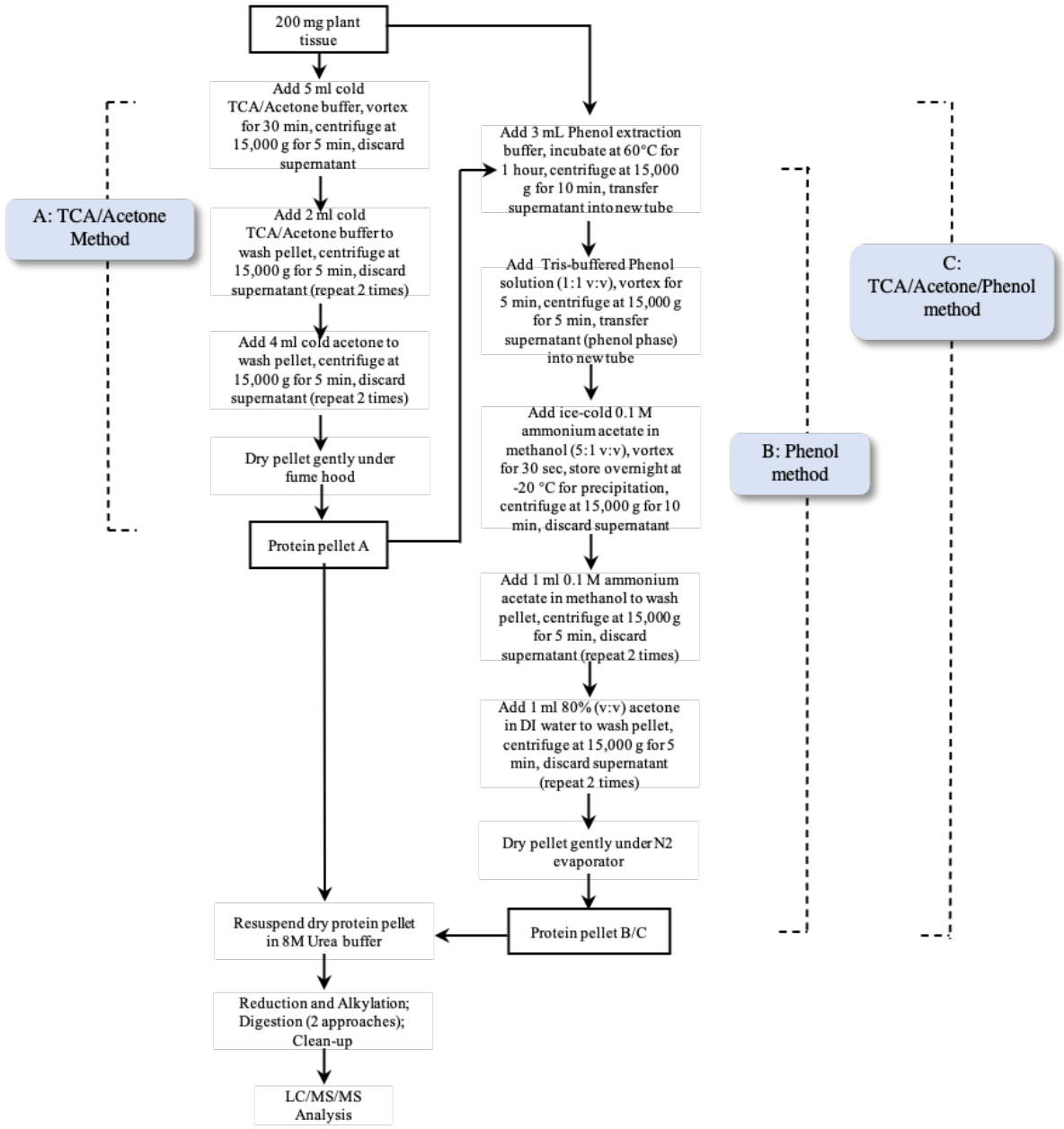

Figure 2. Flowchart of 3 protein extraction and precipitation methods, including A: TCA/acetone method, B: Phenol method and C: TCA/acetone/phenol method

5.2 Protein digestion

Protein pellets A, B & C achieved as per Section 2.5.1 were reduced and alkylated with DTT and IAA. Then protein solution was divided into two aliquots to be digested with 2 digestion approaches, including trypsin digestion and LysC/trypsin digestion. Full details of

protein reduction and alkylation, and 2 protein digestion approaches are in the Supporting Information.

5.3 Peptide purification

Solid phase extraction (SPE) cleanup with C-18 cartridges (Waters Sep-Pak C18 1 cc, 50 mg sorbent) was used for peptide purification after protein digestion. Full details of peptide purification are in the Supporting Information.

6. Statistical analysis

Three replicates were prepared for each method test. The average concentration of three sample replicates was calculated for each peptide to make method comparisons. Among compared extraction methods, the number of peptides showing highest average concentration was counted, and the one with the highest number is considered to be the most efficient method. In addition, the total concentration of all 28 peptides was calculated for each method as another criterion to make the choice of the best method. Data were presented with stacked column using Microsoft Excel to visualize the method comparisons.

C. Results and discussions

1. Selection of signature peptides

The critical step to start a targeted proteomics project is the selection of the proteins that will serve to test the hypothesis and their corresponding "signature" peptides. For specific hypotheses, the selection of proteins can be based on a preliminary non-targeted proteomic analysis, literature knowledge, and/or public data. With the list of targeted proteins, targeted peptides for quantification can be selected using either empirical proteomics data or prediction algorithms.[40] Ideally, candidate peptides can be selected using MS data from in-

house or public empirical data. This is the "gold standard" for targeted proteomics since the selected peptides have already been demonstrated to be present in the proteins of interest, cleavable and detectable via MS.[40] For this study, targeted proteins were selected based on literature review and their signature peptides were selected based on public database.

To assure a successful targeted proteomics assay, there are several criteria for selecting the targeted peptides. First, peptides need to be unique to the protein, which are denominated signature peptides, to enable specificity of the analysis. Second, peptides must be detectable by MS since targeted proteomics utilizes MRM detection. Selection based on empirical MS data is more reliable than predictions. Additionally, to ensure a high-response and stability of the signature peptides, criteria such as proper peptide length, hydropathy, reactive residues and digestion parameters should be considered.[40] Typically, the optimal peptide length for MRM detection is 7 to 20 amino acids, which is the typical length of tryptic peptides produced by trypsin digestion. In addition, reactive amino acid residues that could be modified during sample preparation should be avoided. Reactive residues that potentially lead to modifications include cysteine, methionine and tryptophan (oxidation), n-terminal glutamine (pyroglutamic acid formation), asparagine or glutamine followed by glycine (deamidation), aspartic acid followed by glycine (dehydration), proline (peptide chain cleavage) and histidine (additional charge states).[40] Additional criteria included high abundance of the protein and peptide and a short peptide length to reduce the cost of synthesis. Based on these criteria, 28 signature peptides candidates were selected (Table S1).

2. Optimization of LC-MS/MS analysis for selected peptides

Figure 3 shows the LC-MS/MS chromatograph of 28 peptides standards (100 ng/mL with 50 ng/mL internal standard) using the optimized LC-MS/MS method. With optimized HPLC and MS conditions, the 28 peptides were separated well with great peak shape, which produced high signal to noise ratios and resulted in low LODs (Table 1). The retention time of the 28 peptides ranged from 6.4 min to 9.6 min, and the 4 isotopically-labeled internal standards eluted out at 6.7 min, 7.3 min, 8.2 min and 8.8 min. An internal standard was selected for each of the 28 peptides based on nearest retention time, to adjust for matrix effects and ensure accurate quantitation.

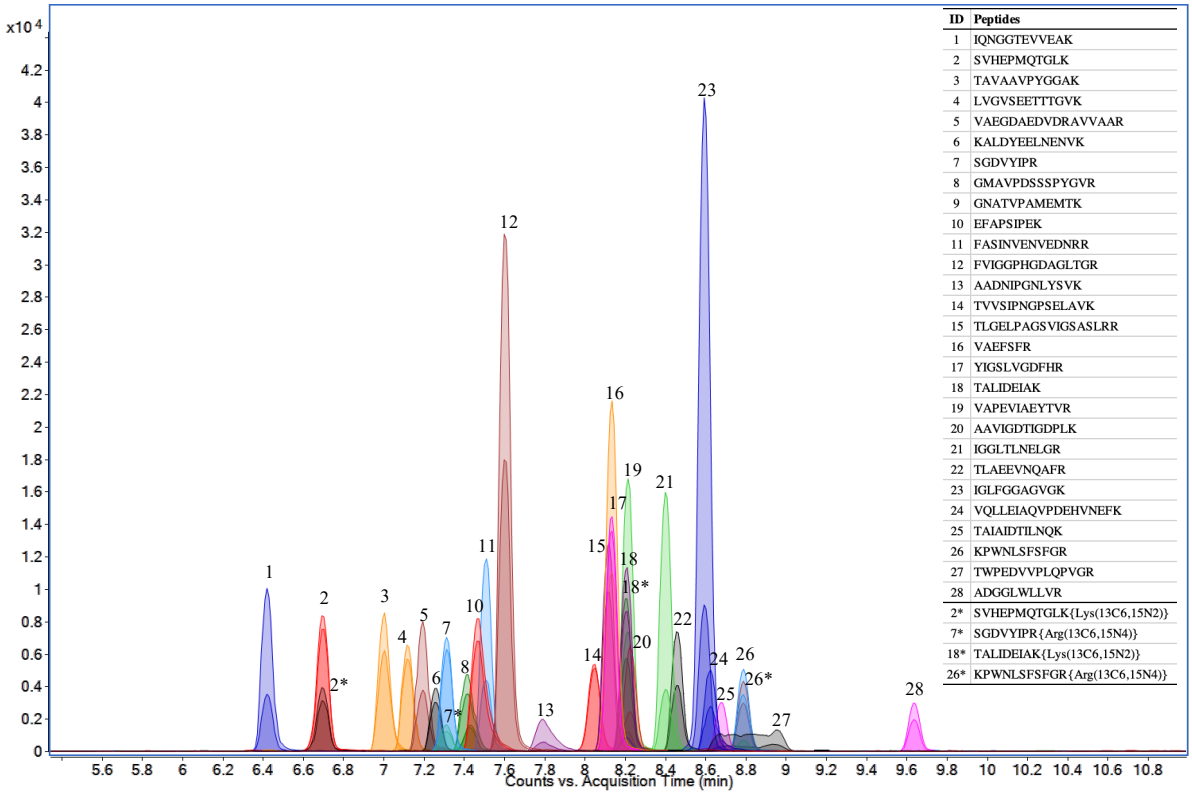

Figure 3. LC-MS/MS chromatograph of 28 peptides standards at 100 ng/mL with 50 ng/mL internal standard.

To optimize HPLC conditions, different chromatography parameter settings including mobile phase and sample solvent were compared to literature conditions. The parameters of this study and previous studies are listed in Table S3. Based on literature review, reverse-

phase columns with silica-based stationary phases such as octadecyl carbon chain (C18)-bonded silica were used to analyze peptides due to their strong affinity for compounds with a wide range of polarity. Ion-paring reagents such as TFA and formic acid in mobile phase can help to deliver highly resolved separations of complex peptide mixtures from tryptic protein digests. In addition, trace amounts of DMSO (3-5%) in mobile phase is also recommended for more efficient ionization and higher signal intensity of peptides.[41,42] After testing several reversed-phase chromatography parameters from previous proteomics studies, the settings of this study were optimized to show the best peak shape and abundance for the targeted peptides.

During LC-MS/MS analysis method optimization, there was a carryover issue that resulted in peaks in solvent blanks immediately after an injection of standard solution. This carryover issue can be caused by insufficient washing of the injection needle and valve of the autosampler since peptides can adsorb to HPLC components. For peptides containing hydrophobic residues, they can even be retained on HPLC columns despite the use of high concentrations of organic solvents for washing.[40] The carryover issue can increase variability of quantification and bias of analysis. In a previous study, Mitulovic et al. recommended the injection of TFE into the HPLC flow path and column to remove strongly bound peptides due to its properties to decoy peptides and ability to clean all parts of HPLC.[43] In our study, we resolved the carryover issue by introducing an autosampler needle wash with 2 μL of TFE between injections.

Table 1. Transitions, LOD and MDL for each peptide.

ID	Sequence	Retention Time (min)	Precursor ion (m/z)	Product ions					LOD (ng/mL)	MDL (ng/g)
				Quant ion (m/z)	Collision energy (V)	Qual ion (m/z)	Collision energy (V)	Fragmentor (V)		
	Peptides									
1	IQNGGTEVVEAK	6.42	623.2	242.1	20	86.1	32	132	0.02	0.08
2	SVHEPMQTGLK	6.70	409.8	110.2	40	84.0	40	96	0.41	2.05
3	TAVAAVPYGGAK	7.00	553.1	173.0	24	72.1	40	112	0.08	0.40
4	LVGVSEETTTGVK	7.12	660.7	86.0	36	72.1	40	137	0.09	0.44
5	VAEGDAEDVDRAVVAAR	7.19	582.0	786.9	16	72.0	40	96	0.16	0.81
6	KALDYEELNENVK	7.25	522.6	102.0	16	86.2	16	96	0.24	1.18
7	SGDVYIPR	7.31	454.0	548.3	16	60.1	40	96	0.01	0.04
8	GMAVPDSSSPYGVR	7.42	712.3	260.0	28	189.2	36	132	0.02	0.09
9	GNATVPAMEMTK	7.43	625.7	172.0	40	70.0	40	117	0.10	0.51
10	EFAPSIPEK	7.46	509.6	335.7	16	70.0	40	96	0.10	0.49
11	FASINVENVEDNRR	7.51	555.3	120.0	24	191.0	16	96	0.00	0.02
12	FVIGGPHGDAGLTGR	7.60	485.5	604.4	12	120.0	32	96	0.00	0.01
13	AADNIPGNLYSVK	7.79	681.8	877.4	20	230.0	32	127	0.08	0.38
14	TVVSIPNGPSELAVK	8.05	756.4	172.8	40	200.9	36	132	0.01	0.06
15	TLGELPAGSVIGSASLRR	8.12	595.7	635.9	16	186.9	20	117	0.00	0.02
16	VAEFSFR	8.13	428.5	171.0	12	72.1	24	96	0.01	0.03
17	YIGSLVGDFHR	8.13	422.1	494.3	8	86.0	28	96	0.01	0.03
18	TALIDEIAK	8.21	487.5	173.0	12	86.0	40	112	0.01	0.03
19	VAPEVIAEYTVR	8.21	674.3	589.0	16	70.0	40	147	0.06	0.28
20	AAVIGDTIGDPLK	8.23	635.7	72.0	32	86.0	32	132	0.06	0.30
21	IGGLTLNELGR	8.40	572.2	228.0	24	86.1	40	122	0.01	0.07
22	TLAEEVNQAFR	8.45	639.7	187.1	28	215.0	20	127	0.04	0.21
23	IGLFGGAGVGK	8.59	488.5	545.2	16	86.1	24	117	0.01	0.05
24	VQLLEIAQVPDEHVNEFK	8.62	703.8	227.8	24	72.1	36	142	0.01	0.06
25	TAIAIDTILNQK	8.68	651.3	173.1	24	86.0	40	112	0.10	0.50
26	KPWNLSFSFGR	8.79	670.3	84.0	36	70.1	40	137	1.17	5.84
27	TWPEDVVPLQPVGR	8.96	797.4	653.7	20	342.1	40	147	1.55	7.75
28	ADGGLWLLVR	9.63	550.7	159.0	40	86.0	40	117	0.02	0.11
	Internal Standards									
2*	SVHEPMQTGLK{Lys(13C6,15N2)}	6.69	412.5	90.1	40	69.9	40	96		
7*	SGDVYIPR{Arg(13C6,15N4)}	7.31	459.0	558.3	12	260.0	16	91		
18*	TALIDEIAK{Lys(13C6,15N2)}	8.21	491.6	172.8	16	86.0	40	81		
26*	KPWNLSFSFGR{Arg(13C6,15N4)}	8.79	675.3	84.1	36	70.0	40	137		

3. Sample preparation optimization for protein extraction, precipitation and digestion

Figure 4 presents the concentration of each targeted peptide in plant tissues processed with 3 protein extraction and precipitation methods, and 2 protein digestion methods (full data in Table S4 in Supporting Information). Three replicates were prepared for each test and the average concentrations were calculated. Among these 6 methods, the phenol method

coupled with trypsin digestion yielded the highest concentration of most targeted peptides (17 out of 28), compared to TCA/Acetone/Phenol method coupled with trypsin digestion (5 out of 28), phenol method coupled with LysC/trypsin digestion (3 out of 28), TCA/Acetone method coupled with trypsin digestion (2 out of 28), TCA/Acetone/Phenol method coupled with LysC/trypsin digestion (1 out of 28) and TCA/Acetone method coupled with LysC/trypsin digestion (0 out of 28). In addition, for the total peptide concentration (Figure 4) the phenol method coupled with trypsin digestion (59,193 ng/g) ranked highest, followed by TCA/Acetone/Phenol method with trypsin digestion (55,107 ng/g), TCA/Acetone method with trypsin digestion (49,765 ng/g), TCA/Acetone method with LysC/trypsin digestion (43,263 ng/g), phenol method with LysC/trypsin digestion (29,172 ng/g) and TCA/Acetone/Phenol method with LysC/trypsin digestion (28,363 ng/g). Overall, trypsin digestion showed higher efficiency than LysC/trypsin digestion when coupled with any of the 3 extraction and precipitation methods. These results indicate that the phenol extraction method coupled with trypsin digestion is the best sample processing method for this study. The procedures of each method are discussed in the following sections.

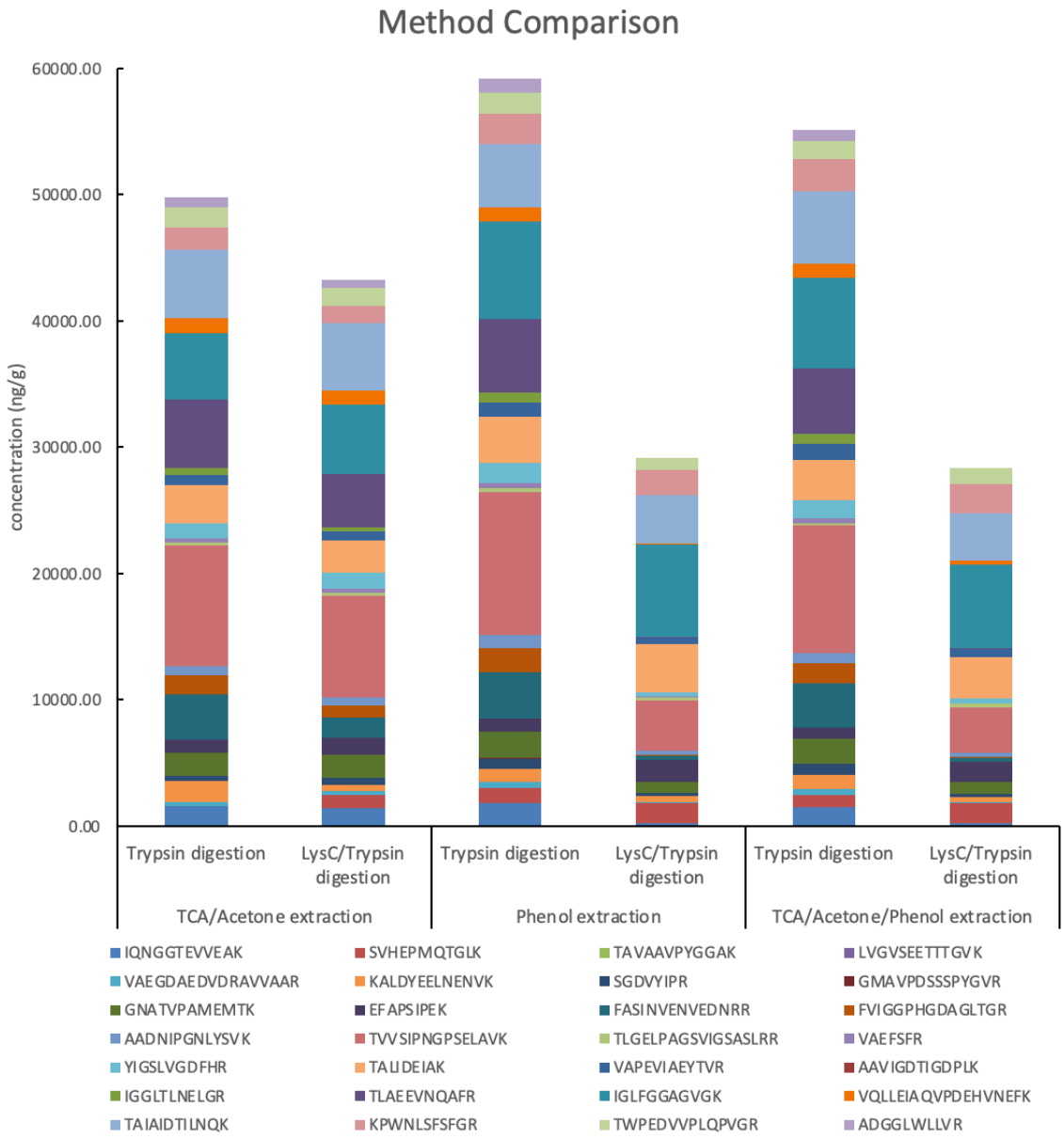

Figure 4. Peptide concentrations in plant tissues processed with 3 protein extraction and precipitation methods and 2 protein digestion methods.

3.1 Protein extraction and precipitation

TCA/acetone-based precipitation methods are commonly used in plant proteomics since they involve a simple organic solution and limited steps. Damerval et al. originally developed this method that combines TCA and acetone precipitation,[44] which can remove many

compounds, particularly ions, lipids, pigments, phenolics, and terpenoids from the samples more effectively than either TCA or acetone alone.[45] This approach employs 10 % TCA in acetone with 2-ME to precipitate proteins by adding the solution directly into the powdered plant tissue. The addition of 2-ME can unfold proteins and prevent formation of disulfide bonds during precipitation thus improving protein recovery.[37] This less time-consuming and easier-to-operate precipitation method is recommended as a starting protocol for plant proteomic analyses and has been widely used in studies with minor modifications.[45] However, the major drawback of this TCA/acetone precipitation approach is that protein pellets are very difficult to fully resolubilize. In the current study, an 8 M urea solution was used to resuspend protein pellets in iced water bath with sonication. Around 1 hr was needed to fully re-solubilize the pellet. The difficulty of protein pellet solubilization from this method could result in the loss of targeted proteins.

A phenol extraction-based methanol precipitation method has also been widely applied in protein extraction from plants, especially for recalcitrant plant tissues.[38,45,46] This method employs the solubility of proteins in phenol to partition the protein from the aqueous extraction buffer into the phenol phase, and then precipitate the protein with ice-cold methanol with addition of ammonium acetate. Isaacson et al. presented the phenol extraction-based methanol precipitation and the TCA/acetone precipitation methods as two protein extraction protocols successfully used with diverse plant tissues including tomato leaves and fruits, maize roots and orange peels, some of which are recalcitrant tissues.[46] Compared to the TCA/acetone method, the phenol method not only includes 2-ME as a reducing agent to prevent protein oxidation, but also contains SDS to solubilize membrane-bound proteins, EDTA to inhibit metalloproteases and polyphenol oxidases, PMSF to irreversibly inhibit

serine proteases, and protease inhibitors to prevent protein degradation. These added components may explain the increased recovery of protein using phenol extraction compared to the TCA/acetone method. In addition, sucrose in the buffer makes the aqueous phase heavier than Tris-buffered phenol, which facilitates separation by making the phenol phase buoyant. This liquid-liquid partitioning can extract protein from an aqueous buffer into the phenol phase, and helps to cleanup protein extract before protein precipitation, which can also lead to better protein recovery.

The TCA/acetone/phenol method integrating TCA/acetone precipitation and phenol extraction was developed by Wang et al. to utilize the advantages of both methods for optimized extraction.[39] It starts with TCA/acetone precipitation, and then a phenol extraction buffer is used to resuspend protein pellets, followed by an aqueous buffer, phenol partition and further protein precipitation using ammonium acetate in methanol. Although some non-targeted proteomics studies recommend this integrated method as an effective approach,[45,47,48] that was not the case in the current study. Therefore, the simpler phenol extraction-based methanol precipitation method was used for sample analysis.

3.2 Protein Digestion

Trypsin digestion is the "gold standard" to cleave proteins into peptides for proteomics since it produces short peptides (0.6-1kDa) with an ideal range for MS analysis (<3 kDa).[49] Trypsin is also highly specific to cleave proteins at the carboxyl site of arginine and lysine residues, making these cleaved sites charged, which will be detectable by MS. However, for some tightly folded proteins, they are resistant to proteolytic digestion due to inaccessibility of cleavage sites that are embedded in the structure. Pre-digestion with LysC before trypsin digestion can be implemented.[49,50] This two-step digestion approach utilizes the

characteristics of LysC, which shares lysine as cleavage site with trypsin, but has more tolerance to protein denaturing reagents such as urea (8M), in which trypsin is inactivated. Thus, LysC can first cleave protein into relatively long peptide sequences at the C-terminal of lysine in 8 M urea, then trypsin can be activated to cleave the peptides further when the urea is diluted below 2M. Thus, LysC/Trypsin can theoretically increase the digestion efficiency if there are huge number of proteins to be digested, especially for non-targeted proteomics. However, for this targeted proteomics study, trypsin digestion proved to be the most effective for the targeted proteins and signature peptides, and is also simpler.

3.3 Peptide Purification

Peptide purification prior to LC-MS/MS analysis is a critical step to ensure the accuracy of peptide quantitation, since it will remove contaminants that would interfere with LC-MS/MS analysis, such as salts from extraction solution, reducing and alkylating reagents, and trypsin from digestion.[51] In the study by Majumdar et al., peptide solutions were desalted using Pierce C18 StageTips.[52] By dispensing and aspirating sample through a monolithic C18 reversed-phase sorbent, followed by elution with 0.1% formic acid in 50%-95% ACN or methanol, C18 StageTips can effectively remove urea, salts and other interfering contaminants before MS analysis. However, the small amount of sorbent can only bind up to 8 µg (10 µL tips) or 80 µg (100 µL tips) of total peptides. Instead, the peptide purification used in this study was solid-phase extraction (SPE) with C18 cartridges (Waters Sep-Pak C18 1 cc, 50 mg sorbent), as recommended by Mikołajczak et al. to purify protein digests with a retention-cleanup-elution strategy.[53] The larger amount of sorbent and loading volume improves purification with a larger sample size (1-10mL), yielding 1.7 mL of diluted peptide solution to be purified after protein digestion.

4. Fresh tissue vs. freeze-dried tissue

To optimize the plant tissue homogenization method, both freeze-dried tissue and fresh tissue were processed using the optimized phenol extraction coupled with trypsin digestion. Three replicates were prepared for each test and the average concentrations were calculated. Full data is in Table S5 in Supporting Information. A comparison of the total peptide and individual targeted peptide concentration extracted from freeze-dried tissue (59,193 ng/g) and fresh tissue (68,831 ng/g) indicated that it is better to use fresh tissue (Figure 5). In addition to a higher total peptide concentration, more peptides (19 out of 28) can be extracted from fresh wheat tissue than freeze-dried tissue (9 out of 28) with higher concentrations. In particular, 3 peptides (i.e., TAVAAVPYGGAK, LVGVSEETTTGVK and AAVIGDTIGDPLK) were only detectable in fresh tissue. Thus, the optimized homogenization method for this study was to grind fresh plant tissue into fine powder using mortar and pestle aided with liquid nitrogen.

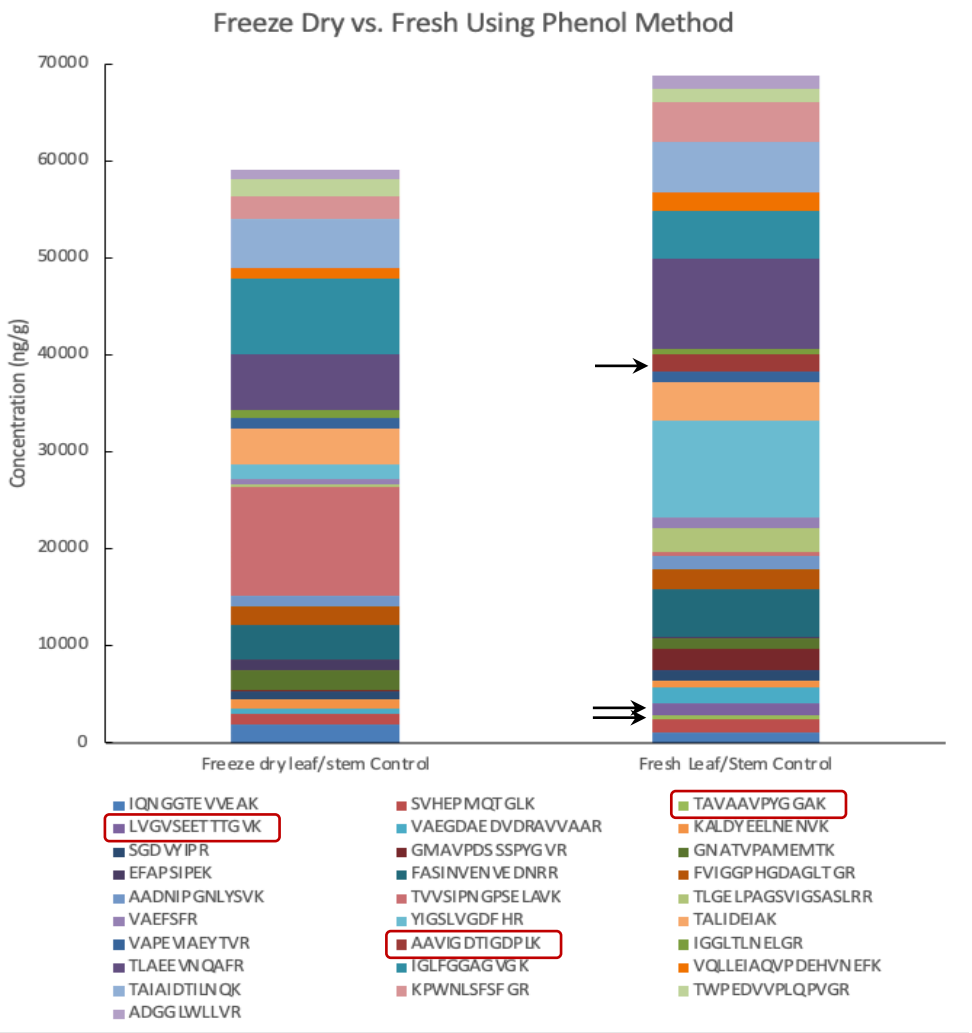

Figure 5. Peptide concentrations extracted from freeze-dried tissue vs. fresh tissue.

D. Conclusions

In this study, an optimized workflow for targeted protein analysis was developed, starting from the selection of targeted proteins and signature peptides to test specific hypotheses concerning metabolomic pathways, followed by optimization of the extraction, digestion and sample preparation methods. A comparison of 3 protein extraction and precipitation methods, and 2 proteolytic digestion methods, indicated that for the wheat proteins of interest the phenol extraction method using fresh plant tissue, coupled with trypsin digestion, was the best sample preparation method for a targeted proteomics study. Overall, the optimized

approach yielded the highest total peptide concentration as well as higher signature peptide concentrations for most peptides (19 out of 28). Three of the signature peptides could only be detected using the optimized approach. Since different plant tissues, or targeted proteins and signature peptides, may be preferentially extracted and digested by other methods, the workflow provides a template for optimizing targeted proteomics for other plant or food samples. Targeted proteomics techniques can also integrate with targeted metabolomics and genomics to provide a more comprehensive understanding of plant response to biotic or abiotic stresses in plant research field.

E. Acknowledgements

This work was supported by the National Science Foundation (NSF) under cooperative agreement number NSF-1901515. Arturo A. Keller would like to give special thanks to Agilent Technologies for their Agilent Thought Leader Award. Any findings and conclusions from this work belong to the authors and do not necessarily reflect the view of NSF.

F. Appendix

1. Three methods of protein extraction and precipitation

A) TCA/Acetone Method:

A 200 mg plant tissue sample was mixed with 5 mL of cold TCA/acetone buffer by vortexing for 30 min at 4 °C, followed by centrifuging at 15,000 g for 5 min, with supernatant discarded. An additional 2 ml of cold TCA/acetone buffer was then added into the tube to wash the pellet, followed by centrifuging at 15,000 g for 5 min with supernatant discarded after each centrifugation (repeated 2 times). Then 4 ml of cold acetone was added into tube to wash TCA off, followed by centrifuging at 15,000 g for 5 min with supernatant

discarded (repeated 2 times). The protein pellet A was dried under the fume hood overnight at room temperature.

B) Phenol Method:

A 200 mg plant tissue sample was mixed with 3 mL phenol extraction buffer, then incubated at 60°C for 1 hour, followed by centrifuging at 15,000 g for 10 min. Then, 3 mL of supernatant was transferred into a new 15 mL centrifuge tube and mixed with 2.5 mL of phenol solution (Tris-buffered) by vortexing for 5 min, followed by centrifuging at 15,000 g for 5 min. Then the phenol phase (supernatant) was transferred into a new 15 mL tube and mixed with 12.5 mL of ice-cold 0.1 M ammonium acetate in methanol by vortexing for 30 sec, and then stored overnight at -20 °C for protein precipitation, followed by centrifuging at 15,000 g for 10 min with supernatant discarded the next day. 1 ml of 0.1 M ammonium acetate in methanol was added into tube to wash pellet, followed by centrifuging at 15,000 g for 5 min with supernatant discarded (repeated 2 times). Then 1 ml of cold 80% (v:v) acetone in DI water was added into the tube to wash the protein pellet and remove phenol, methanol and ammonium acetate, followed by centrifuging at 15,000 g for 5 min with supernatant discarded (repeat 2 times). Then protein pellet B was dried gently under N2 evaporator at room temperature.

C) TCA/Acetone/Phenol Method:

A 200 mg plant tissue sample was processed following the procedure of TCA/Acetone Method to achieve protein pellet A. Then the protein pellet A was resuspended with phenol extraction buffer and processed following procedure of phenol method to produce protein pellet C.

Extraction buffers used for 3 protein extraction/precipitation methods were prepared as following recipe:

TCA/Acetone buffer: 10% (v:v) TCA in acetone with 2% (v:v) 2-ME. Dissolve 50 g of TCA in 400 mL of acetone. Bring the volume to 500 mL by adding acetone. Keep the solution at − 20 °C. Add 2% (v:v) 2-ME just before use.

Phenol extraction buffer: 1% (w:v) SDS, 0.15 M Tris-HCl (pH 8.8), 2% (v:v) 2-ME, 1 mM EDTA, 2 mM PMSF, 1% (v:v) protease inhibitors and 0.7 M sucrose. Prepare buffer by mixing SDS (1%, w:v), Tris-HCl (pH 8.8, 0.15 M), EDTA (1 mM) and sucrose (0.7 M) in water and store at 4 °C. Prepare stock of PMSF (100mM) by dissolving 174 mg of PMSF in 10 mL of IPA and store at − 20 °C. Add 2% (v:v) 2-ME, 2 mM PMSF and 1% (v:v) protease inhibitors just before use.

2. Protein reduction and alkylation

Protein pellets A, B & C achieved after protein extraction and precipitation using 3 methods were resuspended and solubilized with 8 M urea, 50 mM ammonium bicarbonate solution. Then protein in solution was reduced and alkylated by the following steps: 1) add 5 mM DTT and incubate at 56 °C for 30 min with rotation; 2) add 20 mM IAA and incubate at room temperature for 30 min in dark; 3) add additional 20 mM DTT and incubate at room temperature for 30 min to consume unreacted IAA.

3. Two protein digestion approaches

1) Trypsin digestion

Protein solution was diluted with 50 mM ammonium bicarbonate to reduce the concentration of urea from 8 M to 1M. Then 2 μg of trypsin enzyme was added into solution and incubated overnight at 37 °C with rotation.

2) LysC/Trypsin digestion

2 μg of LysC/trypsin enzyme was added into protein solution and incubated at 37 °C for 4 hr with rotation. Then solution was diluted with 50 mM ammonium bicarbonate to reduce the concentration of urea from 8 M to 1M, followed by incubation overnight at 37 °C with rotation. Protein digestion was stopped by adding formic acid into solution to reach a final concentration of 5% (v:v) the next day.

4. Peptide purification

Firstly, the cartridge was conditioned with 1 mL of 80% ACN with 5% formic acid in water. Then the cartridge was re-equilibrated with 1 mL of 5% formic acid, followed by loading digested peptide solution from 2.5.2. After sample loading, the cartridge was washed with 1.5 mL of 5% formic acid. Then peptides adsorbed onto the sorbent was eluted with 1.5 mL of 80 % ACN with 5% formic acid. The eluate was dried gently under N_2 evaporator at room temperature and then reconstituted to 30% ACN in water with 5% formic acid and 3% DMSO for LC-MS/MS analysis.

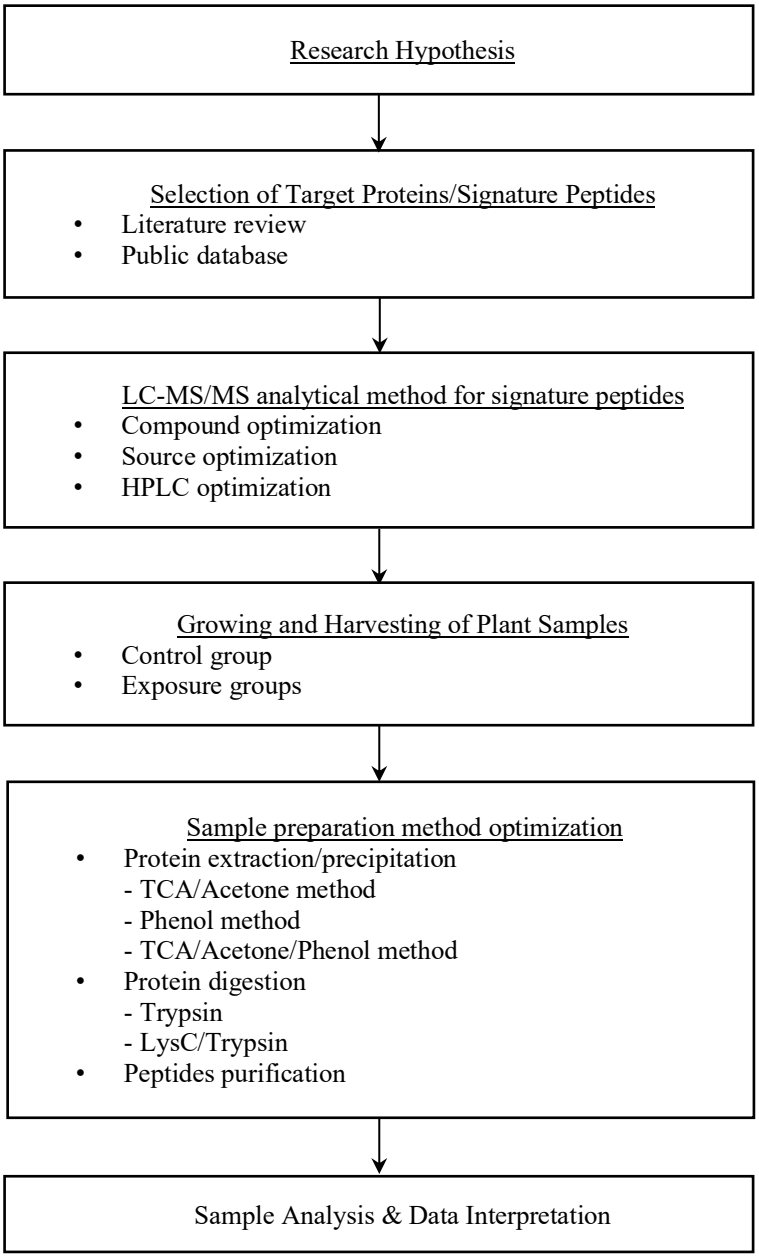

Figure S1. Detailed workflow of a targeted plant proteomics research

Table S1. List of 28 signature peptides for the 24 targeted proteins for this project.

Pathway	Protein	Peptides	Up or Down Regulation	Plant Species	Reference
Amino acid metabolism	AA degradation methionine	LVGVSEETTTGVK		Triticum aestivum	([54])
	AA synthesis methionine	GNATVPAMEMTK		Triticum aestivum	([54])
	S-adenosylmethionine synthase	FVIGGPHGDAGLTGR	+(Ag-NP)	Triticum aestivum	([29])
Fermentation	aldehyde dehydrogenase	VAEGDAEDVDRAVVAAR		Triticum aestivum	([54])
Glycolysis	glycolysis cytosolic branch UGPase	FASINVENVEDNRR		Triticum aestivum	([54])
	glycolysis cytosolic branch aldolase	VQLLEIAQVPDEHVNEFK		Triticum aestivum	([54])
H+ transporting pyrophosphatase	transport H+ transporting pyrophosphatase	AAVIGDTIGDPLK		Triticum aestivum	([54])
Hormone metabolism	lipoxygenase	GMAVPDSSSPYGVR	+(Al2O3-NP); -(Zn-NP, Ag-NP)	Glycine max	([30])
Mitochondrial electron transport / ATP synthesis	transport p- and v-ATPase	SGDVYIPR		Triticum aestivum	([54])
	ATP synthase delta chain	TALIDEIAK		Triticum aestivum	([54])
	ATP synthase beta subunit	IGLFGGAGVGK		Triticum aestivum	([54])
	ATP synthase F1-ATPase	TAIAIDTILNQK		Triticum aestivum	([54])
		SVHEPMQTGLK			
N-metabolism	glutamate dehydrogenase	TAVAAVPYGGAK	+(Al2O3-NP); -(Zn-NP, Ag-NP)	Glycine max	([30])
	glutamate synthase ferredoxin dependent	IGGLTLNELGR		Triticum aestivum	([54])
Photorespiratory pathway	aminotransferases peroxisomal	KALDYEELNENVK		Triticum aestivum	([54])
	photosystem II stability/assembly factor HCF136	AADNIPGNLYSVK	-(Ag-NP)	Triticum aestivum	([29])
		ADGGLWLLVR			
Photosynthesis / Calvin Cycle	calvin cycle aldolase	TVVSIPNGPSELAVK		Triticum aestivum	([54])
	calvin cycle FBPase	YIGSLVGDFHR		Triticum aestivum	([54])
	fructose-bisphosphate aldolase	VAPEVIAEYTVR	+(Ag-NP)	Triticum aestivum	([29])
		KPWNLSFSFGR			
	calvin cycle GAP	TLAEEVNQAFR		Triticum aestivum	([54])
Redox	dismutases and catalases	TWPEDVVPLQPVGR		Triticum aestivum	([54])
TCA / org transformation	malate dehydrogenase	EFAPSIPEK	+(Ag-NP)	Triticum aestivum	([29])
		IQNGGTEVVEAK			
	TCA aconitase	VAEFSFR		Triticum aestivum	([54])
Tetrapyrrole biosynthesis	tetrapyrrole synthesis prophobilinogen deaminase	TLGELPAGSVIGSASLRR		Triticum aestivum	([54])

Table S2. HPLC conditions and MS conditions for LC-MS/MS analysis method.

HPLC Conditions		
Column	Agilent Polaris 3 C18-Ether 150x3.0mm (p/n:A2021150X030)	
Mobile phase A	Water + 0.1% (v:v) formic acid +3% (v:v) DMSO	
Mobile phase B	Acetonitrile + 0.1% (v:v) formic acid +3% (v:v) DMSO	
Flow rate	0.40 mL/min	
Column temperature	25 °C	
Injection volume	2 μL	
Total run time	14 minutes	
Gradient	Time (min)	%B
	0.00	5
	10.00	70
	10.01	5
	14.00	5
MS Conditions		
Ionization mode	ESI Positive	
Gas temperature	340 °C	
Gas flow	12 L/min	
Nebulizer	40 psi	
Sheath gas temperature	250 °C	
Sheath gas flow	9 L/min	
Capillary voltage	Positive	Negative
	3,500 V	3,500 V
Nozzle voltage	Positive	Negative
	2,000 V	2,000 V

Table S3. Chromatography parameters of this study and previous plant proteomics studies

Column	Mobile Phase	Sample Solvent	Gradient	Reference
Agilent Polaris 3 C18-Ether 150 × 3.0mm column	A: 0.1% formic acid and 3% DMSO in water B: 0.1% formic acid and 3% DMSO in ACN	30% ACN with 5% formic acid and 3% DMSO in water	5-70% B	This study
Polaris Ether 3-lm C18 2 × 250 mm column	A: 0.1% aqueous TFA B: 90% ACN and 0.085% aqueous TFA	0.1% formic acid in water	0-50% B	([55])
in house made 75 μm × 40 cm, Reprosil-Gold C18, 3 μm resin, Dr. Maisch, Ammerbuch, Germany	A: 0.1% formic acid and 5% DMSO in water B: 0.1% formic acid and 5% DMSO in ACN	0.1% formic acid in water	4-32% B	([41])
in-house made 17 cm fused silica capillary column (100 μm ID) packed with 3 μm Reprosil-C18 reverse phase material	A: 0.1% formic acid in water B: 0.1% formic acid in 90% ACN	0.1% formic acid in water	0-34% B	([56])
Acclaim Pepmap C18 2 μm 100A, 75 μm i.d. × 15 cm length, Thermo-Fisher Scientific/Dionex	A: 0.1% formic acid in water B: 0.08% formic acid in 90% ACN	1% formic acid in water	4-70% B	([57])
C18 high-capacity nano LC chip	A: 0.1% formic acid in water B: 0.1% formic acid in ACN	2% ACN and 0.1% formic acid in water	2-100% B	([58])
cHiPLC nanoflex microfluidic C18 column 75 mm, 120 Å	A: 0.1% formic acid in water B: 0.1% formic acid in ACN	0.5% formic acid in water	2-90% B	([12])
Acclaim PepMap C18 2 μm 100A, 75 μm i.d. × 15 cm length, Thermo-Fisher Scientific/Dionex	A: 0.1% formic acid in water B: 0.08% formic acid in 90% ACN	1% formic acid in water	4-70% B	([10])
Polaris-HR-Chip-3 C18 column	A: 0.1% formic acid in water B: 0.1% formic acid in ACN	5% ACN and 0.1% formic acid in water	5-35% B	([54])
Agilent Zorbax Eclipse Plus C18 RRHD 2.1 × 150 mm, 1.8 μm pore size column	A: 0.1% formic acid in water B: 0.1% formic acid in 98% ACN	0.1% formic acid in water	3-97% B	([53])
YMC-Triart C18 column pore 12 nm, particle 3 μm, 150 mm length × 0.3 mm id column	A: 0.1% formic acid in water B: 0.1% formic acid in ACN	97% ACN and 0.1% formic acid in water	3-80% B	([59])
in-house made 75 μm I.D. × 400 mm, 1.9 μm beads C18 Reprosil-HD, Dr. Maisch	A: 0.1% formic acid in water B: 0.1% formic acid in 80% ACN	2% ACN and 0.1% formic acid in water	2-56% B	([60])
C18 reversed phase (3 uM, 100A pores, Dr. Maisch GmbH) column, packed in-house with 100uM ID and 18cm resin	A: 3%DMSO in water B: 3% DMSO in ACN	5% formic acid in water	N/A	([52])

Table S4. Peptide concentrations in plant tissues processed with 3 protein extraction and precipitation methods and 2 protein digestion methods.

Peptides (ng/g)	TCA/Acetone Method		Phenol Method		TCA/Acetone/Phenol Method	
	Trypsin digestion	LysC/Trypsin digestion	Trypsin digestion	LysC/Trypsin digestion	Trypsin digestion	LysC/Trypsin digestion
IQNGGTEVVEAK	1577.37	1444.96	1846.93	246.42	1512.87	270.10
SVHEPMQTGLK	0	989.08	1149.65	1620.80	953.50	1547.17
VAEGDAEDVDRAVVAAR	298.85	335.04	491.87	37.68	473.86	89.71
KALDYEELNENVK	1668.41	519.91	1070.43	518.47	1145.45	423.94
SGDVYIPR	449.93	533.46	808.05	163.63	819.90	178.36
GMAVPDSSSPYGVR	0	0	58.72	0	30.97	0
GNATVPAMEMTK	1823.71	1804.15	2048.48	950.98	2012.05	992.22
EFAPSIPEK	1035.12	1366.18	1082.65	1724.25	851.83	1559.58
FASINVENVEDNRR	3581.39	1646.80	3618.37	334.73	3481.21	357.26
FVIGGPHGDAGLTGR	1487.53	955.47	1956.70	62.06	1614.19	86.57
AADNIPGNLYSVK	734.36	607.10	1013.28	278.35	777.54	309.76
TVVSIPNGPSELAVK	9602.24	8000.96	11322.80	4038.47	10144.39	3598.23
TLGELPAGSVIGSASLRR	205.70	261.86	272.85	224.88	177.34	299.89
VAEFSFR	328.27	314.13	417.83	44.42	397.22	0
YIGSLVGDFHR	1146.68	1284.12	1595.43	314.13	1441.63	419.95
TALIDEIAK	3075.50	2599.95	3643.72	3860.42	3133.17	3267.69
VAPEVIAEYTVR	753.35	650.46	1163.97	474.75	1340.03	645.14
IGGLTLNELGR	560.63	336.28	775.57	0	783.65	0
TLAEEVNQAFR	5472.09	4238.38	5793.60	54.12	5195.69	89.67
IGLFGGAGVGK	5202.16	5522.34	7720.47	7338.16	7112.62	6580.29
VQLLEIAQVPDEHVNEFK	1202.93	1112.87	1175.23	93.47	1106.21	351.78
TAIAIDTILNQK	5475.48	5298.47	5015.57	3808.02	5779.68	3691.17
KPWNLSFSFGR	1711.02	1400.37	2380.61	2021.94	2570.85	2364.00
TWPEDVVPLQPVGR	1582.58	1376.84	1697.58	962.01	1430.35	1240.71
ADGGLWLLVR	789.33	664.27	1072.36	0	820.98	0
Total	**49764.61**	**43263.46**	**59192.73**	**29172.15**	**55107.17**	**28363.19**

Table S5. Peptide concentration of each peptide extracted from freeze-dried tissue and fresh tissue.

Peptides (ng/g)	Freeze-dried tissue	Fresh tissue
IQNGGTEVVEAK	1846.93	1047.84
SVHEPMQTGLK	1149.65	1340.42
TAVAAVPYGGAK	0.00	464.67
LVGVSEETTTGVK	0.00	1224.88
VAEGDAEDVDRAVVAAR	491.87	1596.60
KALDYEELNENVK	1070.43	741.79
SGDVYIPR	808.05	1102.14
GMAVPDSSSPYGVR	58.72	2239.22
GNATVPAMEMTK	2048.48	1082.04
EFAPSIPEK	1082.65	121.58
FASINVENVEDNRR	3618.37	4900.71
FVIGGPHGDAGLTGR	1956.70	2028.29
AADNIPGNLYSVK	1013.28	1404.18
TVVSIPNGPSELAVK	11322.80	438.37
TLGELPAGSVIGSASLRR	272.85	2424.43
VAEFSFR	417.83	1029.86
YIGSLVGDFHR	1595.43	10050.64
TALIDEIAK	3643.72	4036.61
VAPEVIAEYTVR	1163.97	1029.60
AAVIGDTIGDPLK	0.00	1755.72
IGGLTLNELGR	775.57	611.32
TLAEEVNQAFR	5793.60	9221.31
IGLFGGAGVGK	7720.47	5029.47
VQLLEIAQVPDEHVNEFK	1175.23	1861.52
TAIAIDTILNQK	5015.57	5273.86
KPWNLSFSFGR	2380.61	4039.33
TWPEDVVPLQPVGR	1697.58	1330.47
ADGGLWLLVR	1072.36	1404.00
Total	**59192.73**	**68830.85**

III. Assessing the Impacts of Cu and Mo Engineered Nanomaterials on Crop Plant Growth Using a Targeted Proteomics Approach

Material from:

Li, W.; Keller, A. A. Assessing the Impacts of Cu and Mo Engineered Nanomaterials on Crop Plant Growth Using a Targeted Proteomics Approach. ACS Agric. Sci. Technol. 2024, 4 (1), 103–117.

Abstract In this study, we investigated the effects of molybdenum (Mo) based nano-fertilizer and copper (Cu) based nano-pesticide exposure on wheat through a multi-faceted approach, including physiological measurements, metal uptake and translocation analysis, and targeted proteomics analysis. Wheat plants were grown under a 16 h photoperiod (light intensity 150 $\mu mol \cdot m^{-2} \cdot s^{-1}$) for 4 weeks at 22 °C and 60% humidity with 6 different treatments, including control, Mo and Cu exposure through root and leaf. The exposure dose was at 6.25 mg of element per plant through either root or leaf. An additional low dose (0.6 mg Mo/plant) treatment of Mo through root was added after phytotoxicity was observed. Using targeted proteomics approach, 24 proteins involved in 12 metabolomic pathways were quantitated to understand the regulation at the protein level. Mo exposure, particularly through root uptake, induced significant upregulation of 16 proteins associated with 11 metabolic pathways, with the fold change (FC) ranging from 1.28 to 2.81. Notably, a dose-dependent response of Mo exposure through the roots highlighted the delicate balance between nutrient stimulation and toxicity, as the high Mo dose led to robust protein upregulation but also resulted in depressed physiological measurements, while low Mo dose resulted in no depression of physiological

measurements but downregulations of proteins, especially in the first leaf ($0.23 < FC < 0.68$) and stem ($0.13 < FC < 0.68$) tissues. Conversely, Cu exposure exhibited tissue-specific effects, with pronounced downregulation (18 proteins involved in 11 metabolic pathways) particularly in the first leaf tissues (root exposure: $0.35 < FC < 0.74$; leaf exposure: $0.49 < FC < 0.72$), which indicated the quick response of plants to Cu induced stress in the early stage of exposure. By revealing the complexities of plants' response to ENMs at both physiological and molecular levels, this study provides insights for optimizing nutrient management practices in crop production and advance towards sustainable agriculture.

A. Introduction

Engineered nanomaterials (ENMs) have gained attention in the field of agriculture, particularly as nano-pesticides and nano-fertilizers, with the aim of enhancing agricultural productivity and sustainability,[13,14] to address the challenges of feeding a growing global population in the face of climate change. By minimizing the quantity of pesticides needed and providing more controlled release mechanisms, nano-pesticides can offer more targeted and efficient delivery of active ingredients, promoting a more environmentally friendly and sustainable agriculture[15]. Similarly, nano-fertilizers are designed to enhance nutrient availability to plants with their controlled release mechanisms to ensure that nutrients are available when needed and make agriculture more sustainable[16]. However, the physicochemical properties of ENMs, such as small particle size and high surface area may increase their toxicity potential.[15,16] Thus, understanding how ENMs interact with plants is essential to ensure both enhanced productivity and minimal negative impacts on the environment and human health.

Omics technologies have revolutionized our ability to understand and analyze the complex molecular responses of plants to various environmental stressors, including ENMs.[61,25] The omics approaches employed in plant stress mechanism responses research include genomics (gene level), transcriptomics (mRNA level), proteomics (protein level) and metabolomics (metabolite level).[18] These approaches allow researchers to delve into different molecular layers to understand how plants react to stressors. Several studies have adopted non-targeted proteomics to investigate plant responses after exposure to nanoparticles (NP) such as Ag-NP[29,30], Al_2O_3-NP and Zn-NP[30]. Responsive protein levels perturbed due to exposure of ENMs are involved in biological pathways such as oxidative stress tolerance, electron transfer and signaling, transcription and protein degradation, nitrogen metabolism, oxidative stress regulation, photosynthesis, and protein biosynthesis and turnover.[29,30,28,31,32] Although non-targeted proteomics is a useful tool to discover disturbed protein pathways, it has limited accuracy and reproducibility due to the characteristics of the full spectrum scan.[62] Targeted proteomics can add a layer of depth by directly analyzing changes in expression of specific proteins, with accuracy and reproducibility since it uses selected reaction monitoring (SRM) and focuses on a defined set of proteins or peptides.[5,12,17] However, the absence of targeted proteomics studies on plant responses to ENMs represents a notable gap in current knowledge. In addition, by employing advanced analytical techniques, researchers can move beyond static snapshots and delve deeper into the temporal aspects of molecular responses. This refined approach can enhance our understanding of complex biological processes, providing insights into the kinetics, dynamics, and adaptability of organisms in response to changing environmental or experimental conditions.

For this study, we considered wheat (*Triticum aestivum*), a crop of global importance, and the effect of two types of ENMs, Cu and Mo based. We selected 24 proteins based on previous studies that reported them to be more likely perturbed by the exposure to ENMs, and their signature peptides were selected based on a public wheat proteome database, as detailed in our previous study (Table 1 and see also Chapter II).[63] These targeted proteins are involved in several key metabolomic pathways, such as photosynthesis related pathways (e.g., photorespiratory pathway and Calvin cycle), and respiration related pathways (e.g., glycolysis, TCA cycle, and mitochondrial electron transport). Previous work reported a significant increase in the expression of the light-harvesting complex II (LHCII) b gene in *Arabidopsis thaliana* when exposed to titanium dioxide nanoparticles (TiO_2-NPs).[64] Another study observed that zinc oxide nanoparticles (ZnO-NPs) improved antioxidant capacity and enhanced photosynthetic efficiency in tomato plants.[65] This improvement in antioxidant mechanisms and photosynthesis could contribute to better plant growth and stress tolerance. In addition, nitrogen cycle related pathways, such as nitrogen metabolism and amino acid metabolism, were reported to promote productivity of cucumber due to the 51% more nitrogen accumulation from the application of TiO2-NPs[66]. Another study indicated that the application of iron (Fe), cobalt (Co), and copper (Cu) nanoparticles resulted in increased nitrogen accumulation and up to a 16% increase in crop yield in soybean plants.[67] Moreover, tolerance related pathways such as oxidative stress regulation were reported to strength abiotic stress resistance caused by ENMs in crop plants.[68]

Cu based nano-pesticide ($Cu(OH)_2$-NMs) and Mo based nano-fertilizer (MoO_3-NMs) were selected as ENMs treatments to wheat plants. To determine a realistic yet impactful experimental does, recommended field application doses, previous studies, and the potential

for eliciting significant plant responses were considered. According to the fertilizer institute (tfi.org), the recommendation for field application of Cu and Mo is 3 to 16 kg/hectare and 0.6 to 2 kg/hectare respectively, which is 0.8-5 mg Cu/plant and 0.2-0.6 mg Mo/plant based on the wheat population of 3.2 to 3.7 million plants/hectare. The application dose will also support the nutritional requirements of Cu (5 ppm)[69] and Mo (0.1 ppm)[70], which are essential micronutrients for plants. Previous ENM related metabolomics studies revealed significant alterations of metabolites at 12 mg Cu/plant exposure dose for spinach[71], 6.7 mg Cu/plant exposure dose for cucumber[72], 6 mg Cu/plant exposure dose for soybean[73] and 8 mg Mo/plant exposure dose for corn and wheat (no significance with a lower dose of 1.6 mg Mo/plant for wheat)[35]. Considering both recommended field application doses and previous studies, we initially chose 6.25 mg element/plant for both Cu and Mo. Then, the recommended dose for field application of Mo (0.6 mg Mo/plant) was added to the experiment. Two different exposure techniques were studied, including root exposure and leaf exposure. For each exposure approach, 3 treatment groups were considered, including control group, Cu exposure group and Mo exposure group.

This study aims to address this gap by pioneering the application of targeted proteomics for investigating plant response to these micronutrients in nanoscale form, to provide focused and precise insights into the specific proteins and pathways impacted. The study will also shed light on the potential applications and risks associated with utilizing these nanomaterials in agriculture, offering valuable insights for optimizing nutrient supplementation strategies and minimizing adverse effects on plant growth.

Table 1. List of selected 24 targeted proteins with related pathways and signature tryptic peptides.

Pathway ID	Pathway	Protein ID	Accession Number	Protein	Signature Peptide
A	Amino acid metabolism	P1	AT3G23810	AA degradation methionine	LVGVSEETTTGVK
		P2	AT5G17920	AA synthesis methionine	GNATVPAMEMTK
		P3	AT1G02500	S-adenosylmethionine synthase	FVIGGPHGDAGLTGR
B	Fermentation	P4	AT1G23800	aldehyde dehydrogenase	VAEGDAEDVDRAVVAAR
C	Glycolysis	P5	AT2G36460	glycolysis cytosolic branch UGPase	FASINVENVEDNRR
		P6	AT5G17310	glycolysis cytosolic branch aldolase	VQLLEIAQVPDEHVNEFK
D	H+ transporting pyrophosphatase	P7	AT1G15690	transport H+ transporting pyrophosphatase	AAVIGDTIGDPLK
E	Hormone metabolism	P8	AT1G55020	lipoxygenase	GMAVPDSSSPYGVR
F	Mitochondrial electron transport / ATP synthesis	P9	AT4G09650	ATP synthase delta chain	TALIDEIAK
		P10	AT5G08670	ATP synthase beta subunit	IGLFGGAGVGK
		P11	AT2G07698	ATP synthase F1-ATPase	TAIAIDTILNQK
		P12	AT1G78900	transport p- and v-ATPase	SGDVYIPR
G	Nitrogen-metabolism	P13	AT5G07440	glutamate dehydrogenase	TAVAAVPYGGAK
		P14	AT5G04140	glutamate synthase ferredoxin dependent	IGGLTLNELGR
H	Photorespiratory pathway	P15	AT1G70580	aminotransferases peroxisomal	KALDYEELNENVK
		P16	AT5G23120	photosystem II stability/assembly factor HCF136	AADNIPGNLYSVK
I	Photosynthesis / Calvin Cycle	P17	AT2G21330	calvin cycle aldolase	TVVSIPNGPSELAVK
		P18	AT3G54050	calvin cycle FBPase	YIGSLVGDFHR
		P19	AT2G36460	fructose-bisphosphate aldolase	VAPEVIAEYTVR
		P20	AT3G26650	calvin cycle GAP	TLAEEVNQAFR
J	Redox	P21	AT1G20620	catalase	TWPEDVVPLQPVGR
K	TCA / org transformation	P22	AT5G43330	malate dehydrogenase	EFAPSIPEK
		P23	AT4G35830	TCA aconitase	VAEFSFR
L	Tetrapyrrole biosynthesis	P24	AT5G08280	tetrapyrrole synthesis prophobilinogen deaminase	TLGELPAGSVIGSASLRR

B. Materials and Methods

1. Materials

$Cu(OH)_2$-NMs (99.5% purity, US3078) and MoO_3-NMs (99.94% purity, US3330) were purchased from U.S. Research Nanomaterials Inc. (Houston, TX, USA). *Triticum aestivum*

(wheat) seeds were purchased from Harmony Farms KS (Jennings, KS, USA). Reagents used during sample processing, such as sodium hypochlorite solution, Triton X-100, dithiothreitol (DTT), iodoacetamide (IAA), trypsin protease, trifluoroethanol (TFE), protease inhibitors cocktail, formic acid, ammonium acetate, trichloroacetic acid (TCA), dimethyl sulfoxide (DMSO), 0.5M pH 8.0 ethylenediaminetetra-acetic acid (EDTA), sucrose, HPLC grade water, methanol, acetone, and Isopropyl alcohol (IPA) were purchased from Sigma Aldrich (St. Louis, MO, USA). Urea, ammonium bicarbonate and acetonitrile (ACN) were obtained from Spectrum Chemicals (New Brunswick, NJ, USA). Other reagents including Tris-buffered phenol solution, 1.5 M pH 8.8 Tris-HCl solution, LysC/trypsin protease mix, phenylmethanesulfonyl fluoride (PMSF), 2-mercaptoethanol (2-ME), sodium n-dodecyl sulfate (SDS), and materials such as 5 mL and 15 mL Eppendorf centrifuge tube were purchased from Fisher Scientific (Waltham, MA, USA). C-18 cartridges (Waters Sep-Pak C18 1 cc, 50 mg sorbent) were purchased from Waters Corporation (Milford, MA, USA). The analytical standards of the 24 selected peptides (Table 1) and 4 isotopic labeled peptide standards to use as internal standard, including SVHEPMQTGLK{Lys($^{13}C_6$,$^{15}N_2$)}, SGDVYIPR{Arg($^{13}C_6$,$^{15}N_4$)}, TALIDEIAK{Lys($^{13}C_6$,$^{15}N_2$)} and KPWNLSFSFGR{Arg($^{13}C_6$,$^{15}N_4$)} were purchased from GenScript (Piscataway NJ, USA). These standards were synthesized as ordered in white lyophilized powder phase with ≥95% HPLC purity.

2. Wheat growth and exposure conditions

Wheat seeds were planted in 6 groups according to treatments and exposure methods (Figure 1A), including root exposure control, Cu exposure through root, Mo exposure through root, leaf exposure control, Cu exposure through leaf, and Mo exposure through leaf.

First, all wheat seeds were sterilized in 1% sodium hypochlorite solution for 10 min and then rinsed for 5 times with NANOpure water, followed by soaking in NANOpure water overnight for germination. Then germinated seeds were planted into vermiculite saturated with 10% Hoagland solution with 4 seeds per pot following the same procedure as in previous studies.[63] Plants were grown under a 16 h photoperiod (light intensity 150 $\mu mol \cdot m^{-2} \cdot s^{-1}$) for 4 weeks at 22 °C and 60% humidity, and watered with 20 mL of diluted 10% Hoagland solution daily to maintain a 70%-90% water content and provide sufficient nutrients for plant growth.[63,35]

For root exposure groups, ENM suspensions were prepared in 10% Hoagland solution at 1250 mg Cu or Mo element per liter. On day 7, in contrast to watering with 20 mL of 10% Hoagland water for root exposure control group, Cu and Mo exposure groups were watered with 20 mL ENMs suspensions. At the 4 seedling locations, 5 mL of the ENM suspensions were applied to the pots with a 5 mL pipette to ensure evenly exposure, for a total of 20 mL/pot. The total amount of ENMs exposure is 25 mg Cu or Mo per pot, which is 6.25 mg element per plant. For leaf exposure groups, surfactant (Triton X-100, BioXtra, p/n: T9284) was employed to improve wettability of leaf surfaces and prevent off-target drift.[74] ENM suspensions were prepared with 500 mg of Cu or Mo element per liter in surfactant solution (0.2% Triton X-100 in NANOpure water). From day 22 to day 28, plant leaves were soaked 3 times per day into 50 mL centrifuge tube with freshly prepared ENM suspensions for exposure groups, or into surfactant solution for leaf control group (Figure 1 B). The amount of applied ENMs suspensions was calculated considering the weight of solutions measured before and after leaf soaking and the concentration of solution. On average, the daily exposure volume for both Cu and Mo suspensions was around 7 mL. After 7 days of leaf

exposure, the total amount of ENMs exposure was 25 mg Cu or Mo per pot, which is 6.25 mg element per plant as well. For both exposure approaches, at least 40 plant replicates (in 10 pots, 4 plants per pot) were grown for each treatment.

After the initial studies with 6.25 mg Mo/plant, it became clear that the excessive concentration of Mo had a negative physiological effect, particularly when exposed to Mo ENMs via roots. To further study the dose effect to Mo exposure through the roots, a lower concentration of 0.6 mg Mo/plant via the roots, which is the recommended dose for field application of Mo, was added to the experiment.

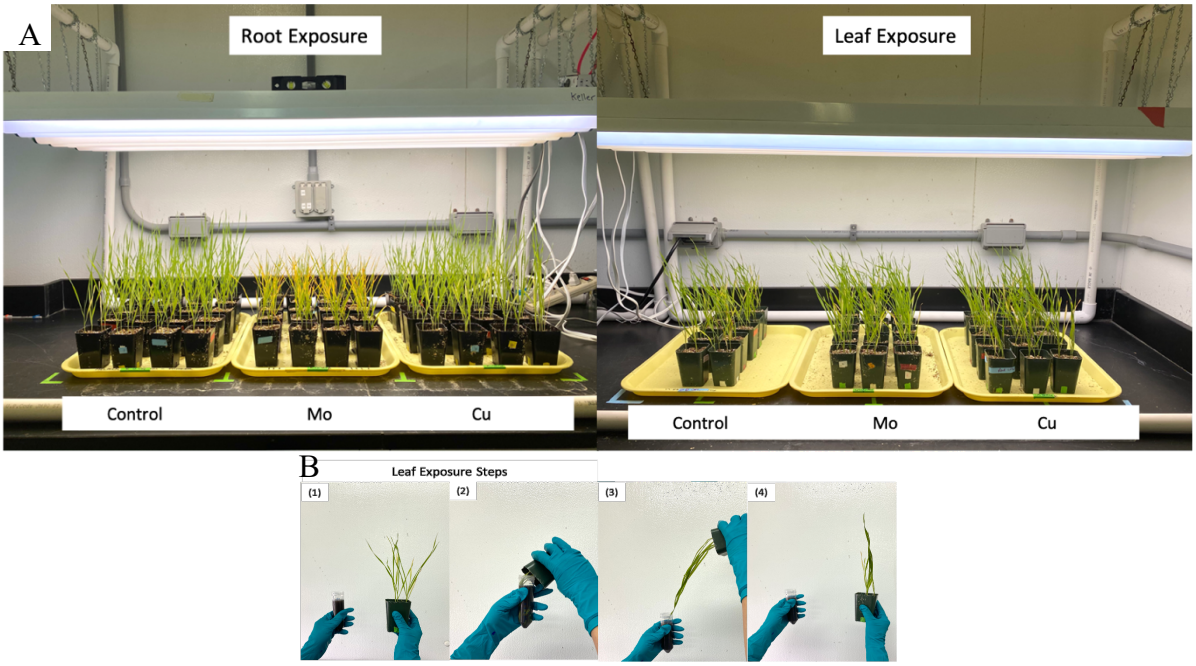

Figure 1. Wheat plant growth and exposure. A) Images of plant growth with two different exposure techniques (root exposure and leaf exposure) and 3 treatment groups (control group, Mo exposure group (6.25 mg Mo/plant) and Cu exposure group (6.25 mg Cu/plant)); B) Leaf exposure steps: 1) prepare ENMs suspensions in 50 mL centrifuge tube; 2) insert all leaves into tube, swirling the leaves gently and soaking the leaves in solution for 10 seconds; 3) remove leaves and let them dry for 10 seconds; 4) bring plant upright and let it dry for 15 mins, then repeat steps 2-4 for another 2 times for a total of 3 daily exposures.

3. Wheat harvesting, physiological measurements and tissue homogenization

After 28 days, plants were harvested and grouped into the 6 treatments followed by rinsing with NANOpure water. Physiological measurements, including leaf color, biomass and length of the shoot (tissues above the soil) and root parts were recorded for each group. Three leaves emerged from each plant during the 4-week growth period. The harvested leaves were labeled as leaf #1 (L1), leaf #2 (L2), and leaf #3 (L3) with L1 being the first leaf to emerge and L3 the third leaf to emerge. To calculate biomass distribution, the biomass was also measured for L1, L2, L3, stem and root parts separately after cutting plants into these five parts. After measurements, each of the 5 tissues from each treatment group were pooled and ground using mortar and pestle with liquid nitrogen added for homogenization. The homogenized plant tissues (5 tissues × 6 treatment groups = 30 tissue samples) were stored in 50 mL centrifuge tubes at -80°C until analyzed.

4. Metal uptake and translocation analysis

In a previous study we determined the dissolution rate of Cu and Mo based ENMs.[75] The dissolution of Cu ENMs was relatively slow in both DI water and root exudate solution, around 1% after 6 days, and a rate of 0.001% per hour. In contrast, Mo ENMs dissolve relatively fast when placed in either DI or root exudate solution, releasing around 31-35% of Mo ions within the first 6 hours, and 0.026% to 0.047% per hour thereafter. Thus, wheat plants exposed via roots to Mo ENMs will also be exposed to a substantial amount of Mo^{6+}, and even those exposed via the leaves would be exposed to released Mo ions. In contrast, plants exposed to Cu ENMs would be exposed to low concentrations of Cu^{2+}, in either exposure path.

To reveal the effect on metal element accumulation and distribution caused by ENMs exposure during growth, the concentration of elements including Cu, Mo and other nutrient elements such as K, Mg, Ca, P, Mn, Fe and Zn in plant tissues were quantified via ICP-MS analysis (Agilent 7900, Agilent Technologies). A 100 mg of homogenized plant sample was weighed into a 50 mL digestion tube and mixed with 2 mL of PlasmaPure HNO_3 (trace metals equal to or less than 1 ppb). Then tubes were covered with watch glasses and placed into a hot block digestion system (DigiPREP MS, SCP Science) to heat for 20 mins at 115 °C, followed by an addition of 8 mL of H_2O_2 to continue to heat for 60 mins at 115 °C. The digested solution was diluted to a total volume of 50 mL with NANOpure water. Finally, 4 mL of diluted digests were transferred into 15 mL metal free centrifuge tube and mixed with 4 mL of NANOpure water for the final dilution to ensure < 2% acid content for ICP-MS analysis. Six points of calibration standards ranging from 1 ppb to 1000 ppb were prepared for each analyzed element for quantification. For QA/QC purpose, a mid-level of calibration standards followed by a solvent blank were injected after every 6 sample injections and the recovery for QC injections were all within 80% to 120%. The ICP-MS results were adjusted by the dilution factors.

5. Protein extraction and targeted proteomics analysis

To measure the concentration of selected proteins, plant tissues were processed through protein extraction and precipitation, proteolytic digestion, and peptide purification before analysis using an Agilent 6470 triple quadrupole mass spectrometer coupled with an Agilent InfinityLab 1290 Infinity II Series liquid chromatography system.[63] Three replicates were prepared for each sample. Firstly, samples were processed using the optimized phenol extraction method from our previous study.[63] Generally, 200 mg of plant tissue sample was

extracted using a phenol extraction buffer then partitioned with phenol solution (Tris-buffered). Then, ice-cold 0.1 M ammonium acetate in methanol was mixed with phenol extracts and stored overnight at -20 °C for protein precipitation. The protein pellet was washed with 0.1 M ammonium acetate in methanol followed by 80% (v:v) acetone in DI water to remove phenol, methanol and ammonium acetate, followed by solubilization with 8 M urea, 50 mM ammonium bicarbonate solution. Then protein in solution was reduced and alkylated with 5 mM DTT and 20 mM IAA followed by peptide digestion with 2 μg of trypsin enzyme overnight at 37 °C with rotation. Finally, the digested peptides were purified via solid-phase extraction (SPE) with C-18 cartridge (Waters Sep-Pak C18 1 cc, 50 mg sorbent). Samples were reconstituted to 30% ACN in water with 5% formic acid and 3% DMSO for LC-MS/MS analysis.

An Agilent Polaris 3 C18-Ether column (150x3.0mm, p/n: A2021150X030) coupled with a gradient mobile phase (A: Water + 0.1% (v:v) formic acid + 3% (v:v) DMSO; B: ACN + 0.1% (v:v) formic acid + 3% (v:v) DMSO) was used to analyze peptides in the processed samples.[63] The HPLC conditions and MS conditions are detailed in the Supporting Information (SI, Table S1). The total run time for each sample was 14 min, and a needle wash with TFE was done between injections to reduce carryover. The transitions and limit of detection (LOD) for each peptide can be found in Table S2. Eight levels of calibration standards ranging from 1 ng/mL to 100 ng/mL with 50 ng/mL of internal standards were prepared for quantitation.[63] For QA/QC purpose, a mid-level of calibration standards followed by a solvent blank were injected after every 6 sample injections and the recovery for QC injections were all within 80% to 120%.

6. Statistical analysis

Box-and-whisker plots coupled with one way Analysis of Variance (ANOVA) followed by t-test were used to compare physiology measurements across different treatment groups with a significant threshold (p-value) at 0.05. Heatmaps were used to visually represent the patterns of metal uptake and transport for Cu, Mo and other nutrient elements. A heatmap of protein abundance across different treatments also helped to identify clusters of proteins with similar expression profiles and highlight differences or trends between experimental groups. Partial Least Squares - Discriminant Analysis (PLS-DA) was conducted to visualize the separation between different treatment groups.[76] Volcano plots were used to depict fold changes versus statistical significance (negative logarithm of p-values), which helped to highlight proteins with significant changes in expression. Then fold change bar plots were generated to prioritize proteins that exhibit substantial changes with a magnitude bigger than 1.25-fold or smaller than 0.75-fold. In addition, Venn diagrams were used to visualize the overlaps and differences between different treatment groups and help to identify common or unique proteins that are significantly affected by ENMs.

C. Results and discussions

1. Physiology measurements

Plants were grouped into 6 treatments after harvest and washing (Figure 2A). Among all 6 groups, the Mo exposure through root group (Root-Mo) was particularly distinct in its response to the ENMs. The Root-Mo group exhibited smaller plant mass and especially less root mass compared to all other groups (Figure 2B), which suggests that the Mo exposure through roots has a substantial impact on plant growth and development. In addition, the Root-Mo group produced the most yellow leaves while the root exposure control group (Root-Control) produced the least yellow leaves (Figure 2C). The leaf color changes

indicated the changes in photosynthetic efficiency and overall plant health. Additionally, the control of leaf exposure group (Leaf-Control) produced more yellow leaves than Root-control, likely due to the usage of Triton X-100 as the surfactant for the leave treatments, which suggests the potential interactions between surfactants and plant physiology.[74]

Box-and-whisker plots coupled with one way ANOVA followed by t-tests were employed to compare the length and biomass of shoot or root tissues among the 6 treatment groups (Figure 3). The ANOVA tests with p-values smaller than 0.05 for all comparisons (shoot length: p=2.57E-63; root length: p=4.10E-3; shoot biomass: p=3.47E-32; root biomass: p=2.39E-32) determined the statistically significant differences between these multiple treatment groups. To identify and understand the magnitude of the observed difference, t-tests were made within the same exposure technique (control vs. Cu exposure, control vs. Mo exposure, and Cu exposure vs. Mo exposure for root exposure and leaf exposure respectively) and between different exposure techniques (root exposure-control vs. leaf exposure-control, root exposure-Cu vs. leaf exposure-Cu, and root exposure-Mo vs. leaf exposure-Mo). Within the root exposure technique, Mo exposure group was significantly different from the control and Cu exposure groups for all physiology measurements. These statistically significant differences indicated that root exposure to Mo ENMs has a distinct effect on the physiological response. However, exposure to Mo ENMs via the leaves did not have a significant effect compared to the control, indicating that there is very significant difference depending on the exposure route. The absence of significance might be due to various factors, such as differing absorption rates or sensitivity of tissues to Mo ENMs and Mo ions between roots and leaves.

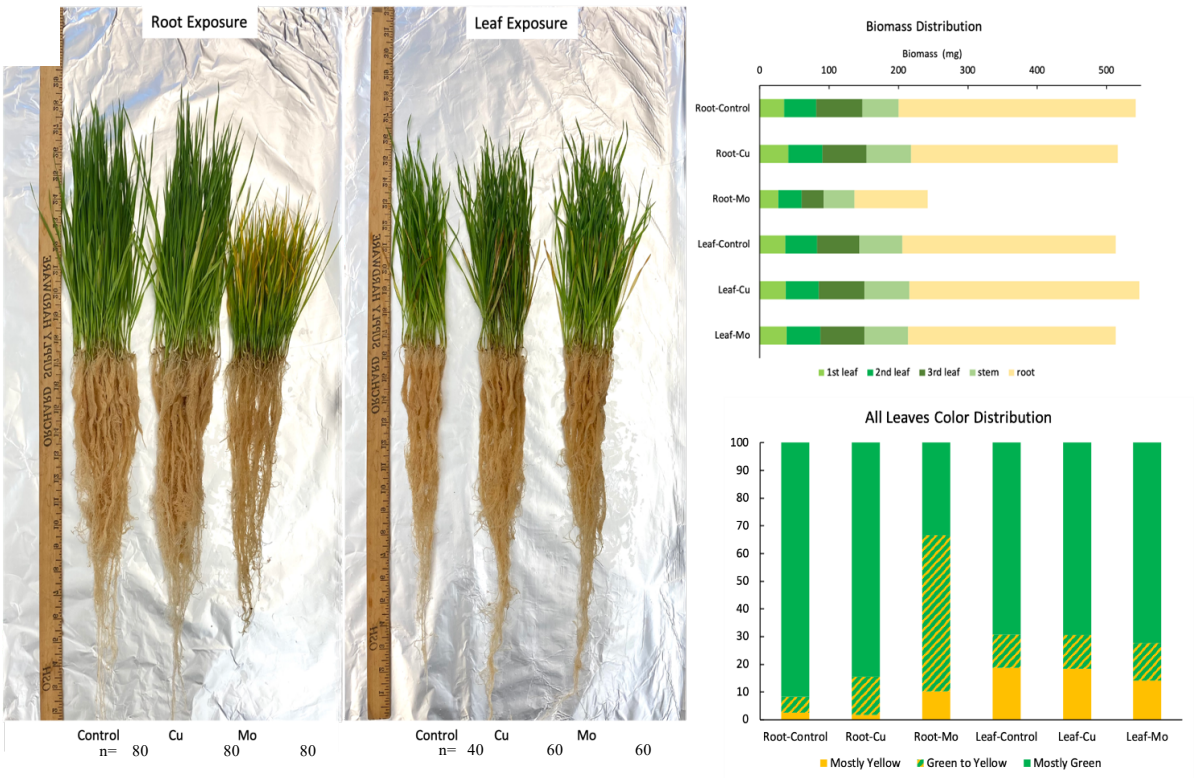

Figure 2. Wheat plant harvest. A) Plants after harvest and wash (From left to right: root exposure control, Cu exposure through root (6.25 mg Cu/plant), Mo exposure through root (6.25 mg Mo/plant), leaf exposure control, Cu exposure through leaf (6.25 mg Cu/plant), and Mo exposure through leaf (6.25 mg Mo/plant)); B) Biomass distribution of 6 groups; C) Leaves color distribution of 6 groups.

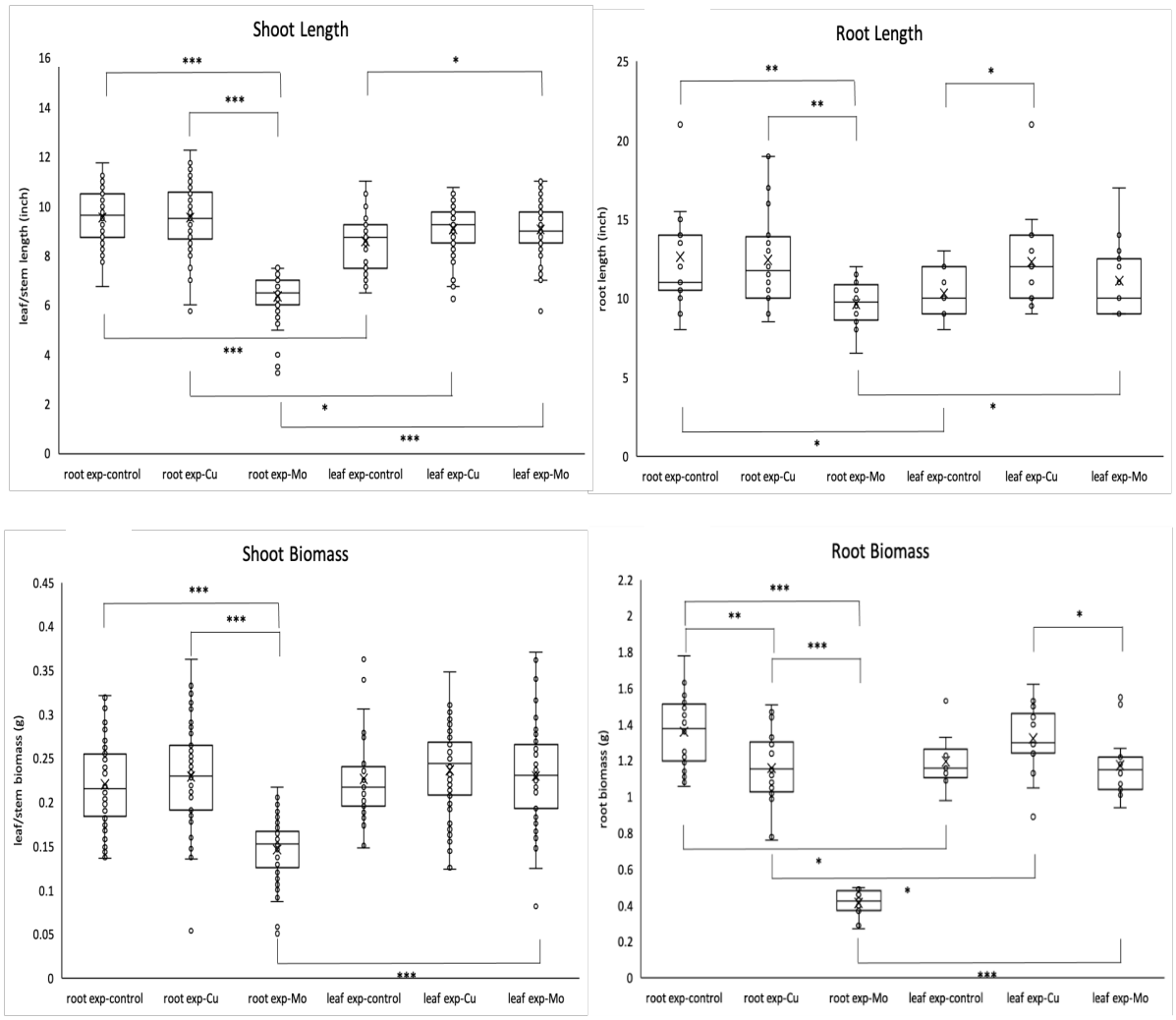

Figure 3. The box-and-whisker plot of a) shoot length, b) root length, c) shoot biomass and d) root biomass of 6 treatment groups. T-test results indicated as *: $p \leq 0.05$; **: $p \leq 0.01$; ***: $p \leq 0.001$.

2. Metal accumulation and distribution

The heatmap analysis (Figure 4 a, b) presented the concentrations of Cu, Mo, and other nutrient elements in different tissues and exposure scenarios, and highlighted some interesting findings regarding the distribution of these elements across different tissues and exposure techniques, as well as their potential interactions with other nutrient elements. First, Mo concentration increased significantly with root exposure to Mo-NP, with the highest Mo

concentration in leaf 1 (L1) (1823.97 ± 48.45 μg/g), followed by L2 (1178.93 ± 5.05 μg/g), L3 (779.74 ± 2.84 μg/g), stem (S) (757.81 ± 42.84 μg/g), and root (R) (386.53 ± 28.88 μg/g). Leaf exposure to Mo-NP also caused increased Mo concentration (e.g., 89.88 ± 16.05 μg/g in L1), but the effect was less pronounced compared to root exposure. It is not surprising since soil application is recommended in agriculture due to the low solubility of molybdenum trioxide (MoO_3).[77] On the contrary, Cu concentration increased significantly with leaf exposure to Cu-NP, with the highest concentration observed in L2 (740.04 ± 23.31 μg/g), followed by L1 (688.92 ± 5.29 μg/g), L3 (493.24 ± 1.77 μg/g), S (89.05 ± 0.42 μg/g), and R (12.24 ± 0.16 μg/g). Meanwhile, the root exposure to Cu-NP only slightly increased Cu concentration in the root tissues (28.87 ± 0.03 μg/g). These findings illuminate the differential uptake strategies and translocation dynamics of Mo and Cu within the plant. Mo exhibits a strong root-to-leaf translocation, indicating a clear pathway from root uptake to subsequent transport in the leaves. Cu, on the other hand, demonstrates a distinct preference for leaf uptake, with less emphasis on accumulation in the roots or translocation. This aligns to a previous studies which observed higher efficiency of Cu uptake through foliar spray rather than via soil irrigation.[78,79] This distinction highlights the nuanced strategies plants employ in assimilating different elements.

Moreover, correlation analysis (Figure 4c) reveals different relationships between Cu and Mo with other nutrient elements. For example, there is a strong positive correlation between Mo and Mg concentrations, which suggests that there might be shared uptake or transport mechanisms for these two elements. The strong negative correlation between Mo and Mn concentrations suggests that there might be competitive interaction between these two elements. On the contrary, the weaker correlation between Cu and Mg concentrations, as well

as the strong positive correlation between Cu and Mn concentrations, indicates that the relationships between Cu and these elements are distinct from those of Mo. In addition, Na and Fe also show opposite correlations with Mo or Cu concentrations. This suggests that Cu might have different uptake dynamics and interactions compared to Mo, which aligns to the observed negative correlation between Mo and Cu (Figure 4C). The antagonistic effects between Cu and Mo uptake have been observed in several plant species, including berseem (Egyptian clover)[80] and wheat[81]. The antagonistic effects of Cu with Mo can also explain the leaf yellowing observed in Mo treatment through root (Figure 2C), since the decreased availability of copper due to excess molybdenum uptake could disrupt chlorophyll formation and impair photosynthetic activity due to the importance of Cu as cofactor of various enzymes in chlorophyll.[82,83] The correlations observed in our study provide insights into potential elemental interactions and complex nutrient uptake dynamics and transport mechanisms within the wheat plant.

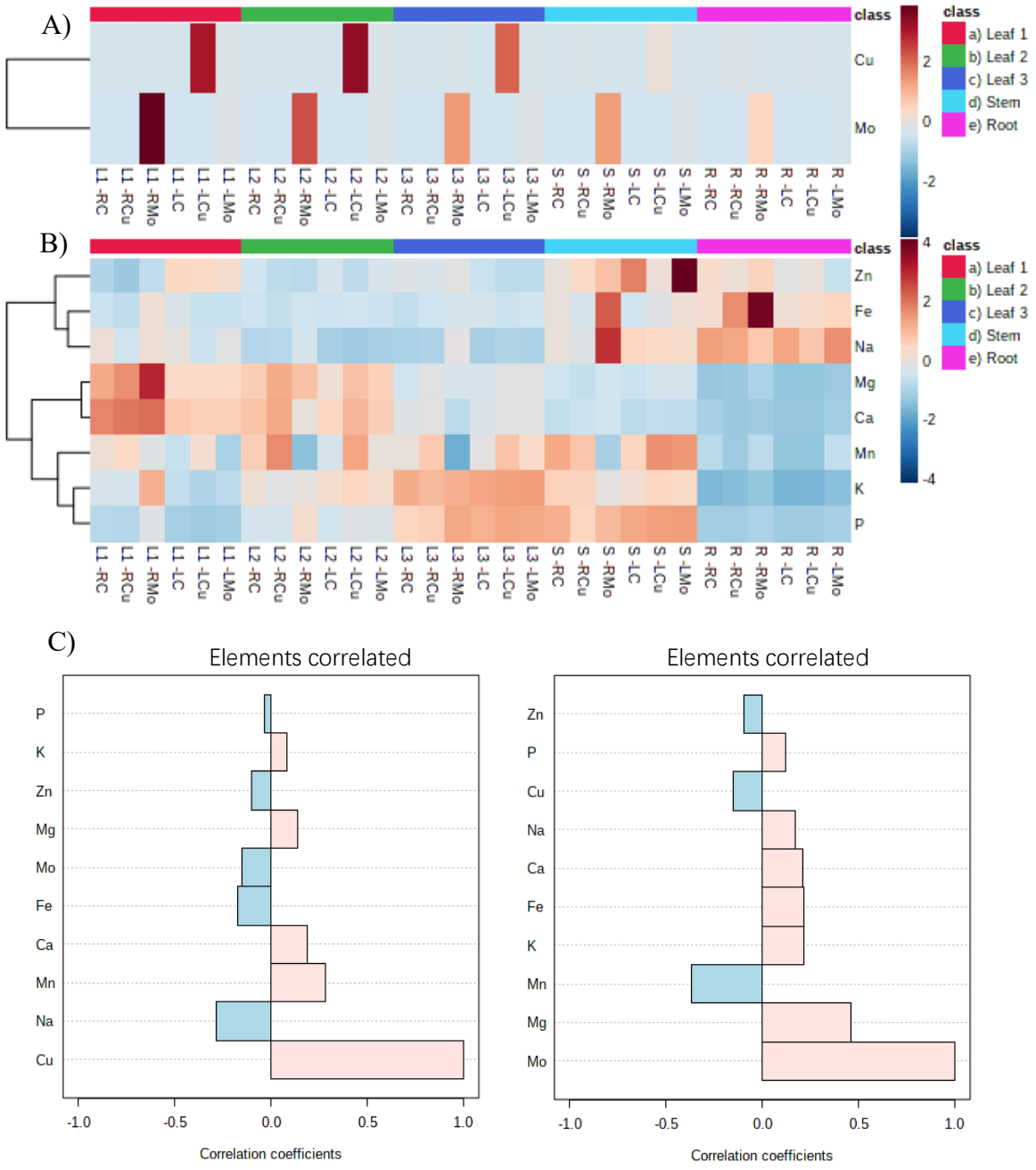

Figure 4. Heatmap of metal concentration in plant tissues. A) Cu and Mo concentration in plant tissues; B) Nutrient element concentration in plant tissues. C) Correlation analysis between Cu and Mo and other nutrient elements. RC: root exposure control; RCu: Cu exposure through root; RMo: Mo exposure through root; LC: leaf exposure control; LCu: Cu exposure through leaf; LMo: Mo exposure through leaf. Element concentration data in Table S3.

3. Targeted proteomics analysis

The heatmap of protein concentrations provided interesting trends of the distribution and clustering patterns of proteins across different tissues and exposure techniques (Figure 5). The first ten proteins in the cluster #1 exhibit a pattern where L3 has the highest protein concentrations, followed by L2, L1, stem and roots. Conversely, the 11 proteins in clusters #2 and #3 show a pattern where stem has the highest concentrations, followed by L3 (very similar as in stem for cluster #3), L2, L1 and roots. The three proteins in cluster #4 have the highest concentrations in L2, closely followed by L3, then S, L1 and roots. Overall, roots and L1 had the lowest protein concentrations, and L3 and S had the highest ones. This suggests tissue-specific distribution patterns for these proteins, indicating that different tissues might have varying protein expression profiles, even among leaves. These observations align with the expected metabolic demands and functional distribution of proteins in different plant tissues. For example, the presence of proteins associated with the Calvin cycle and photosynthesis (e.g., calvin cycle GAP, calvin cycle FBPase and calvin cycle aldolase) in cluster #1 is consistent with the higher metabolic activity of these pathways in leaves, which are the most important photosynthetic tissues. In addition, the presence of proteins related to the photorespiratory pathway (e.g., aminotransferases peroxisomal and photosystem II stability/assembly factor HCF136) in cluster #1 further emphasizes the active engagement of leaves in these processes. Moreover, since mitochondrial electron transport and ATP synthesis play a crucial role in synthesizing ATP, which supports the energetic demands of photosynthetic tissues and plant growth,[84] it's logical to find the related proteins in high concentrations in leaves (e.g., ATP synthase beta subunit and ATP synthase delta chain). However, ATP synthase F1-ATPase (cluster #3) and transport p- and v-ATPase (cluster #4),

which are also involved in ATP synthesis pathway, showed high concentration in stem other than leaves. Similar distinction was found for proteins related to amino acid metabolism and N-metabolism, with proteins separately grouped in cluster #1 and cluster #2. This finding suggests that while proteins within the same pathway might have related functions, their expression patterns in different tissues could be influenced by factors beyond their pathway interactions.

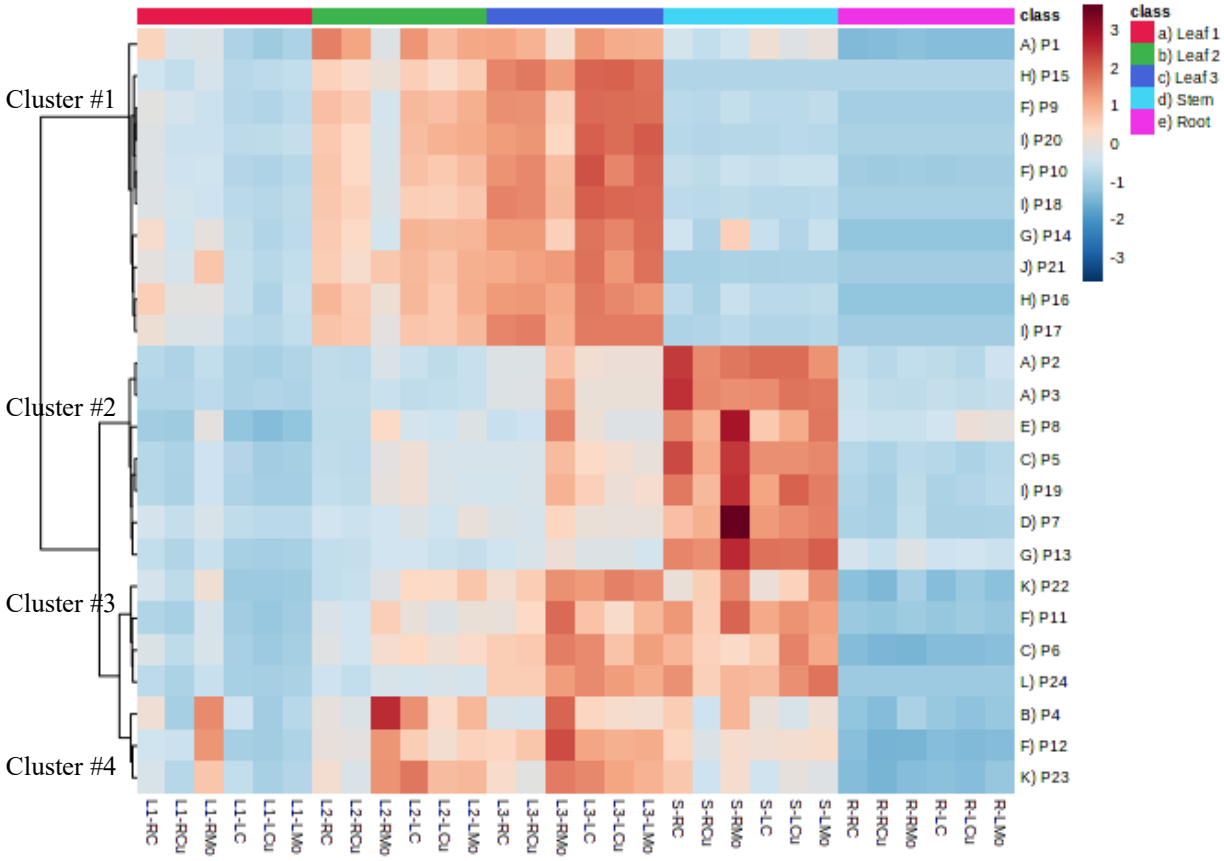

Figure 5. Heatmap of protein concentrations in different plant tissues with different treatments.

Due to the tissue-specific distribution of proteins, protein concentrations were analyzed within each tissue part respectively. PLS-DA was used to visualize the separation between the six treatment groups at the protein level, which offers an effective means to discern distinct patterns in the proteomic responses (Figure 6). For all tissues, there is a strong

separation between root exposure of Mo (yellow dots) from all other treatments. This separation aligns with the pattern observed in physiological measurements, reinforcing the idea that Mo exposure through root has a distinct impact on plant response across different levels of analysis. In addition, it shows separation between treatment groups based on exposure techniques (e.g., red vs. blue), which suggests that the choice of exposure method (leaf exposure vs. root exposure) has a discernible effect on the proteomic responses of the plants. This separation also aligns with physiological measurements and metal analysis, and it supports the notion that the exposure approach itself influences the proteomic profiles, indicating that different tissues and pathways might be engaged based on how the exposure occurs.

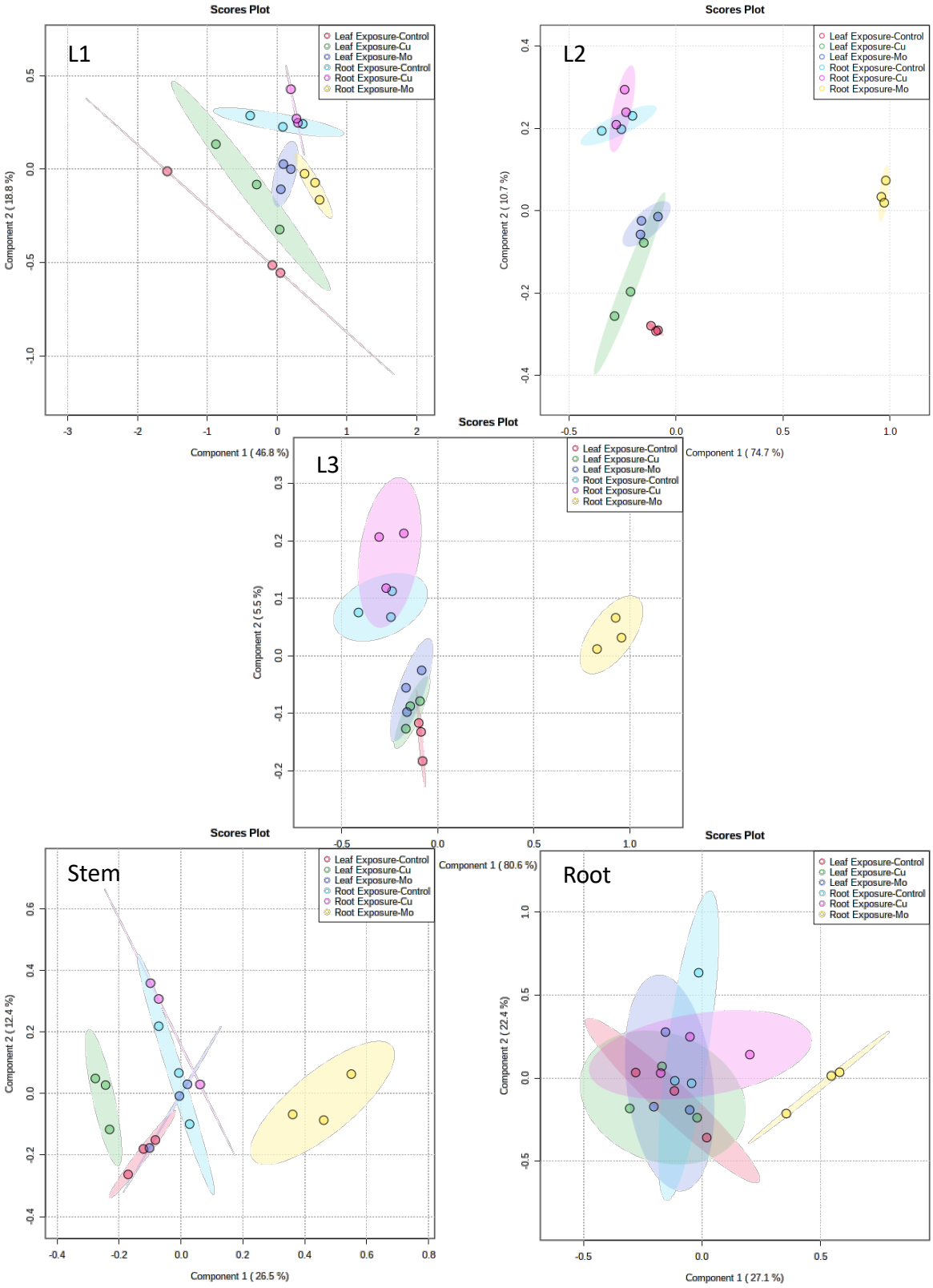

Figure 6. Partial Least Squares Discriminant Analysis (PLS-DA) of protein concentrations in each plant tissues with different treatments.

To quickly identify proteins that exhibit both substantial changes in expression and statistical significance, volcano plots were used to visualize the relationship between significance (p-values) and fold changes (FC) in each tissue (Figure 7). Grey spots represent data points with p-values greater than 0.05, indicating that these changes are not statistically significant. Blue points indicate significant changes with $0.75 < FC < 1.25$. While these changes are statistically significant, their relatively small magnitude suggests that they might not have a substantial impact on the biological response. Yellow and red points represent significant changes with $FC \geq 1.25$ or ≤ 0.75 (yellow) and $FC \geq 1.5$ or ≤ 0.5 (red), which represent alterations in protein expression that are both statistically significant and of biologically relevant due to their considerable magnitude.

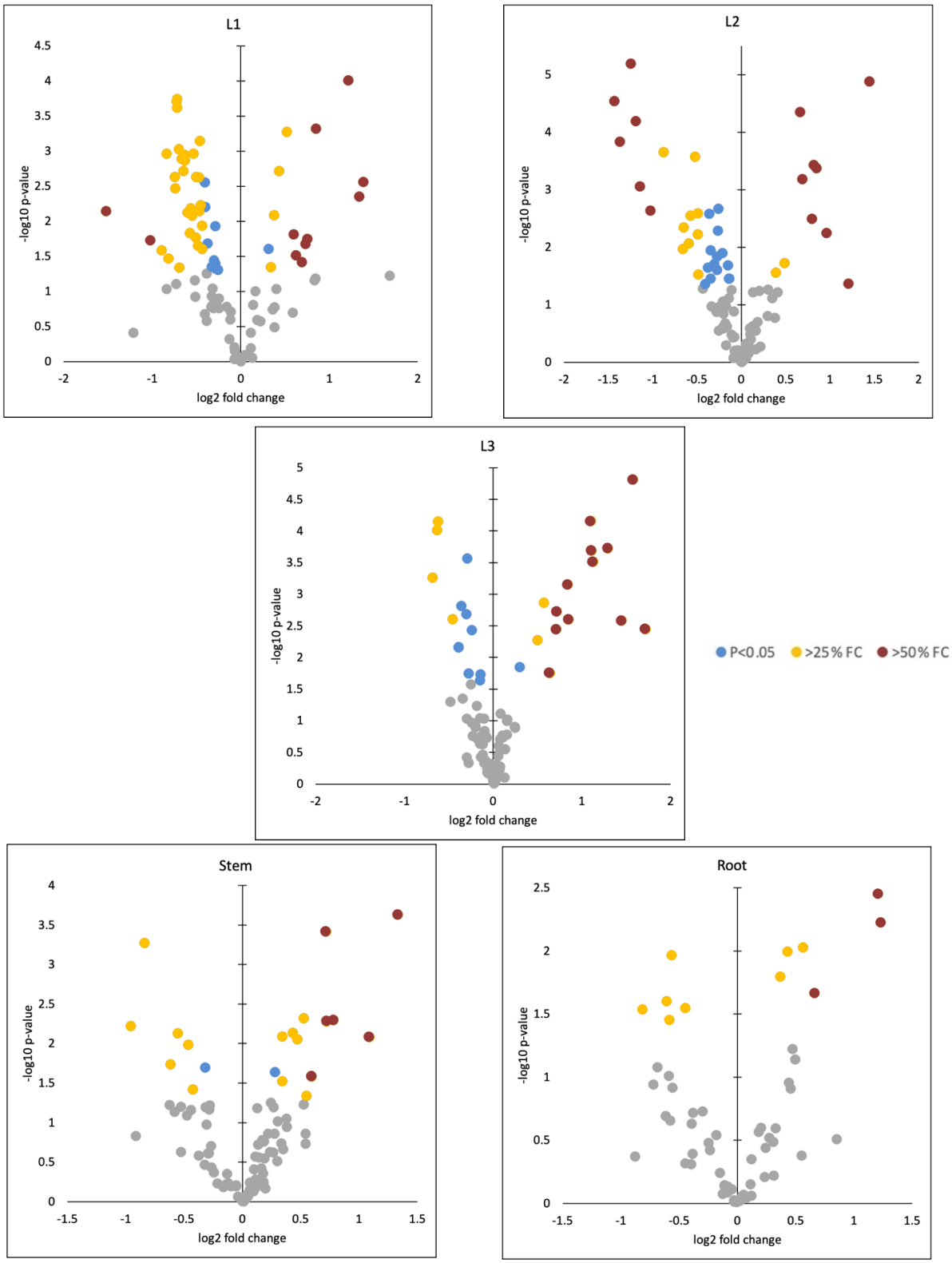

Figure 7. Volcano plots to visualize the relationship between significance (p-values < 0.05) and fold changes (FC) in each tissue. Grey points: not significant; blue color points: significant but 0.75 < FC < 1.25; yellow color points: significant and FC ≥ 1.25 or ≤ 0.75; red color points: FC ≥ 1.5 or ≤ 0.5

To better interpret the results, the data were filtered and fold change bar plots were made focusing on the yellow and red data points (Figure 8). Proteins exhibited different regulation patterns between Cu and Mo exposures, particularly in leaf tissues (L1-L3) where Mo causes protein upregulation and Cu causes downregulation. This finding highlights the specificity of protein responses to different metal exposures. Moreover, most of the regulation caused by Mo is through root exposure, which aligns with the elemental concentration and emphasizes the significance of root exposure of Mo in driving protein expression changes. In addition, the pattern of regulation activity from high to low in leaves to roots aligns with the metal release from the Mo ENMs, Mo uptake and translocation results as well. This suggests that the physiological and molecular responses of different tissues are connected, with leaves being the most sensitive and responsive, possibly due to their prominent role in Mo accumulation. Another interesting finding is that, proteins within the same metabolic pathway can have diverse regulation patterns (e.g., within pathway F, P9 and P10 downregulated while P11 and P12 upregulated). This suggests that even within the same metabolic pathway, the expression levels of individual proteins can be regulated independently.

To get a comprehensive overview of the changes occurring in the entire plant in response to ENMs exposure, targeted protein concentrations for the whole plant were calculated by the adjustment of biomass distribution (Figure 2B) for five different tissues. It shows that among 24 selected proteins (involved in 12 metabolic pathways), 16 proteins (involved in 11 metabolic pathways) were significantly upregulated ($1.28 < FC < 2.81$) under Mo ENMs exposure through the roots (Figure 9). This is not surprising as Mo is an essential trace

element necessary for various plant metabolic processes, and it is a key component of enzymes involved in nitrogen fixation, nitrate reduction, and amino acids metabolism, which are all fundamental processes that support plant growth and development.[85,86] Increased Mo concentration can potentially lead to higher activity rates of reactions of Mo-dependent enzymes, which play crucial roles in metabolic pathways. This, in turn, could upregulate the proteins involved in metabolic pathways in plants. The coordinated upregulation of multiple pathways suggests the presence of a complex regulatory network that senses Mo availability and coordinates responses across various pathways to ensure optimal metabolic function. However, the excessive presence of Mo in the soil, which is then translocated to the leaves in excess, leads to a negative physiological response (yellowing and stunted growth). The upregulation of proteins could be a strategy to increase Mo tolerance in wheat plants. For example, transport H+ transporting pyrophosphatase (P7), which was the most upregulated protein for the entire plant, has also been reported to upregulate to enhance proton pump expression, improving tolerance to the toxicity of cadmium in tobacco plants.[87]

In contrast to Mo exposure, Cu exposure has a relatively smaller impact on protein expression at the whole plant scale, since only two proteins showed significant changes (Figure 9). However, 18 proteins (involved in 11 pathways) showed significant changes particularly in leaf tissues and when exposure was via leaves (Figure 8), which indicates that Cu has a more localized impact particularly. This result correlated well with the high copper concentrations in leaves exposed via this route, which can lead to oxidative stress in plant cells due to the generation of reactive oxygen species (ROS).[88] The mostly downregulated proteins (root exposure: $0.35 < FC < 0.74$; leaf exposure: $0.49 < FC < 0.72$) observed in response to Cu exposure in leaves suggests that the plant initiated specific responses to

mitigate the effects of copper-induced oxidative stress. This includes regulating the expression of enzymes like catalase (P21), a vital enzyme in the cellular defense against oxidative stress by efficiently breaking down hydrogen peroxide, to help protect cells from the damaging effects of ROS, contributing to overall cellular health and function.[89,90]

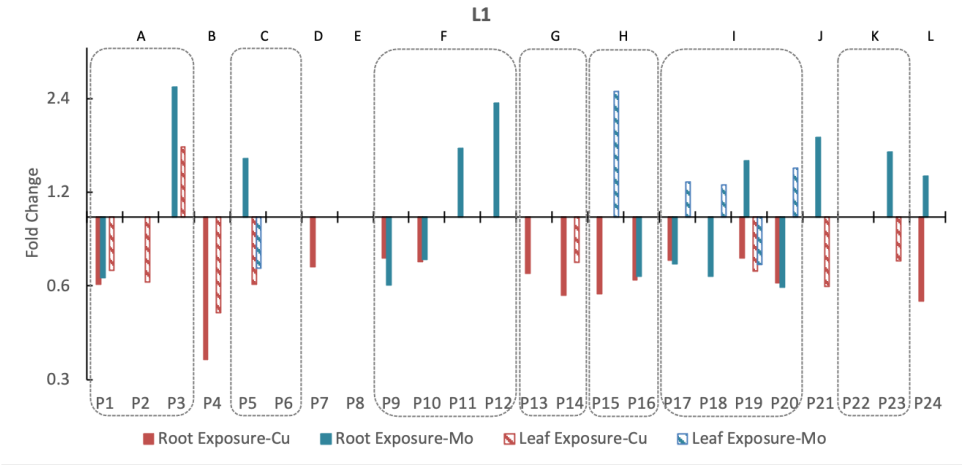

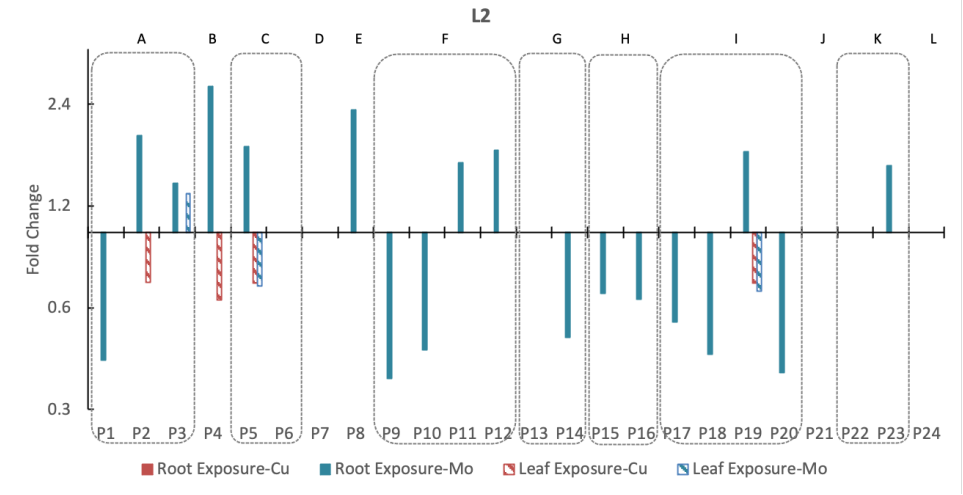

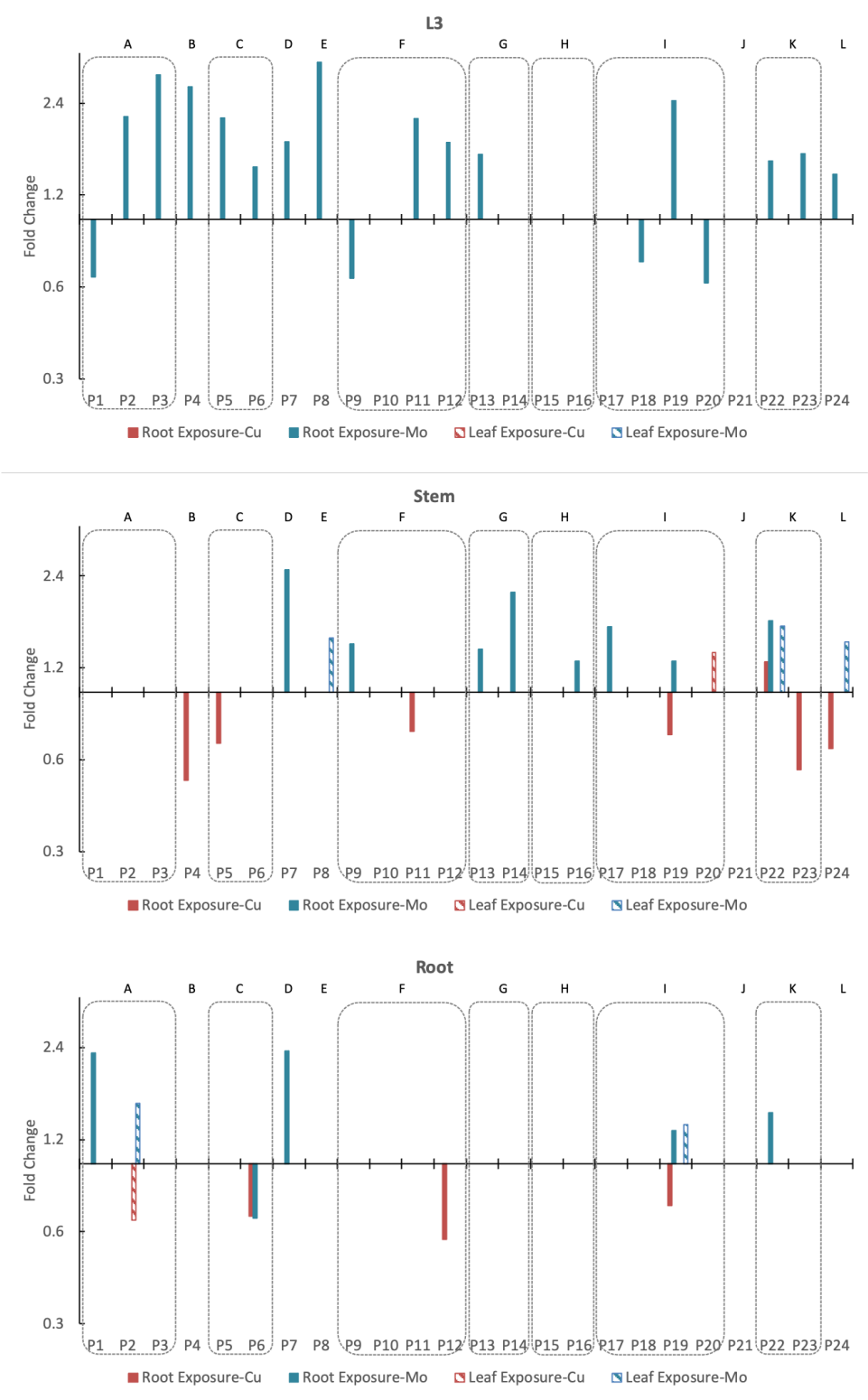

Figure 8. Fold change bar plots of proteins with FC ≥ 1.25 or ≤ 0.75 significant changes in different plant tissues.

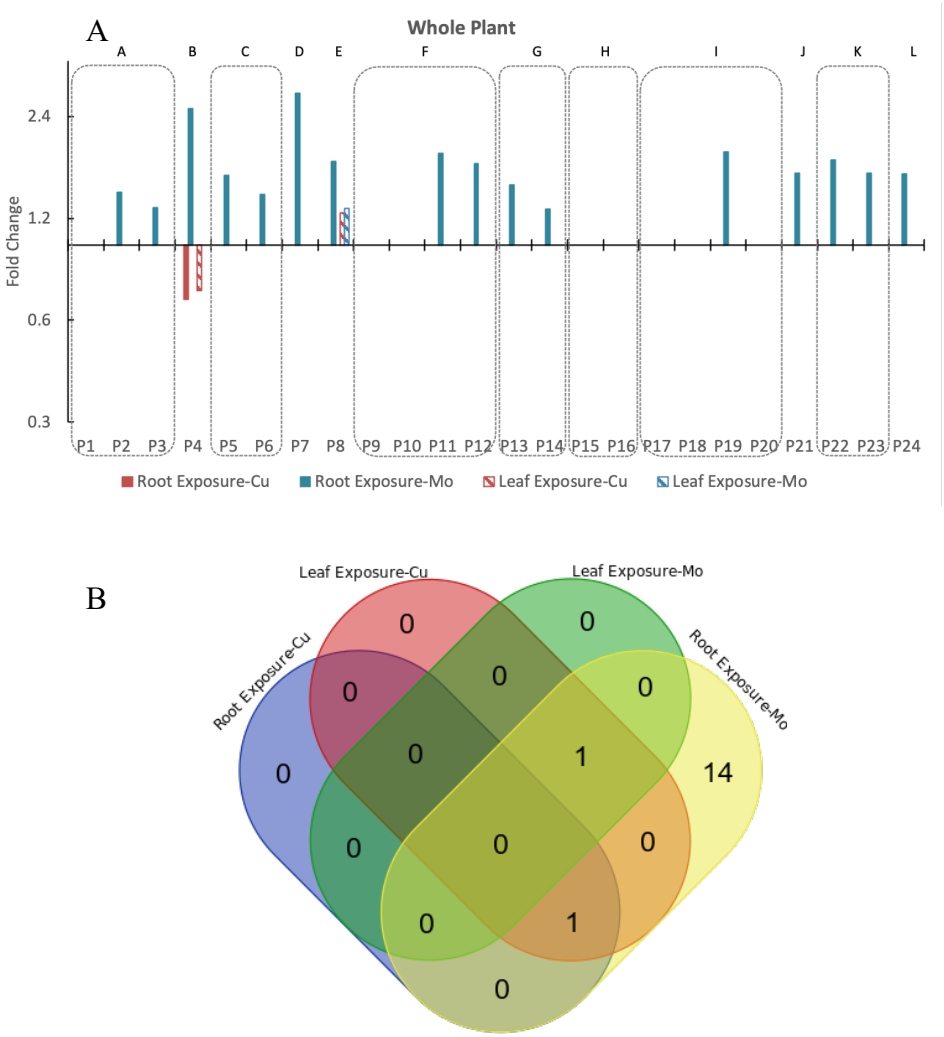

Figure 9. Protein expression in whole plant. A) Fold change bar plot of proteins with FC ≥ 1.25 or ≤ 0.75 significant changes in the whole plant; B) Venn diagram of proteins with FC ≥ 1.25 or ≤ 0.75 significant changes in the whole plant.

4. Effect of exposure to high vs. low Mo ENM concentrations through root

The significant upregulation of most selected proteins under Mo exposure through root indicates that the plant is actively responding to the presence of molybdenum. However, the depressed physiological measurements, despite protein upregulation, suggest that excess molybdenum was negatively affecting plant health. Yellowing of leaves and depressed root growth were also reported in a hydroponic experiment investigating the uptake of Mo in cress (*Lepidium sativum L.*) with 7000 µg/L Mo exposure, which was 35 times higher than

the optimal dose.[91] To further study the dose-dependent response of root exposure to Mo ENMs, a lower concentration of 0.6 mg Mo/plant was added to the experiment. The physiological measurements of the low Mo exposure group, including total biomass and biomass distribution (Figure S1 A), leaf color (Figure S1 B), and shoot and root length (Figure S1 C) were not significantly different from the control, but were significantly different from the high Mo exposure group. The slight and significant increase in shoot biomass and the decreased root biomass under low Mo exposure, suggests that lower concentration of Mo improves plant health compared to the control, and the difference between the low and high Mo exposure groups is substantial. In terms of metal uptake, plants with low Mo exposure exhibit even higher Mo concentrations in leaves (1.77, 2.67 and 3.40 times higher in L1, L2 and L3 respectively) than those with high exposure (Figure S2). This surprising observation implies that nutrient uptake by plants follows complex kinetics, and at lower Mo concentration, plants might enhance their uptake mechanisms.

At the protein level, there is a similar tissue-specific distribution of proteins (Figure S3) as noticed in Figure 5, which suggests that the distribution pattern was determined by the metabolic demands and function in each tissue. However, the clear separations observed in the PLS-DA between dose-specific treatments underscores the distinct molecular responses triggered by the different Mo concentrations (Figure S4). Particularly, in contrast to the upregulation with high Mo exposure, the proteins were significantly downregulated under low Mo exposure, especially in L1 ($0.23 < FC < 0.68$) and stem ($0.13 < FC < 0.68$) tissues. (Figure S5). Considering the protein expression in the whole plant using the adjustment of biomass distribution, levels of 5 (P7, P8, P14, P21 and P22) out of the 16 significantly regulated proteins were consistently upregulated in response to both high and low Mo

exposure (Figure S6). Specifically, the involvement of proteins in pathways like N-metabolism (P14), redox (P21) and TCA cycle (P22) processes underscores their pivotal role in harnessing the growth-promoting benefits of Mo. However, proteins P13 and P23, also involved in N-metabolism and TCA cycle, displayed a contrasting response: downregulated due to low Mo exposure but upregulated in the high Mo exposure. In addition, proteins P9, P10, and P20, crucial for processes like mitochondrial electron transport, ATP synthesis, and the Calvin Cycle, demonstrated no significant change in levels under high Mo exposure but were downregulated under low Mo exposure. These findings indicate a complex relationship between Mo availability and these metabolic processes and a potential requirement for higher Mo levels to effectively drive these energy-related pathways. The opposite trends in protein regulation indicate that the plant is employing distinct strategies to adapt to varying Mo levels, such as optimizing nutrient uptake, altering metabolic pathways, and fine-tuning stress responses. The dose-specific regulation was also reported in a previous study on metabolomic responses of corn and wheat plants due to exposure to 8 or 40 mg Mo/plant.[35] This investigation of dose effects underscores the fine balance between nutrient stimulation and toxicity. While a high dose of Mo induced significant protein upregulation, it also yielded depressed physiological measurements, highlighting the importance of appropriate nutrient dosing for optimal plant health.

D. Conclusions

In conclusion, this study delved into the response of wheat plants to a Mo based nano-fertilizer and a Cu based nano-pesticide through a comprehensive exploration of various aspects, including physiological measurements, metal uptake and translocation, and protein expression. Exposure to Mo ENMs, which release substantial amount of Mo ions, results in

significant Mo root uptake and translocation to leaves, which results in significant upregulation of multiple proteins involved in diverse metabolic pathways, particularly those related to photosynthesis and the Calvin cycle, ATP synthesis, N-metabolism, redox and TCA cycle. This aligns with the pivotal role of Mo as a cofactor for enzymes essential in nitrogen fixation, amino acid biosynthesis, and other fundamental plant processes. Notably, the study highlighted a dose-dependent response, where a higher dose of Mo through root exposure induced robust upregulation of proteins, albeit yellowing and stunted growth, while a lower dose resulted in more translocation but surprisingly induced downregulation of some proteins. The low Mo exposure induced downregulation of these proteins, mostly involved in energy metabolism and carbon fixation, suggests the requirement of higher levels of Mo to maintain their activity effectively. In contrast, Cu ENM exposure demonstrated a distinct pattern. While fewer proteins exhibited significant changes at the whole plant level, the study unveiled pronounced effects on leaf tissues, notably from exposure via leaves. This underlines that while Cu ENMs provide plant protection in terms of fungi and other pests, Cu ENMs have the potential to initiate stress responses and metabolic adaptations, particularly in the initial stages of exposure. To delineate and validate the mechanistic differences arising from nanostructures, future studies incorporating non-nanoscale Cu and Mo controls alongside nanoscale exposures can help to better elucidate nano-specific effects.

This study leveraged targeted proteomics to gain a highly quantitative insight into the nuanced response of plants to Cu and Mo ENMs exposure. The analysis at the tissue level provided a more granular understanding of these responses, allowing us to discern tissue-specific variations that would have been overlooked in a whole-plant approach. This precision was invaluable in unraveling the intricate metabolic shifts triggered by Cu and Mo

availability. Furthermore, the integration of metalomics, which delved into the uptake and translocation of Cu and Mo, enriched our understanding by providing a comprehensive view of nutrient dynamics within the plant. The study's contribution is not only in unraveling proteomic response of wheat under Mo and Cu ENMs exposure but also in illuminating the potential applications and risks associated with their utilization in agriculture. The findings hold relevance for optimizing nutrient supplementation strategies to enhance crop productivity while minimizing adverse effects on plant growth.

E. Acknowledgements

This work was supported by the National Science Foundation (NSF) under cooperative agreement number NSF-1901515. Arturo A. Keller would like to give special thanks to Agilent Technologies for their Agilent Thought Leader Award. Any findings and conclusions from this work belong to the authors and do not necessarily reflect the view of NSF.

F. Appendix

Table S1. HPLC conditions and MS conditions for LC-MS/MS analysis method.

HPLC Conditions		
Column	Agilent Polaris 3 C18-Ether 150x3.0mm (p/n:A2021150X030)	
Mobile phase A	Water + 0.1% (v:v) formic acid +3% (v:v) DMSO	
Mobile phase B	Acetonitrile + 0.1% (v:v) formic acid +3% (v:v) DMSO	
Flow rate	0.40 mL/min	
Column temperature	25 °C	
Injection volume	2 μL	
Total run time	14 minutes	
Gradient	Time (min)	%B
	0.00	5
	10.00	70
	10.01	5
	14.00	5
MS Conditions		
Ionization mode	ESI Positive	
Gas temperature	340 °C	
Gas flow	12 L/min	
Nebulizer	40 psi	
Sheath gas temperature	250 °C	
Sheath gas flow	9 L/min	
Capillary voltage	Positive	Negative
	3,500 V	3,500 V
Nozzle voltage	Positive	Negative
	2,000 V	2,000 V

Table S2. Transitions, LOD and MDL for each peptide.

ID	Sequence	Retention	Precursor ion (m/z)	Product ions					LOD (ng/mL)	MDL (ng/g)
				Quant	Collision	Qual	Collision	Fragm		
	Peptides									
1	IQNGGTEVVEAK	6.42	623.2	242.1	20	86.1	32	132	0.02	0.08
2	SVHEPMQTGLK	6.70	409.8	110.2	40	84.0	40	96	0.41	2.05
3	TAVAAVPYGGAK	7.00	553.1	173.0	24	72.1	40	112	0.08	0.40
4	LVGVSEETTTGVK	7.12	660.7	86.0	36	72.1	40	137	0.09	0.44
5	VAEGDAEDVDRAVVAAR	7.19	582.0	786.9	16	72.0	40	96	0.16	0.81
6	KALDYEELNENVK	7.25	522.6	102.0	16	86.2	16	96	0.24	1.18
7	SGDVYIPR	7.31	454.0	548.3	16	60.1	40	96	0.01	0.04
8	GMAVPDSSSPYGVR	7.42	712.3	260.0	28	189.2	36	132	0.02	0.09
9	GNATVPAMEMTK	7.43	625.7	172.0	40	70.0	40	117	0.10	0.51
10	EFAPSIPEK	7.46	509.6	335.7	16	70.0	40	96	0.10	0.49
11	FASINVENVEDNRR	7.51	555.3	120.0	24	191.0	16	96	0.00	0.02
12	FVIGGPHGDAGLTGR	7.60	485.5	604.4	12	120.0	32	96	0.00	0.01
13	AADNIPGNLYSVK	7.79	681.8	877.4	20	230.0	32	127	0.08	0.38
14	TVVSIPNGPSELAVK	8.05	756.4	172.8	40	200.9	36	132	0.01	0.06
15	TLGELPAGSVIGSASLRR	8.12	595.7	635.9	16	186.9	20	117	0.00	0.02
16	VAEFSFR	8.13	428.5	171.0	12	72.1	24	96	0.01	0.03
17	YIGSLVGDFHR	8.13	422.1	494.3	8	86.0	28	96	0.01	0.03
18	TALIDEIAK	8.21	487.5	173.0	12	86.0	40	112	0.01	0.03
19	VAPEVIAEYTVR	8.21	674.3	589.0	16	70.0	40	147	0.06	0.28
20	AAVIGDTIGDPLK	8.23	635.7	72.0	32	86.0	32	132	0.06	0.30
21	IGGLTLNELGR	8.40	572.2	228.0	24	86.1	40	122	0.01	0.07
22	TLAEEVNQAFR	8.45	639.7	187.1	28	215.0	20	127	0.04	0.21
23	IGLFGGAGVGK	8.59	488.5	545.2	16	86.1	24	117	0.01	0.05
24	VQLLEIAQVPDEHVNEFK	8.62	703.8	227.8	24	72.1	36	142	0.01	0.06
25	TAIAIDTILNQK	8.68	651.3	173.1	24	86.0	40	112	0.10	0.50

26	KPWNLSFSFGR	8.79	670.3	84.0	36	70.1	40	137	1.17	5.84
27	TWPEDVVPLQPVGR	8.96	797.4	653.7	20	342.1	40	147	1.55	7.75
28	ADGGLWLLVR	9.63	550.7	159.0	40	86.0	40	117	0.02	0.11
	Internal Standards									
2*	SVHEPMQTGLK{Lys(13C6,15N2)}	6.69	412.5	90.1	40	69.9	40	96		
7*	SGDVYIPR{Arg(13C6,15N4)}	7.31	459.0	558.3	12	260.0	16	91		
18*	TALIDEIAK{Lys(13C6,15N2)}	8.21	491.6	172.8	16	86.0	40	81		
26*	KPWNLSFSFGR{Arg(13C6,15N4)}	8.79	675.3	84.1	36	70.0	40	137		

Table S3. Metal concentration in different plant tissue samples with different treatments

Sample ID	Exposure Elements (µg/g)		Nutrient Elements (µg/g)							
	Cu	Mo	K	Mg	Ca	P	Mn	Fe	Zn	Na
L1-RC	2.05± 0.00	0.75± 0.02	5554.72 ± 221.67	1155.45 ± 4.30	556.85 ± 8.92	170.68 ± 7.36	34.27± 0.02	11.99± 0.15	2.77± 0.02	41.63 ± 0.35
L1-RCu	5.17± 0.04	0.76± 0.03	5516.42 ± 83.19	1304.96 ± 50.74	585.87 ± 4.57	155.52 ± 7.03	37.55± 1.53	9.05± 0.12	1.83± 0.11	29.36 ± 1.58
L1-RMo	3.43± 0.77	1822.97 ± 48.45	9151.55 ± 180.25	1808.21 ± 17.94	605.34 ± 4.80	369.21 ± 10.54	30.75± 0.65	26.15± 0.23	3.41± 0.00	43.19 ± 0.34
L1-LC	1.92± 0.15	1.03± 0.04	4815.98 ± 20.84	849.81± 18.03	397.01 ± 0.57	91.97± 0.74	27.24± 0.31	17.35± 0.01	6.85± 0.18	38.75 ± 1.20
L1-LCu	688.92 ± 5.29	1.59± 0.03	4256.47 ± 3.47	848.10± 5.76	385.13 ± 3.48	67.25± 3.10	35.19± 0.14	10.57± 0.03	6.62± 0.12	27.89 ± 0.01
L1-LMo	28.08± 1.97	89.88± 16.05	4630.07 ± 374.73	859.26± 146.26	385.17 ± 46.06	84.64± 34.55	22.94± 4.15	10.64± 1.27	6.07± 1.26	36.14 ± 6.61
L2-RC	1.83± 0.00	0.65± 0.11	6713.77 ± 629.39	947.88± 179.00	413.88 ± 56.11	307.51 ± 79.21	39.39± 7.65	12.86± 1.67	4.15± 1.57	20.17 ± 4.15
L2-RCu	2.68± 0.04	1.28± 0.00	6002.09 ± 3.41	1143.59 ± 1.56	479.77 ± 1.57	296.05 ± 0.98	49.67± 0.07	10.25± 0.01	3.30± 0.36	21.29 ± 0.27
L2-RMo	1.68± 0.01	1178.93 ± 5.05	6354.39 ± 76.71	1014.21 ± 9.82	282.08 ± 0.74	502.39 ± 3.22	19.10± 0.20	13.59± 0.10	3.18± 0.06	30.98 ± 0.65
L2-LC	6.75± 0.99	0.48± 0.02	6969.96 ± 647.16	765.70± 80.46	363.13 ± 52.05	287.49 ± 43.17	29.67± 3.04	12.70± 1.77	4.34± 0.75	16.06 ± 2.16
L2-LCu	740.04 ± 23.31	1.61± 0.05	7578.29 ± 536.84	1024.16 ± 32.83	447.87 ± 34.68	362.75 ± 16.56	45.70± 1.82	14.06± 1.10	3.28± 0.33	13.59 ± 0.19
L2-LMo	26.05± 2.20	85.11± 16.98	6985.79 ± 505.81	927.34± 187.37	389.66 ± 47.04	351.66 ± 105.24	33.09± 6.45	12.41± 1.41	4.44± 1.49	16.75 ± 3.42
L3-RC	3.72± 0.00	0.50± 0.05	9218.28 ± 645.71	528.30± 39.64	251.10 ± 24.98	581.94 ± 47.89	33.48± 2.51	9.84± 0.98	4.86± 0.85	17.54 ± 1.73
L3-RCu	4.31± 2.24	0.54± 0.09	8749.80 ± 617.85	644.38± 120.82	269.03 ± 29.49	621.63 ± 129.43	40.21± 7.62	13.27± 1.48	4.55± 1.42	18.81 ± 3.58
L3-RMo	18.56± 0.14	779.74± 2.84	9120.38 ± 6.14	572.64± 5.19	165.84 ± 4.54	809.35 ± 4.58	15.66± 0.00	15.38± 0.10	5.07± 0.11	38.02 ± 0.50
L3-LC	2.80± 1.01	0.59± 0.02	9456.88 ± 100.81	570.60± 46.79	238.61 ± 9.08	778.90 ± 67.19	31.94± 2.59	15.07± 0.44	3.82± 0.73	16.48 ± 1.30
L3-LCu	493.24 ± 1.77	1.97± 0.01	9646.79 ± 64.27	660.81± 7.25	262.01 ± 1.02	833.01 ± 7.89	41.28± 0.24	11.91± 0.19	3.38± 0.03	19.74 ± 0.16
L3-LMo	20.12± 0.10	98.75± 0.52	9764.08 ± 2.38	653.44± 0.51	263.13 ± 7.49	806.52 ± 13.66	36.53± 0.30	13.85± 0.28	3.25± 0.09	17.66 ± 0.41
S-RC	4.09± 2.33	0.60± 0.12	7746.65 ± 529.05	528.66± 93.30	180.92 ± 22.15	783.85 ± 155.13	45.67± 8.59	23.35± 2.83	5.56± 1.46	40.67 ± 7.51
S-RCu	19.20± 0.26	0.48± 0.06	7772.32 ± 1925.10	466.56± 46.16	200.30 ± 59.21	580.22 ± 74.76	40.73± 3.99	15.48± 4.49	6.59± 0.71	35.78 ± 4.54
S-RMo	5.26± 2.12	757.81± 142.84	6149.11 ± 543.98	552.50± 112.10	220.60 ± 22.53	728.94 ± 159.88	22.79± 4.34	69.77± 8.06	7.91± 0.66	101.68± 21.50

S-LC	2.41± 0.02	0.57± 0.03	6870.02 ± 5.98	500.54± 0.94	166.05 ± 2.89	810.60 ± 14.99	38.49± 0.41	14.02± 0.07	10.75± 0.23	51.14 ± 0.17
S-LCu	89.05± 0.42	1.50± 0.02	7574.34 ± 62.51	560.95± 1.45	180.64 ± 4.09	854.80 ± 6.39	49.09± 0.34	19.00± 0.17	5.71± 0.03	49.06 ± 0.09
S-LMo	13.01± 0.01	70.63± 0.22	7308.35 ± 404.93	565.45± 4.81	176.71 ± 12.84	864.13 ± 8.37	47.61± 0.17	26.19± 1.88	17.22± 0.11	45.78 ± 0.11
R-RC	9.48± 0.19	0.17± 0.00	2662.01 ± 261.67	221.47± 7.75	116.07 ± 13.89	88.30± 5.00	25.28± 0.97	27.34± 2.59	6.33± 0.00	70.15 ± 1.17
R-RCu	28.87± 0.03	0.14± 0.00	2872.15 ± 5.01	242.19± 2.28	91.84± 1.97	78.51± 1.92	21.03± 0.19	56.87± 0.25	5.81± 0.28	67.67 ± 0.36
R-RMo	10.13± 0.06	386.53± 28.88	3250.91 ± 81.64	335.95± 25.04	104.00 ± 7.33	129.75 ± 18.26	25.60± 1.60	101.91± 5.84	7.15± 0.08	55.92 ± 3.25
R-LC	8.63± 0.13	0.16± 0.02	2554.23 ± 3.43	203.50± 4.81	90.18± 2.14	62.55± 3.93	19.93± 0.51	26.29± 0.17	4.98± 0.09	68.83 ± 1.14
R-LCu	12.24± 0.16	0.18± 0.01	2619.34 ± 22.56	208.30± 1.08	84.19± 5.80	63.14± 2.44	19.74± 0.18	29.51± 0.48	5.55± 0.01	57.31 ± 0.09
R-LMo	8.21± 1.51	13.11± 1.85	2944.04 ± 141.16	261.63± 38.92	108.47 ± 3.02	105.13 ± 28.60	26.57± 3.85	33.55± 1.80	3.70± 1.67	75.01 ± 8.57

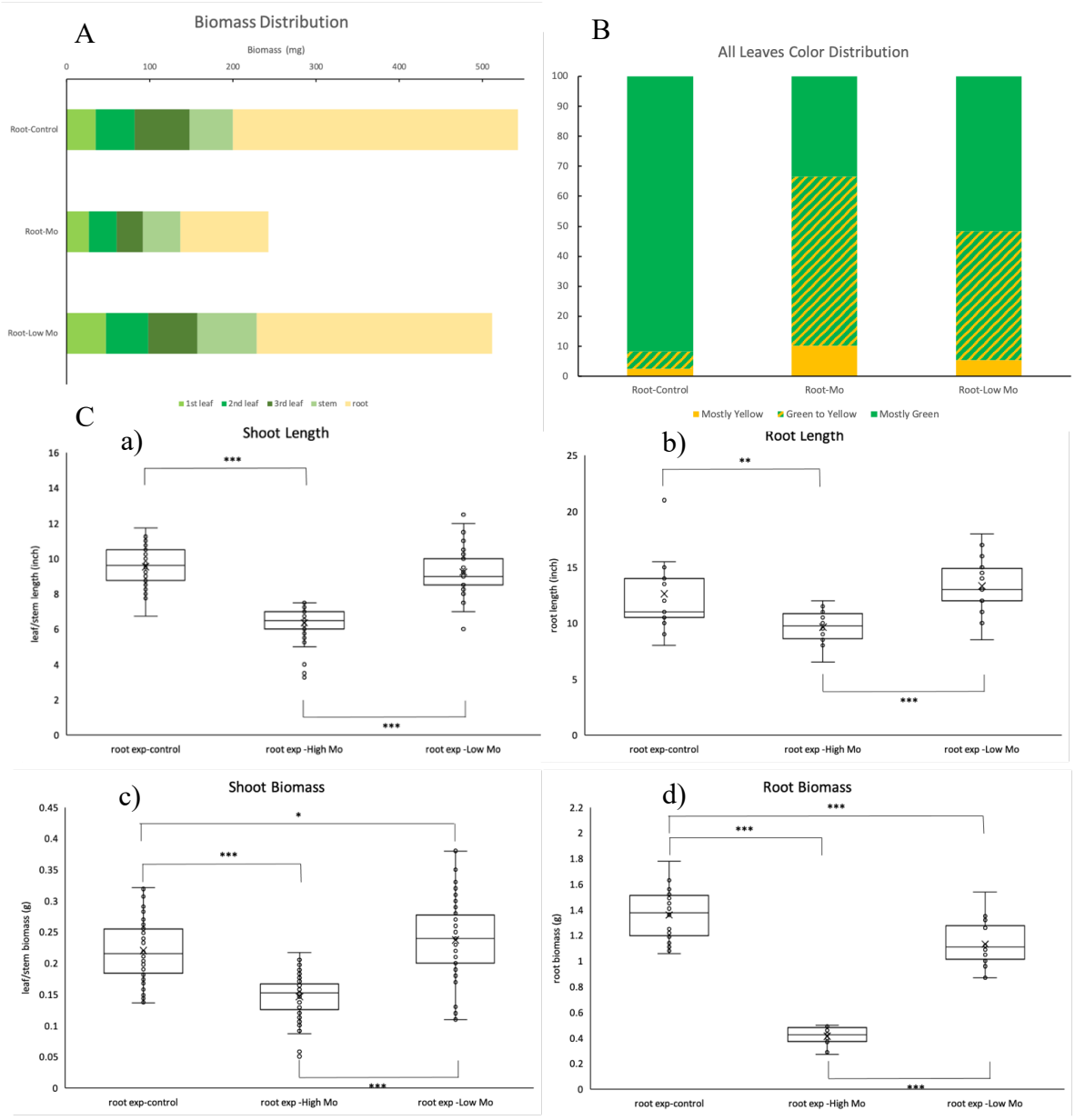

Figure S1. Physiology measurements of plants with high and low Mo exposure treatments. A) Biomass distribution; B) Leaves color distribution; C) The box-and-whisker plot of a) shoot length, b) root length, c) shoot biomass and d) root biomass of Mo treatment groups through root exposure (Control, High Mo and Low Mo). T-test results indicated as *: $p \leq 0.05$; **: $p \leq 0.01$; ***: $p \leq 0.001$

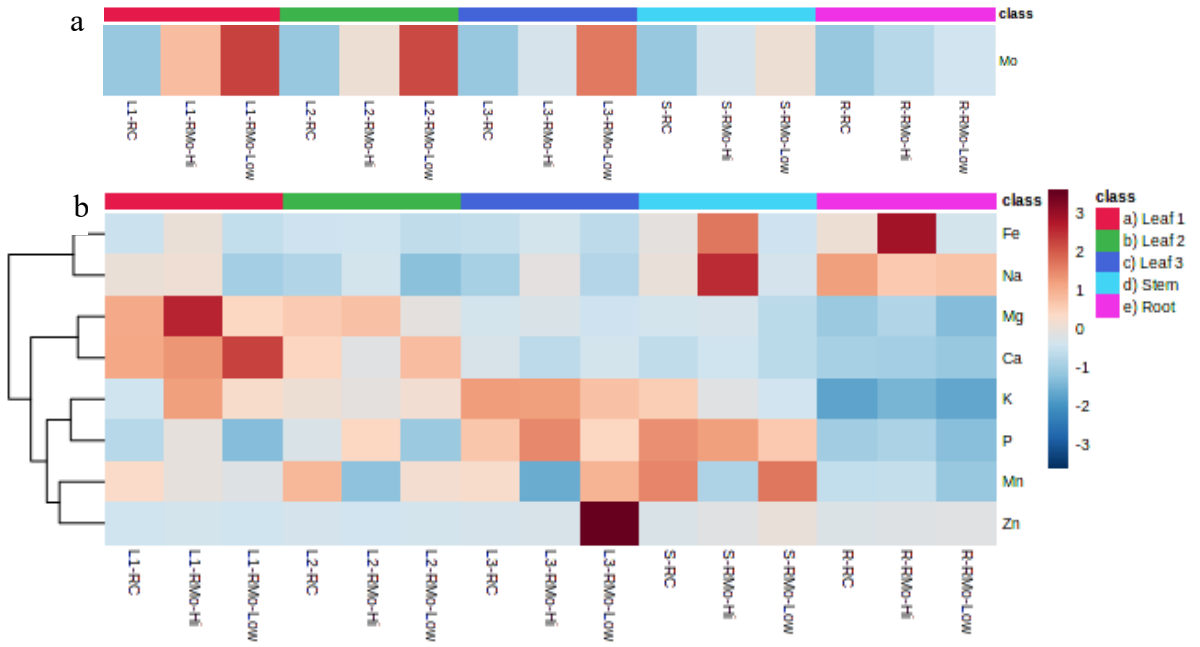

Figure S2. Heatmap of metal concentration in plant tissue samples with high and low Mo exposure treatments. a) Mo concentration in plant tissues; b) Nutrient elements concentration in plant tissues. RC: root exposure control; RMo-Hi: root exposure to Mo-NP with high dose; RMo-Low: root exposure to Mo-NP with low dose.

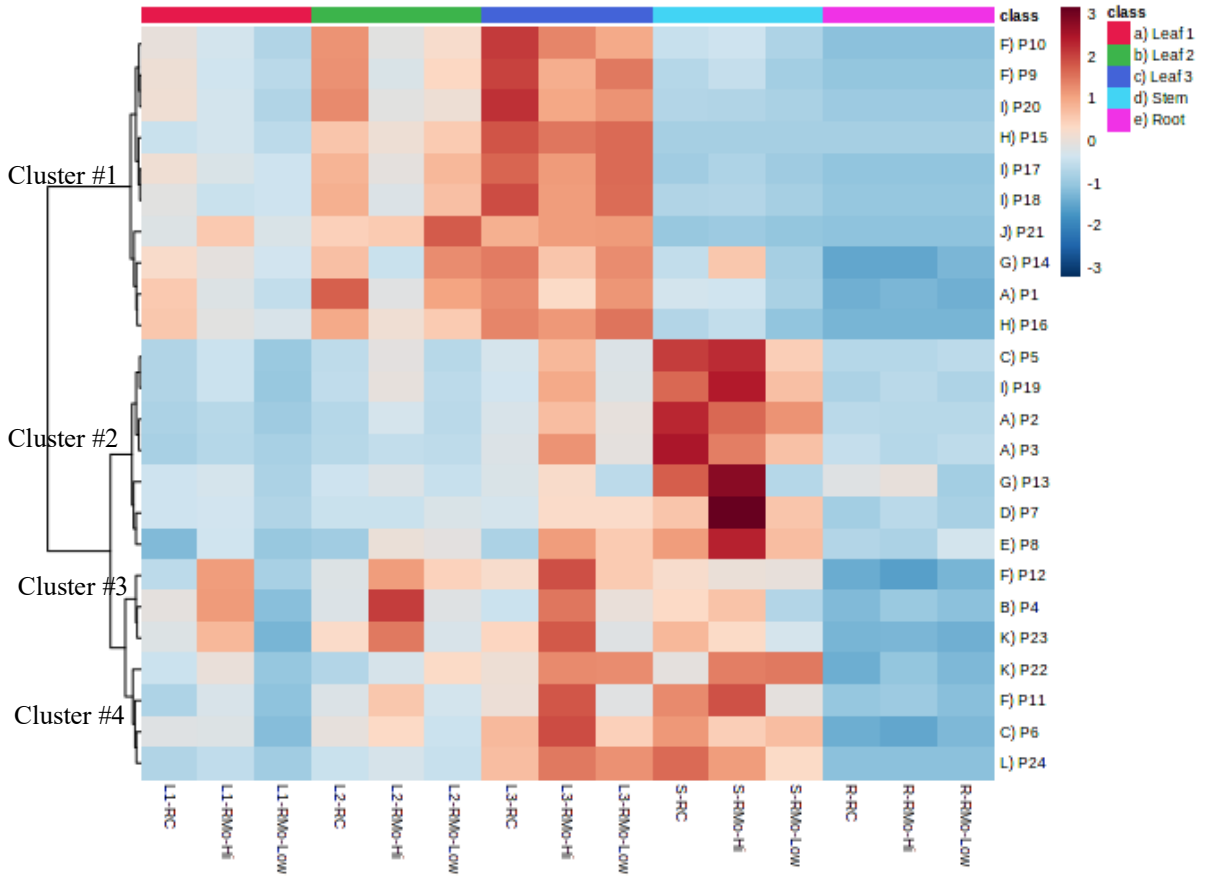

Figure S3. Heatmap of protein concentrations in plant tissues with high and low Mo exposure treatments.

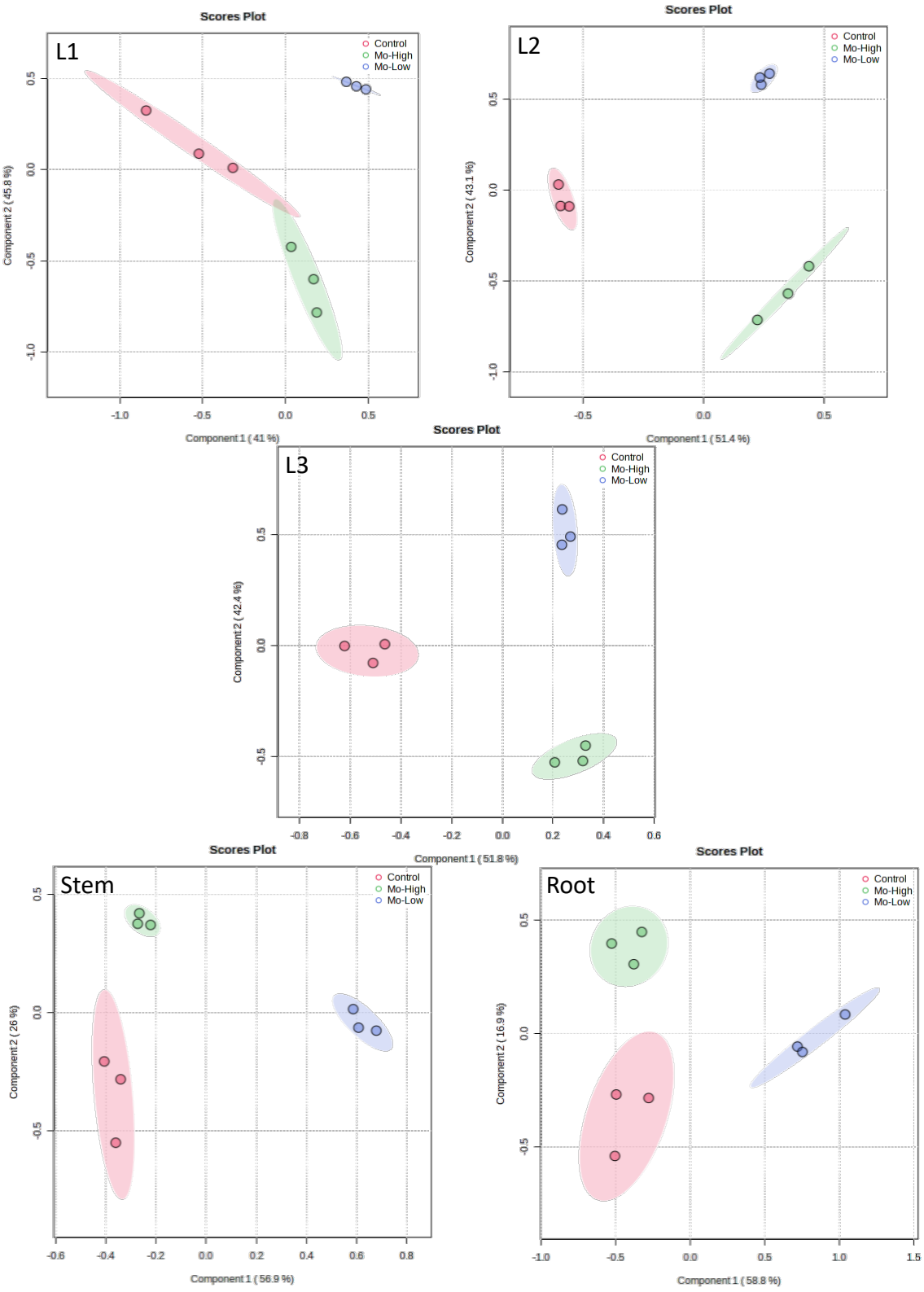

Figure S4. Partial Least Squares Discriminant Analysis (PLS-DA) of protein concentrations in different plant tissues exposed to high and low Mo doses via the roots.

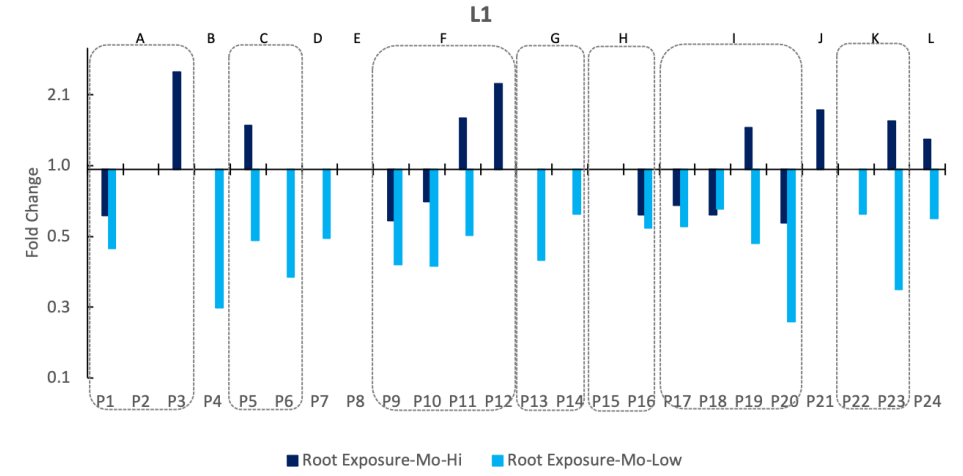
L1
A B C D E F G H I J K L
2.1
1.0
0.5
0.3
0.1
Fold Change
P1 P2 P3 P4 P5 P6 P7 P8 P9 P10 P11 P12 P13 P14 P15 P16 P17 P18 P19 P20 P21 P22 P23 P24
Root Exposure-Mo-Hi
Root Exposure-Mo-Low

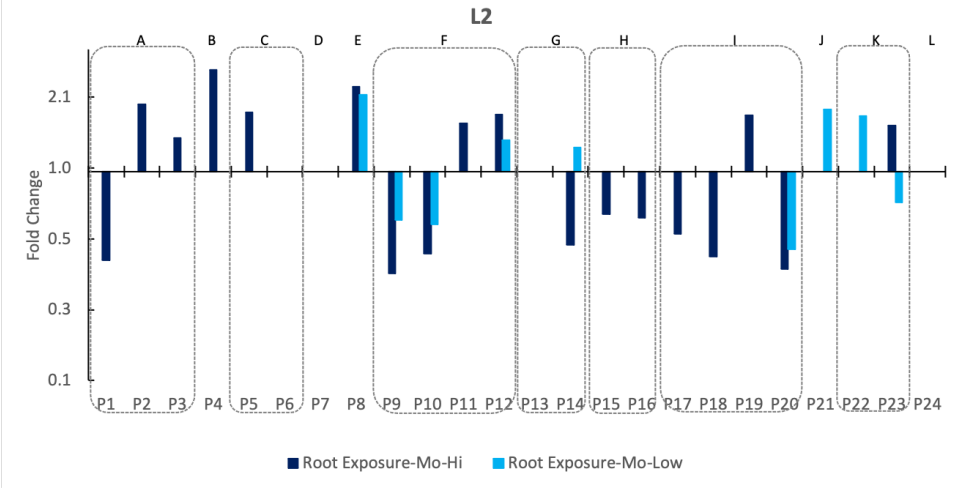
L2
A B C D E F G H I J K L
2.1
1.0
0.5
0.3
0.1
Fold Change
P1 P2 P3 P4 P5 P6 P7 P8 P9 P10 P11 P12 P13 P14 P15 P16 P17 P18 P19 P20 P21 P22 P23 P24
Root Exposure-Mo-Hi
Root Exposure-Mo-Low

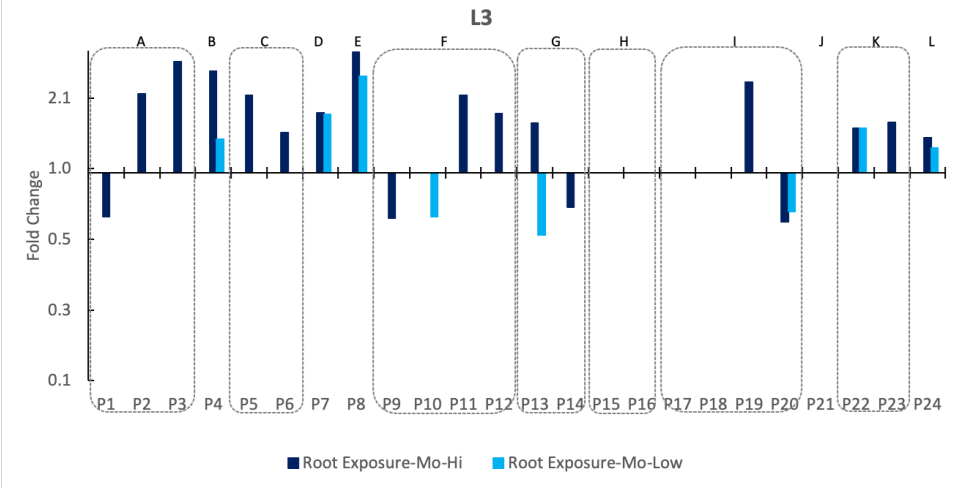
L3
A B C D E F G H I J K L
2.1
1.0
0.5
0.3
0.1
Fold Change
P1 P2 P3 P4 P5 P6 P7 P8 P9 P10 P11 P12 P13 P14 P15 P16 P17 P18 P19 P20 P21 P22 P23 P24
Root Exposure-Mo-Hi
Root Exposure-Mo-Low

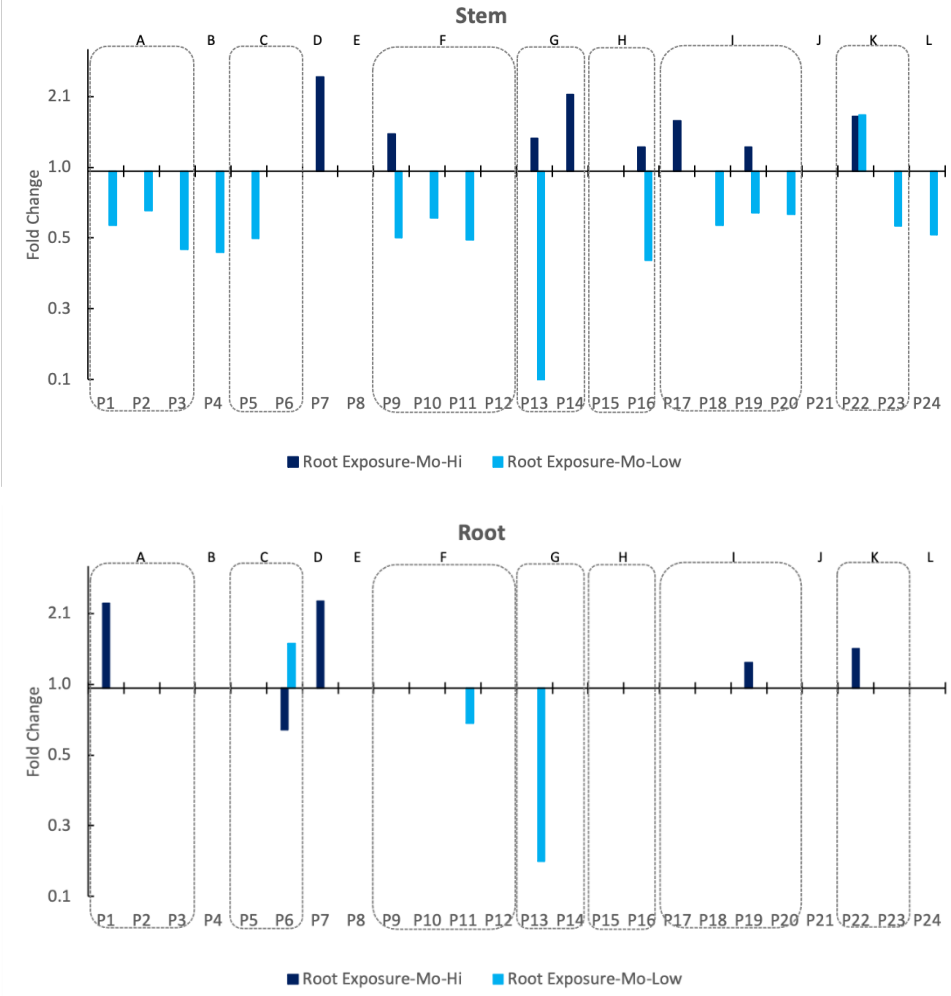

Figure S5. Fold change bar plots of proteins with FC ≥ 1.25 or ≤ 0.75 significant changes in different plant tissues with high and low Mo exposure treatments.

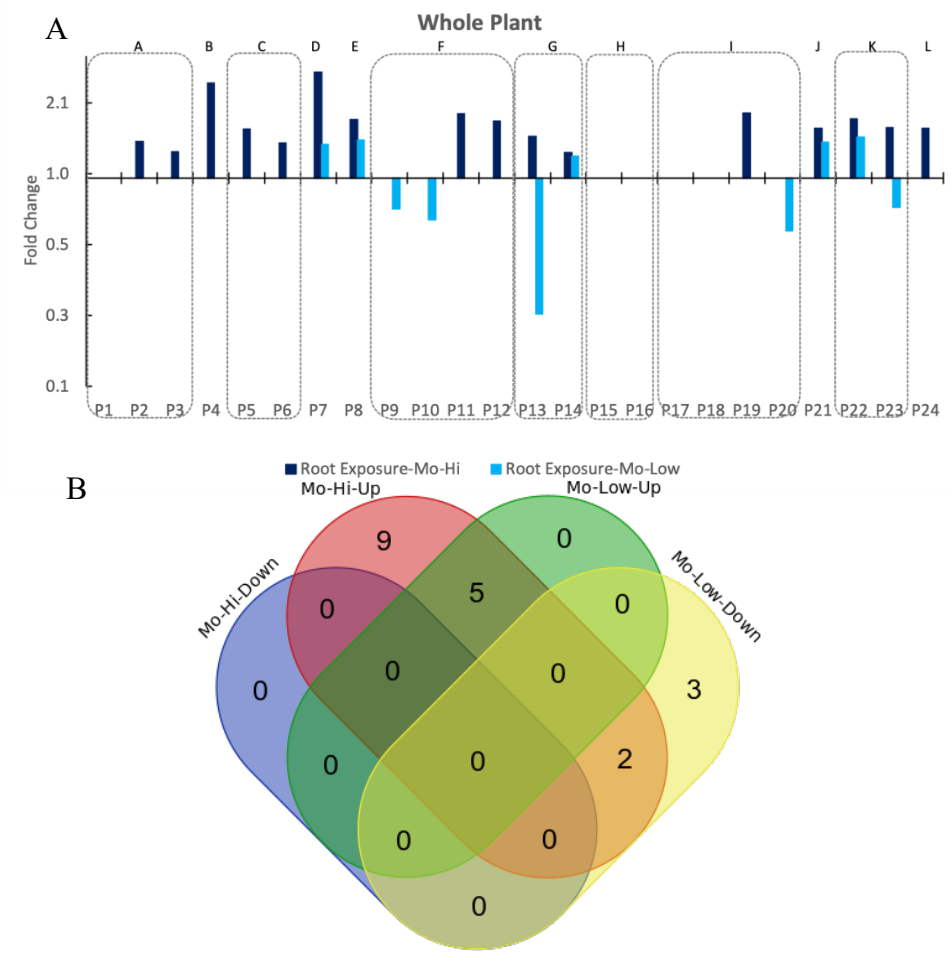

Figure S6. Protein expression in whole plant. A) Fold change bar plot of proteins with FC ≥ 1.25 or ≤ 0.75 significant changes in the whole plant with high and low Mo exposure treatments.; B) Venn diagram of proteins with FC ≥ 1.25 or ≤ 0.75 significant changes in the whole plant.

IV. Integrating Targeted Metabolomics and Targeted Proteomics to Study the Responses of Wheat Plants to Engineered Nanomaterials

Abstract Understanding the intricate response of plants to exposure of nanomaterials like molybdenum (Mo) based nano-fertilizer and copper (Cu) based nano-pesticide is pivotal for assessing their environmental impact and agricultural applications. Here, a multi-omics investigation into the metabolic and proteomic responses of wheat to Mo and Cu based ENMs exposure via root and leaf application methods is presented. Utilizing LC-MS/MS analysis, 82 metabolites across various classes and 24 proteins were assessed in different plant tissues (roots, stems, leaves) under diverse treatments. The investigation identified 58 responsive metabolites and 19 responsive proteins for Cu treatments, 71 responsive metabolites and 24 responsive proteins for Mo treatments, mostly through leaf exposure for Cu and root exposure for Mo. Distinct tissue-specific preferences for metabolite accumulation were revealed, highlighting the prevalence of organic acids and fatty acids in stem or root tissues, while sugars and amino acids were abundant in leaves, mirroring their roles in energy storage and photosynthesis. Joint pathway analysis revealed 23 perturbed pathways across treatments, among which Mo exposure through roots affected all identified pathways while through leaf exposure influenced 15, emphasizing the dependance on exposure route and tissue specific inducement of metabolic and proteomic responses. The coordinated response observed in protein and metabolite concentrations, particularly in amino acids, highlighted a dynamic and interconnected proteomic-to-metabolic-to-proteomic relationship. Furthermore, the contrasting expression patterns observed in glutamate dehydrogenase (upregulation at $1.38 \leq FC \leq 1.63$ with high Mo dose, and downregulation at

$0.13 \leq FC \leq 0.54$ with low Mo dose) and its consequential impact on glutamine expression ($7.67 \leq FC \leq 39.60$ with high Mo dose and $1.50 \leq FC \leq 1.95$ with low Mo dose) following Mo root exposure highlighted dose-dependent regulatory trends influencing proteins and metabolites. These findings offer a multi-dimensional understanding of plant responses to ENMs exposure, guiding agricultural practices and environmental safety protocols while advancing knowledge on nanomaterial impacts on plant biology.

A. Introduction

Understanding the intricate mechanisms governing cellular responses to varying environmental stimuli is pivotal in unraveling the complexity of biological systems. The advent of high-throughput technologies in various 'omics' fields such as genomics, transcriptomics, proteomics, and metabolomics has significantly expanded our capacity to explore biological systems at different molecular levels.[18,61] In general, genomics (gene level) provides collective characterization and quantification of the organism's genes, while transcriptomics (mRNA level) looks into gene expression patterns determined by RNA transcripts. Proteomics (protein level) studies dynamic protein products and their interactions, while metabolomics (metabolites level) profiles metabolites at a specific time under specific environmental conditions. When a plant is exposed to any xenobiotic, the processes triggered are interconnected, involving gene expression regulation, subsequent protein regulation, and alterations in metabolic processes that ultimately manifest in the plant's phenotype. Integrating these datasets through multi-omics can serve to comprehensively understand the complex interactions and regulatory networks within biological systems.[19,20] For example, by integrating metabolomics and transcriptomics, a study revealed the regulation of the genes in the flavonoid biosynthesis pathway that

promoted the biosynthesis of quinone chalcones in safflower under MeJA treatment.[92] Another study integrated proteome and metabolome profiling with alterations in the levels of enzymes of glycolysis and TCA cycle pathways and relative metabolites revealed protein profiling and metabolism disturbances induced by the differential transformation process in glyphosate tolerant genetically modified maize.[93]

The existing multi-omics investigations have primarily employed untargeted approaches, enabling a broad and comprehensive view at each level of omics analysis. However, untargeted approaches have limitations in terms of accuracy and reproducibility compared to targeted methods, which focus on specific molecules or pathways of interest.[21,22,23,5] Thus, in our study, we opted to utilize our previously optimized targeted metabolomics (see Chapter II)[35] and targeted proteomics (see Chapter III)[63] approaches. We aimed to investigate the specific molecular responses of plants to engineered nanomaterials (ENMs). This strategic approach allows us to focus on particular molecules or pathways of interest, providing a more precise and detailed understanding of how plants respond to ENM exposure.

Engineered nanomaterials (ENMs) have emerged as significant elements in agriculture, notably as nano-pesticides and nano-fertilizers, aiming to augment agricultural productivity and sustainability.[94,13,14,15] This is crucial in meeting the challenges posed by feeding an expanding global population amidst the backdrop of climate change. Nanotechnology represents a potential solution to address the evolving agricultural demands by providing innovative methods to enhance crop yield and plant resilience in the face of environmental stressors. Thus, gaining a deeper understanding of how these nanomaterials interact with biological systems at the cellular level is crucial for developing safer and more efficient applications in agricultural practices. Especially owing to the rapid analytical improvements

in liquid chromatography-mass spectrometry (LC-MS), targeted analytical approaches enable tissue specific analysis, to provide more detailed understanding of the effects of ENMs on particular plant tissues.[95] This level of analysis contributes to refining the design and application of ENMs in agriculture, to ensure their effectiveness while concurrently mitigating potential risks or adverse impacts on plants, soil, and the surrounding environment.

In this study, we focused on wheat (*Triticum aestivum*), a globally significant crop, to investigate the impact of two types of ENMs, specifically molybdenum (Mo) based nano-fertilizer and copper (Cu) based nano-pesticide. We investigated two exposure routes: root exposure and leaf exposure since they represent two common application approaches in agriculture. This investigation aids in understanding the potentially different effects and responses of plants to ENMs administered through different application techniques.[95] We selected 24 proteins for analysis based on previous research indicating their susceptibility to perturbation upon exposure to ENMs (see Chapter III).[63] A total of 82 metabolites that were actively involved in plant central metabolism were selected for targeted metabolomics analysis, including antioxidants, organic acids, phenolics, nucleobase/side/tide, amino acids, sugar/sugar alcohol and fatty acids.[35, 74,96]

B. Materials and Methods

1. Wheat growth and harvest

Triticum aestivum (wheat) seeds purchased from Harmony Farms KS (Jennings, KS, USA) were sterilized using a 1% sodium hypochlorite solution for 10 minutes followed by rinsing with NANOpure water and soaking in NANOpure water overnight before

germination. Vermiculite saturated with 10% Hoagland water was prepared and transferred into plant pots to serve as soil. Soaked seeds (four seeds per pot) were planted in the soil with their tips facing up to ensure successful germination. Each pot was watered daily with 20 ml of 10% Hoagland water to maintain adequate moisture. Plants were grown under specific conditions: 16-hour photoperiod, light intensity of 150 $\mu mol \cdot m^{-2} \cdot s^{-1}$, temperature of 22 °C, and 60% relative humidity for 4 weeks. $Cu(OH)_2$-NMs (99.5% purity, US3078) and MoO_3-NMs (99.94% purity, US3330) were purchased from U.S. Research Nanomaterials Inc. (Houston, TX, USA) and applied to wheat as ENMs treatments through two exposure routes, root and leaf. For root exposure, ENM suspensions containing Cu or Mo (1250 mg element /L) were prepared in 10% Hoagland solution. On day 7, instead of regular watering, Cu and Mo exposure groups were watered with ENMs suspensions (25 mg Cu or Mo per pot) evenly distributed in pots to ensure root exposure. For leaf exposure, ENMs suspensions containing Cu or Mo (500 mg element /L) were prepared in a surfactant solution (0.2% Triton X-100 in NANOpure water). From day 22 to day 28, plant leaves were soaked 3 times daily in ENM suspensions to receive 7 mL/day for exposure groups or in surfactant solution for the leaf control group. The total ENM exposure for both root and leaf exposure routes were 6.25 mg Cu or Mo per plant (25 mg per pot). At least 40 plant replicates were raised for each treatment group in both exposure approaches. In addition to the existing treatment levels, an extra lower concentration of 0.6 mg of Mo per plant was introduced via the roots. This lower concentration was included in the experiment to evaluate the recommended field application dose of Mo. The selection of all dosage levels, including this lower concentration, was based on findings and recommendations from prior studies to ensure a comprehensive assessment of Mo.[95,74,71,72,73]

In total, 6 treatment groups, including root exposure control, Cu exposure through root, Mo exposure through root, leaf exposure control, Cu exposure through leaf, and Mo exposure through leaf, were harvested on day 28. Three leaves emerged from each plant during the 4-week growth period. The harvested plants were cut into 5 parts, including leaf #1 (L1), leaf #2 (L2), leaf #3 (L3), stem and root, with L1 being the first leaf to emerge and L3 the third leaf to emerge. The pooled tissue of each part was homogenized using mortar and pestle coupled with liquid nitrogen, and then stored in 50 mL centrifuge tubes at -80 °C until analyzed.

2. Metabolites extraction and targeted metabolomics analysis

To extract metabolites from harvested plants, a universal extraction method from our previous studies was used.[35] Generally, a portion of 100 mg plant tissue from each homogenized part was mixed with 1 ml of 80% methanol in water with 2% formic acid in a 1.5 ml centrifuge tube by vortexing at 3000 rpm for 20 min, followed by sonication in water bath for 20 min at room temperature. Then the extraction was centrifuged at 20,000 g for 20 min, and the 1ml of supernatant was divided and transferred into 4 vials with 200 μL in each, followed by reconstitution into proper solvent for LC-MS/MS analysis grouped by 6 metabolite categories, including antioxidants (vial #1), organic acids and phenolics (vial #2), nucleobase/side/tides (vial #2), amino acids (vial #3), sugar/sugar alcohol (vial #3), and fatty acids (vial #4) (Figure S1). A full list of metabolites analyzed using our targeted metabolomics analysis is presented in Table S1, detailing the information of reconstitution solvent, optimized LC-MS/MS column and mobile phase. The LC-MS/MS analysis parameters for targeted metabolomics analysis are detailed in Table S2. LC-MS/MS

chromatograph of the 6 groups of metabolites using optimized methods are shown in Figure S2.

3. Protein extraction and targeted proteomics analysis

Tissue samples were processed using a phenol extraction method coupled with trypsin digestion.[63, 95] Generally, 200 mg of plant tissue was extracted using a phenol extraction buffer and partitioned with Tris-buffered phenol solution. Then protein was precipitated using 0.1 M ammonium acetate in methanol overnight at -20 °C. The protein pellet was solubilized in 8 M urea with 50 mM ammonium bicarbonate solution followed by reduction with 5 mM DTT, alkylation with 20 mM IAA, and digestion with 2 µg of trypsin enzyme overnight at 37 °C with rotation. The digested peptides were purified using a C-18 solid-phase extraction cartridge and finally reconstituted in 30% acetonitrile in water with 5% formic acid and 3% DMSO for LC-MS/MS analysis. Based on our previous study[95], twenty-four proteins were selected and analyzed using targeted proteomics (Table S3). The peptide analysis was conducted using an Agilent Polaris 3 C18-Ether column (150×3.0mm, p/n: A2021150X030) coupled with a gradient mobile phase system (A: Water + 0.1% (v:v) formic acid + 3% (v:v) DMSO; B: ACN + 0.1% (v:v) formic acid + 3% (v:v) DMSO)) developed in our previous studies.[63,95] A needle wash with TFE was added between injections to reduce carryover.

4. Statistical analysis and integrated pathway analysis

Partial Least Squares - Discriminant Analysis (PLS-DA) was employed to visualize the separation between different treatment groups.[76] Volcano plots were used to illustrate the relationship between fold changes in metabolites expression and statistical significance (represented by negative logarithm of p-values), to help in pinpointing responsive

metabolites and proteins with significant changes.[92,97] Heatmaps were utilized to display metabolites abundance across different treatments, enabling identification of clusters of metabolites with similar expression profiles and highlighting differences or trends among experimental groups. Fold change bar plots were generated to prioritize metabolites that exhibit substantial changes with a magnitude bigger than 25%. In addition, Venn diagrams were used for visualizing overlaps and differences between different treatment groups. Pathway analysis was performed with identified responsive metabolites and proteins for each treatment using MetaboAnalyst 5.0 coupled with KEGG pathway library. The threshold of impact value calculated from pathway topology analysis (Relative-betweenness Centrality) was set at 0.1 for the identification of perturbed pathways.[35,74] Moreover, a pathway mapping based on KEGG templates was created with responsive metabolites and proteins involved in perturbed pathways to provide a comprehensive visual representation, demonstrating the interplay between responsive metabolites, proteins, and the perturbed pathways and exploring their relationships across different omics layers.

C. Results and discussions

1. Targeted metabolites analysis

A total of 82 metabolites, including 23 amino acids, 15 nucleobase/side/tides, 15 organic acids and phenolics, 13 sugar/sugar alcohol, 8 antioxidants and 8 fatty acids in plants were analyzed by LC-MS/MS for each tissue with different treatments. PLS-DA was employed to analyze the concentration of different metabolites in various tissues across six different treatment groups (Figure 1). Specifically, there was a noticeable and robust separation between the treatment involving Mo exposure through root (represented by yellow dots) and all other treatments across all tissues analyzed. This separation aligns consistently with

patterns observed in previous studies that involved physiological measurements and proteomics analysis in other plant species.[95,35,74] The findings suggest that exposure to Mo via the root system significantly disrupted metabolic regulations at both the proteomic and metabolomic levels. Volcano plots were used to efficiently identify metabolites that display significant changes in expression levels alongside statistical significance across different treatments (Figure 2). Data points were plotted based on their fold change (FC) on the x-axis and their significance level (p-values) on the y-axis. Grey spots indicate data points where the p-values were greater than 0.05, suggesting not statistically significant. Meanwhile, red and blue points denote significant upregulations ($FC \geq 1.25$) and downregulations ($FC \leq 0.75$), respectively. These red and blue points represent alterations in metabolomic expression that were both statistically significant and of biological relevance due to their substantial magnitude. The metabolites corresponding to these red and blue points were filtered as "responsive metabolites" for the respective treatments. Out of the 82 analyzed metabolites, 58 responsive metabolites were identified for Cu treatments, and 71 responsive metabolites for Mo treatments.

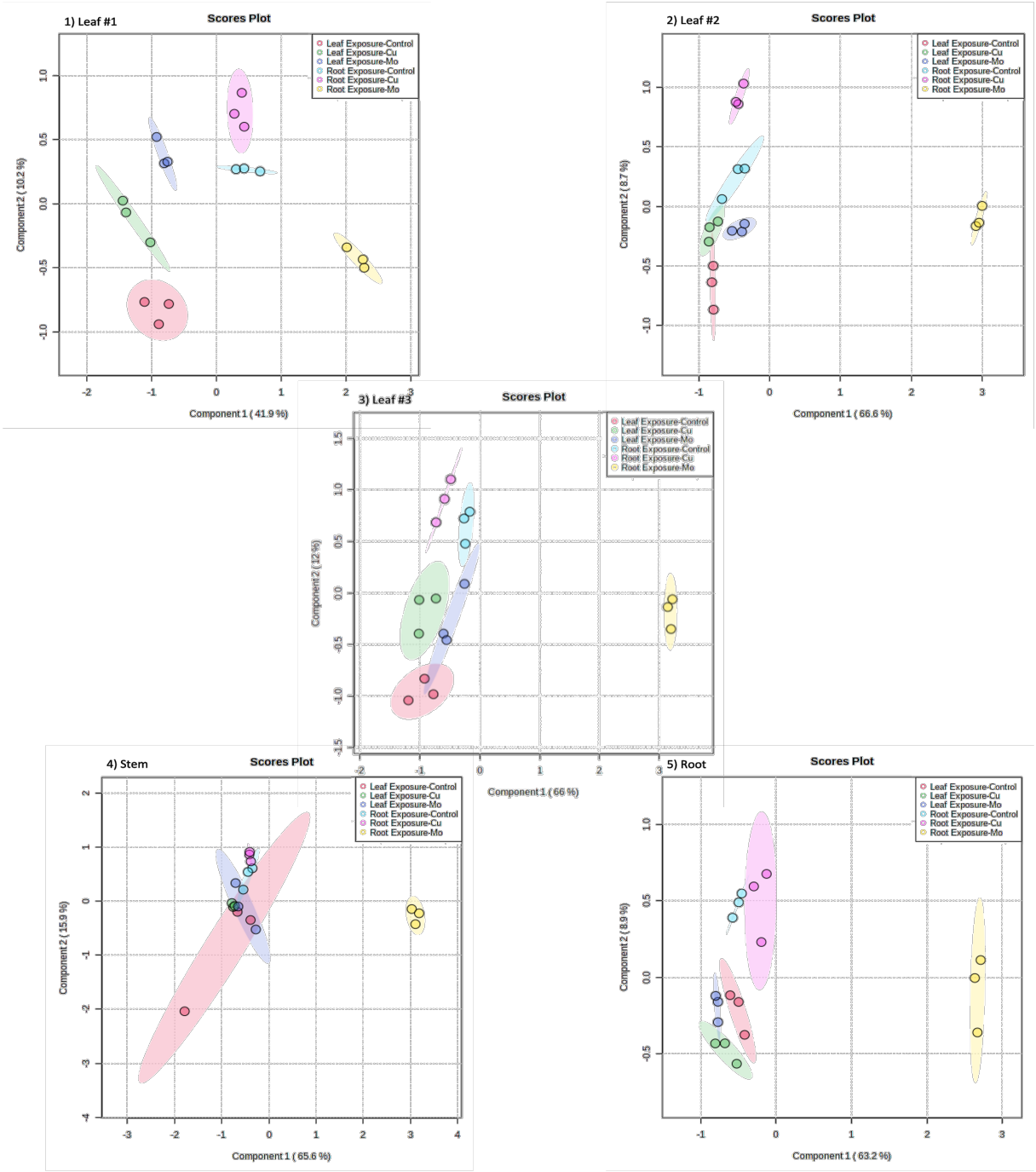

Figure 1. Partial Least Squares Discriminant Analysis (PLS-DA) of metabolite concentrations in each plant tissue with different treatments and exposure routes.

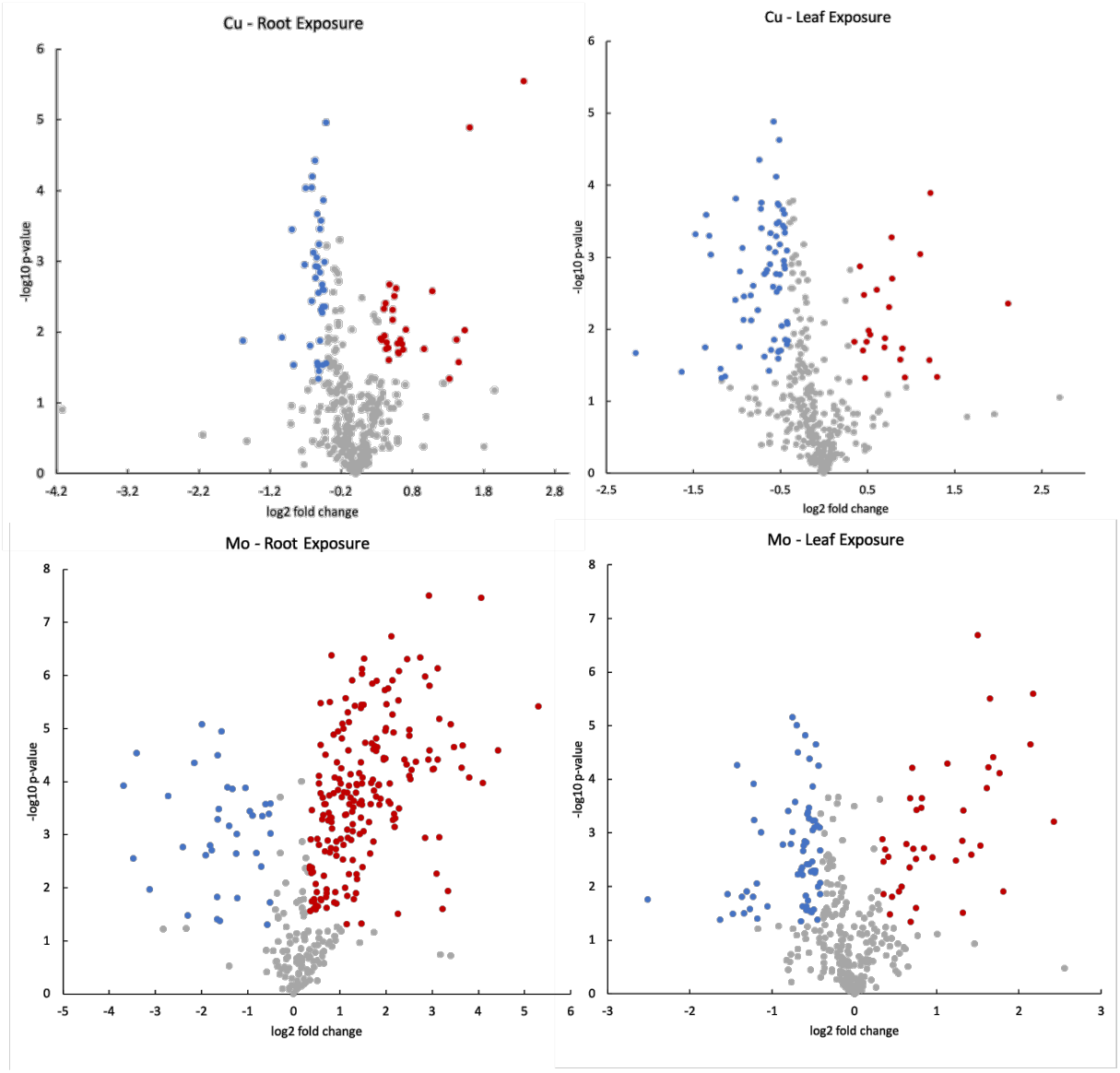

Figurer 2. Volcano plots to visualize the relationship between significance (p-values < 0.05) and fold changes (FC) for each indicated treatment. Grey points: not significant; red points: significant and FC ≥ 1.25; blue color points: FC ≤ 0.75.

Subsequently, a heatmap was generated to visualize the concentrations of these responsive metabolites across different tissues for Cu treatments (Figure 3A) and Mo treatments (Figure 3B). There were 58 responsive metabolites identified for Cu exposure and 71 for Mo exposure. The heatmap depicts a tissue-specific distribution of responsive

metabolites under both Cu and Mo treatments, suggesting distinct preferences for the accumulation of different metabolite groups in specific plant tissues. In general, Cluster 1, primarily composed of organic acids and fatty acids, indicates a tendency for the accumulation of these metabolites in stem or root tissues. Organic acids and fatty acids are commonly associated with energy storage and structural components in plant biology.[98,99] The functions of these metabolites also aligns to the roles of stem and root tissues in energy storage and structural integrity within the plant's overall physiology.[100] On the other hand, Cluster 2, consisting mainly of sugars and amino acids, demonstrates a preference for accumulation in leaf tissues, particularly in L1 or L3. Sugars and amino acids play crucial roles in various processes vital to plant growth and development, particularly in photosynthesis and protein synthesis. Their abundance in leaves is associated with their essential functions within chloroplasts and the cytosol, which are particularly rich in leaf tissues.[101,102]

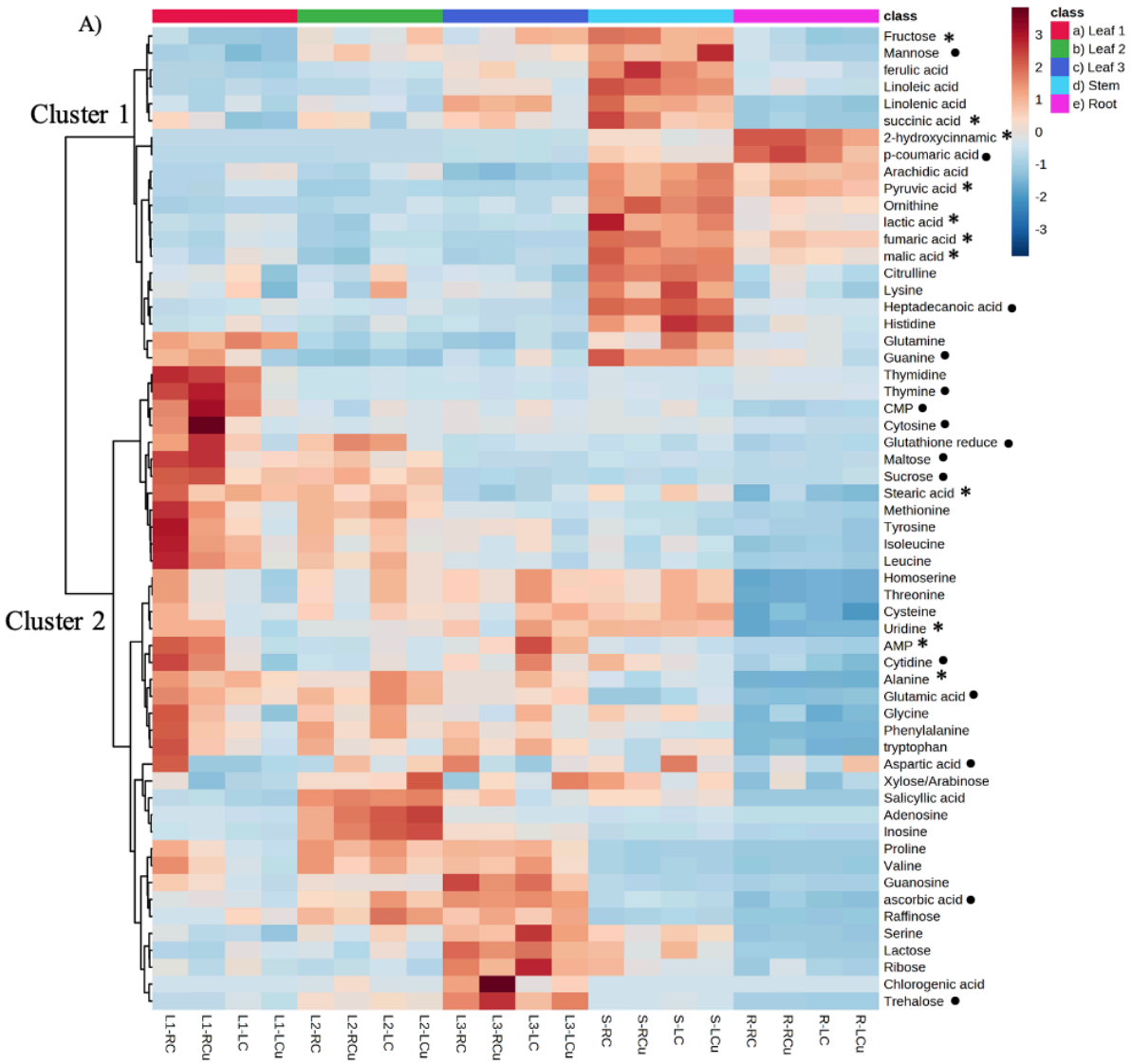
A)
Cluster 1
Cluster 2
class
Fructose ✱
Mannose ●
ferulic acid
Linoleic acid
Linolenic acid
succinic acid ✱
2-hydroxycinnamic ✱
p-coumaric acid ●
Arachidic acid
Pyruvic acid ✱
Ornithine
lactic acid ✱
fumaric acid ✱
malic acid ✱
Citrulline
Lysine
Heptadecanoic acid ●
Histidine
Glutamine
Guanine ●
Thymidine
Thymine ●
CMP ●
Cytosine ●
Glutathione reduce ●
Maltose ●
Sucrose ●
Stearic acid ✱
Methionine
Tyrosine
Isoleucine
Leucine
Homoserine
Threonine
Cysteine
Uridine ✱
AMP ✱
Cytidine ●
Alanine ✱
Glutamic acid ●
Glycine
Phenylalanine
tryptophan
Aspartic acid ●
Xylose/Arabinose
Salicyllic acid
Adenosine
Inosine
Proline
Valine
Guanosine
ascorbic acid ●
Raffinose
Serine
Lactose
Ribose
Chlorogenic acid
Trehalose ●
L1-RC
L1-RCu
L1-LC
L1-LCu
L2-RC
L2-RCu
L2-LC
L2-LCu
L3-RC
L3-RCu
L3-LC
L3-LCu
S-RC
S-RCu
S-LC
S-LCu
R-RC
R-RCu
R-LC
R-LCu
class
a) Leaf 1
b) Leaf 2
c) Leaf 3
d) Stem
e) Root
3
2
1
0
-1
-2
-3

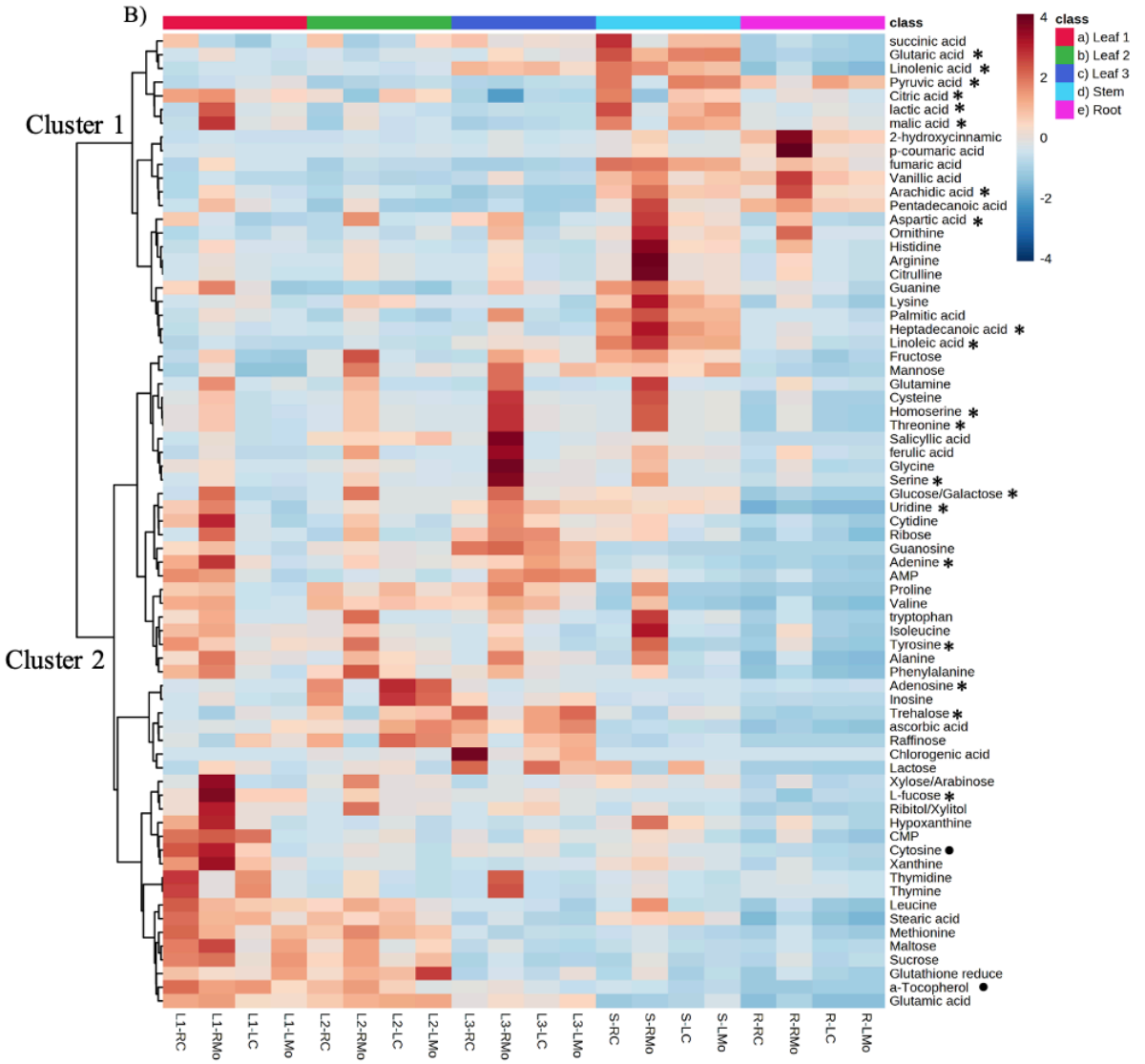

Figure 3. Heatmap of A) 58 responsive metabolites concentrations in different plant tissues with Cu treatments. B) 71 responsive metabolites concentrations in different plant tissues with Mo treatments. L1: leaf #1; L2: leaf #2; L3: leaf #3; S: stem; R: root; RC: root exposure control; LC: leaf exposure control; RCu: Cu exposure through root; LCu: Cu exposure through leaf; RMo: Mo exposure through root; LMo: Mo exposure through leaf. ✱: only responsive through root exposure; ● : only responsive through leaf exposure

The analysis using Venn diagrams showcased the overlaps and unique aspects of responsive metabolites among exposure to Cu and Mo, distinguishing between root and leaf exposures (Figure 4a). Notably, all 58 metabolites that showed responsiveness to Cu exposure were also identified as responsive metabolites in the Mo exposure groups. The

overlap in responsive metabolites between the Cu and Mo exposure groups highlights a shared set of metabolic alterations induced by both Cu and Mo treatments, indicating potential similarities or interactions in their effects on the metabolic pathways. Among the 58 responsive metabolites for Cu exposure, 11 metabolites were responsive solely to root exposure, 15 metabolites were responsive solely to leaf exposure, and 32 metabolites were responsive to both root and leaf exposure. Among the 71 responsive metabolites for Mo exposure, 20 metabolites were responsive solely to root exposure, 2 metabolites (cytosine and a-tocopherol) were responsive solely to leaf exposure, and 49 metabolites were responsive to both root and leaf exposure. The exposure-specific responsive metabolites are labeled on heatmaps (Figure 3), with "∗" as responsive exclusively due to root exposure while labeled with "•" as responsive exclusively due to leaf exposure. Metabolites without symbols were responsive to either root or leaf exposure. Notably, for Mo exposure, the higher number of metabolites specifically responding to root exposure signifies that this exposure route triggers a more active and distinct metabolic response in the plant compared to leaf exposure. This emphasizes the importance of considering exposure route when assessing the effects of agrochemicals, particularly ENMs, on plant metabolomics, as different exposure approaches can lead to varying and distinctive metabolic responses. Another noteworthy observation is that, among the 71 responsive metabolites identified across all treatments, a subset of 25 metabolites demonstrated responsiveness across all different treatments. This group of 25 metabolites comprises 15 amino acids, 4 sugars, 3 nucleobases/nucleosides/nucleotides, 2 phenols and 1 antioxidant, highlining a core set of metabolites that consistently responded across various treatments.

To better understand the tissue-specific response of these metabolites, Venn diagrams were also used to illustrate the responsive metabolites in each tissue for different treatments (Figure 4b-e). In the case of Mo exposure through roots (Figure 4d), among the responsive metabolites identified in different tissues, there were 20 metabolites that displayed responsiveness across every tissue analyzed, including 13 amino acids, 2 fatty acids, 2 antioxidant, 2 phenolics and 1 organic acid. This uniform responsiveness in multiple tissues indicates a potentially systemic or global impact of Mo exposure on plant metabolism across various tissue types.

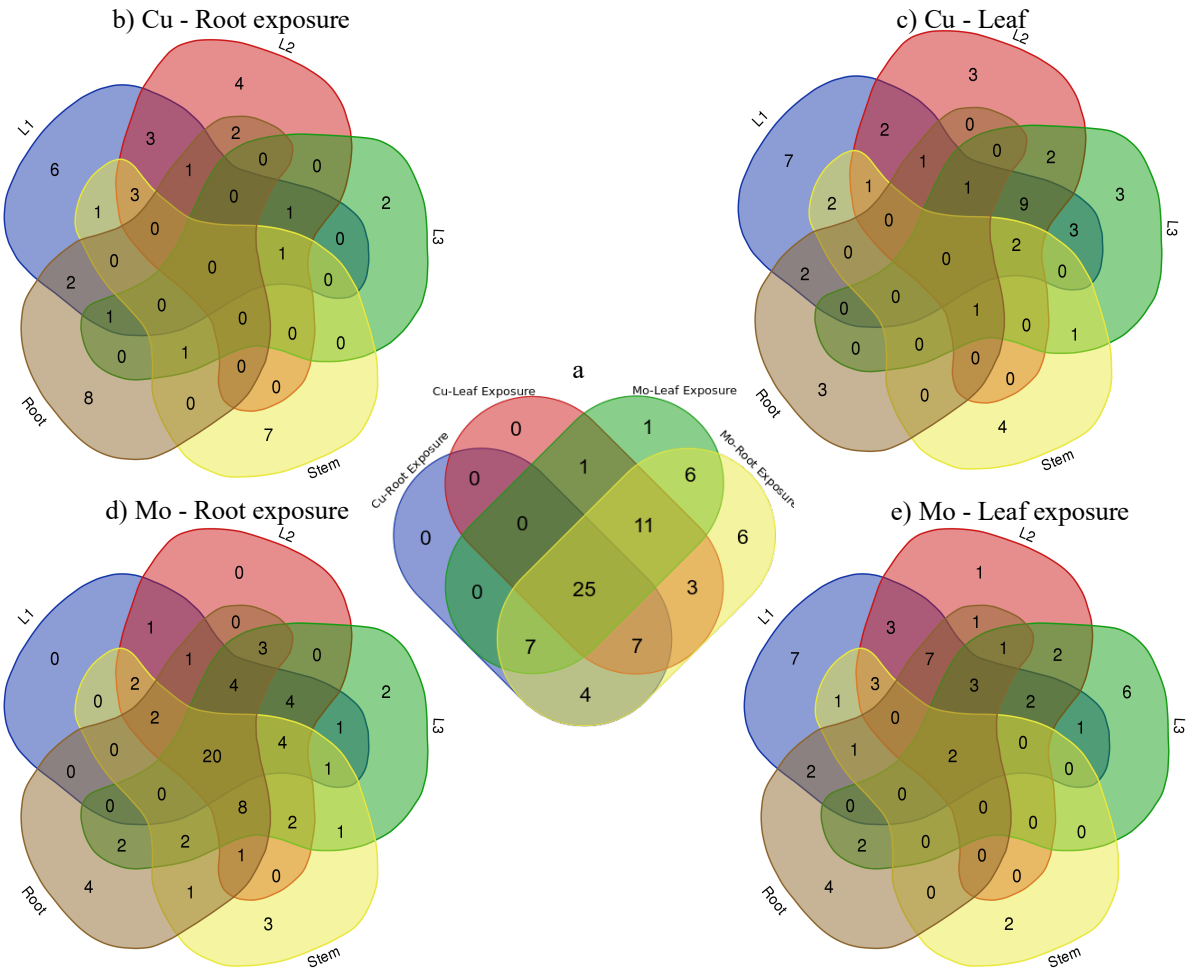

Figure 4. Venn diagram of a) responsive metabolites with Cu and Mo exposure through root and leaf; b) tissue specific distribution of responsive metabolites with Cu exposure through root; c) tissue specific distribution of responsive metabolites with Cu exposure through leaf; d) tissue specific distribution of responsive metabolites with Mo exposure through root; e) tissue specific distribution of responsive metabolites with Mo exposure through leaf.

To delve into the detailed regulation of responsive metabolites across various tissues for each treatment, fold change bar plots categorized by metabolite classes were generated (Figure 5, Figure S3-S5). Among various classes of metabolites, amino acids exhibited the most notable regulations, displaying significant fold changes and involvement across multiple tissues in response to different treatments. Mo exposure through roots resulted in a considerable upregulation ($1.28 \leq FC \leq 39.60$) of all analyzed amino acids across various plant tissues, except for leucine (in L1), methionine (in L1 and L3), and proline (in L2) that exhibited downregulation ($0.52 \leq FC \leq 0.71$) specifically in certain leaf samples under this exposure condition (Figure 5). Since Mo is actively involved in nitrogen metabolism, incorporated into molybdoenzymes to assimilate inorganic nitrogen into organic forms such as amino acids,[85] Mo exposure through roots may enhance the activity of molybdoenzymes and induce the observed upregulation of amino acids. Moreover, the significant alterations in amino acid levels align with their crucial roles in the central metabolism of plants. For example, glutamine, which showed the strongest upregulation ($7.67 \leq FC \leq 39.60$) in all tissues, serves as a nitrogen storage molecule and plays a vital role in nitrogen metabolism.[103] Specifically, during stress conditions, glutamine acts as a vital nitrogen donor, providing readily available nitrogen for protein synthesis and other essential metabolic pathways, to cope with stress-induced changes by supporting crucial cellular processes under adverse conditions.[104] This notable upregulation of glutamine reflects an Mo-induced stress due to the excess molybdenum uptake with root exposure, which aligns with the phytotoxic effect

observed in our previous study.[95] However, the amino acids in plants exposed to Mo via leaves were mostly down regulated ($0.59 \leq FC \leq 0.75$) across different tissues, except for methionine (in L1), cysteine (in L1), alanine (in stem), glutamine (in L1), glutamic acid (in stem) and ornithine (in L1, L2 and L3) that exhibited upregulation ($1.28 \leq FC \leq 3.39$) (Figure S5). These findings highlight contrasting patterns in amino acid regulation depending on exposure route.

In contrast to Mo exposure, Cu exposure through either root or leaf induced downregulation for most of the amino acids (Figure S3-S4). However, ornithine, among all the amino acids studied, stands out as the only one consistently upregulated across all tissues subjected to different Cu and Mo treatments. Ornithine plays a pivotal role in plant metabolism as it stands at the critical juncture of multiple essential metabolic pathways that lead to the production of various crucial compounds functional in several cellular processes related to growth, stress tolerance, and overall plant health.[105] The noteworthy upregulation of ornithine despite the overall downregulation of other amino acids underscores its resilience mechanism, suggesting its involvement in stress adaptation and tolerance. This aligns with a study that indicated accumulation of ornithine delayed the stress- and age-dependent progression of leaf senescence by fueling the TCA cycle.[106]

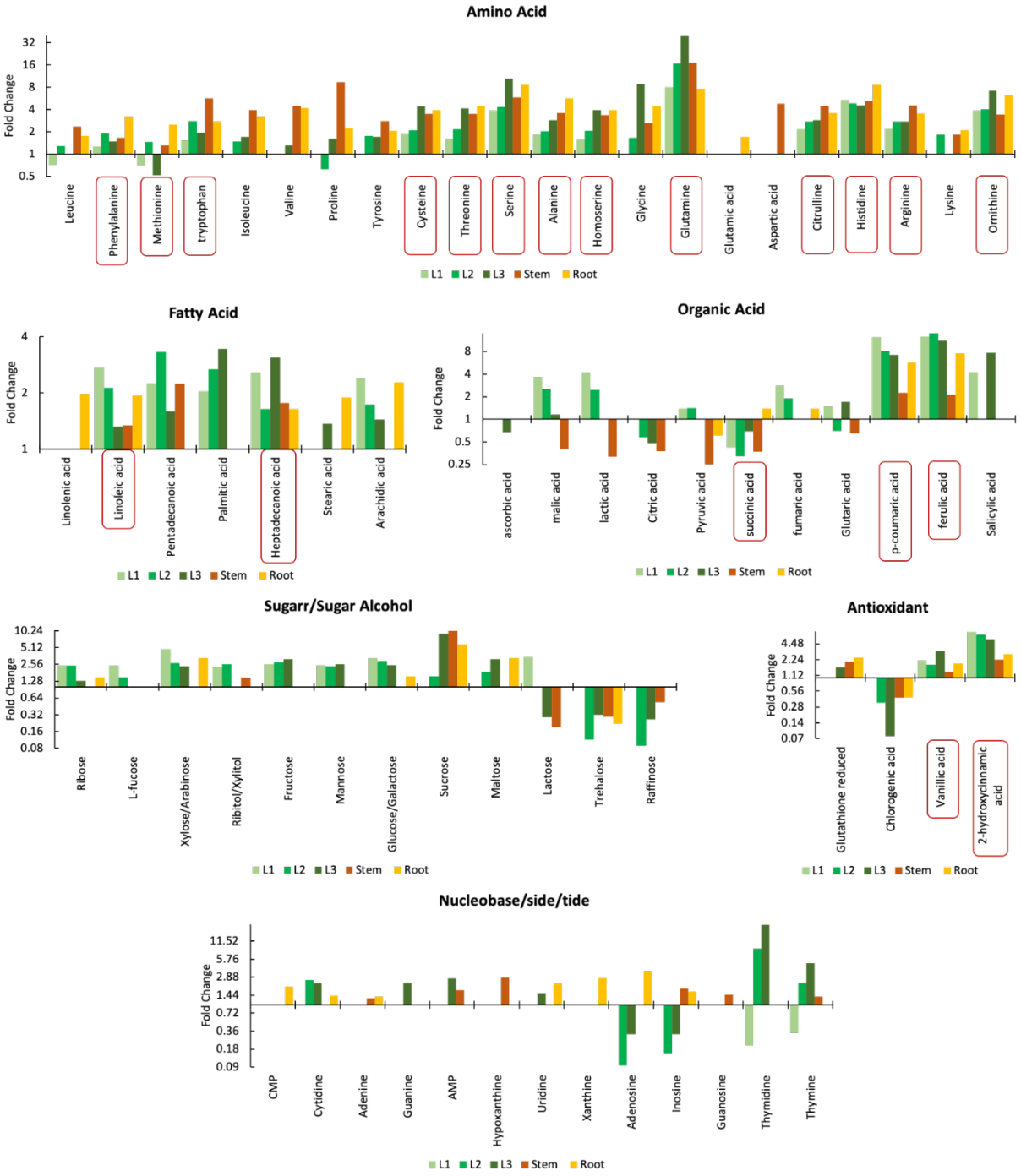

Figure 5. Fold change bar plots of 69 responsive metabolites (grouped by metabolite classes) in different plant tissues with Mo exposure through Root. Metabolites highlighted with red square are the ones responsive across all tissues.

2. Targeted proteomics analysis

Similar to the identification of responsive metabolites, proteins meeting both criteria, significant changes in abundance with a p-value smaller than 0.05 and a fold change of ≥ 1.25 or ≤ 0.75, were identified as "responsive proteins." These proteins were considered to have undergone biologically relevant alterations in their concentrations in response to the experimental treatments. The Venn diagram revealed distinct patterns in the responsiveness of proteins to different exposure treatments of Mo and Cu through root and leaf exposure methods (Figure 6a). For Mo treatments, all 24 proteins analyzed demonstrated responsiveness to Mo exposure through root application. In contrast, only 11 proteins showed responsiveness to Mo exposure through leaf application. This suggests a more limited impact or alteration in the abundance of proteins when Mo was applied through leaves compared to root exposure. For Cu treatments, 19 proteins were responsive when exposed through the root, while 10 proteins showed responsiveness when exposed through the leaf, with 7 proteins shared with root exposure. Notably, 3 proteins related to carbohydrate metabolism (P5-glycolysis cytosolic branch UGPase, P19-fructose-bisphosphate aldolase, and P20-Calvin cycle GAP) exhibited responsiveness across all treatments. The consistent response of these proteins across various treatments implied their significant role in maintaining carbohydrate metabolism under different environmental conditions or treatments. The regulation of these proteins may be a plant's way of adapting its carbohydrate metabolism to optimize energy production, carbon fixation, or storage based on changing environmental cues or stressors.

Moreover, the tissue-specific distribution of responsive proteins reveals distinct patterns in their presence across different plant parts under Cu and Mo treatments through root and

leaf exposure routes. For Cu exposure through roots, the responsive proteins predominantly appeared in L1 (13 proteins), followed by the stem (7 proteins), and fewer in the roots (3 proteins) (Figure 6b). On the other hand, Cu exposure through leaf showed a different distribution- 9 responsive proteins were observed in L1, with 4 shared proteins in L2, and one protein each in the stem and roots (Figure 6c). This indicates a stronger impact on protein abundance in the early emerged leaves compared to other tissues when Cu was applied, especially via the roots. Interestingly, under Mo treatments through root exposure, the responsive proteins were present in every tissue (Figure 6d). However, when Mo was applied through leaf exposure, the responsive proteins were absent in L3 (Figure 6e). The absence of responsive proteins in L3 (the last emerged leaf) for leaf exposure treatments with both Cu and Mo might be anticipated due to the shorter duration of exposure experienced by this leaf compared to the other tissues. The metabolic responses at the protein level might not have been fully induced or manifested within this shorter exposure timeframe.

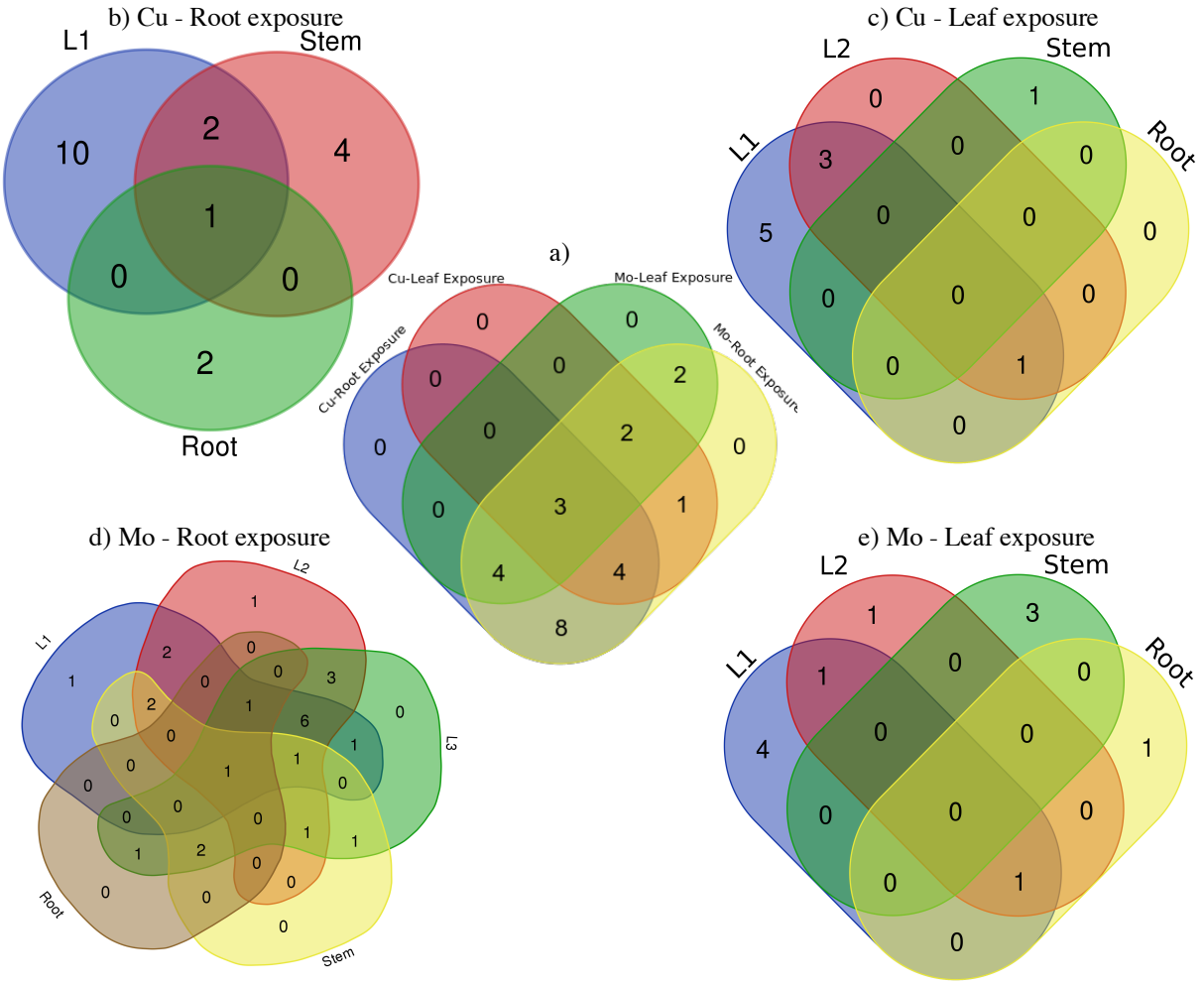

Figure 6. Venn diagram of a) responsive proteins with Cu and Mo exposure through root and leaf; b) tissue specific distribution of responsive proteins with Cu exposure through root; c) tissue specific distribution of responsive proteins with Cu exposure through leaf; d) Tissue specific distribution of responsive proteins with Mo exposure through root; e) tissue specific distribution of responsive proteins with Mo exposure through leaf.

The detailed fold changes of responsive proteins in different treatments were visualized in bar plots, delineating tissue-specific responses (Figure S6). An observation similar to the metabolomics data emerged: Mo exposure through the root exhibited the most pronounced perturbations among the treatments, primarily characterized by upregulation trends, indicating an increased biosynthesis or accumulation of these proteins in response to the treatment. The aligned upregulation observed in both amino acids at the metabolomics level

and proteins at the proteomics level indicates a significant interplay and interconnectedness between metabolomic and proteomic perturbations in the plant's response to the treatments. For instance, in the case of Mo exposure through root, the upregulation of specific amino acids provides the necessary building blocks for the increased synthesis of particular proteins. Simultaneously, the increased expression of these proteins enhances the assimilation of nitrogen, contributing to the elevated production of amino acids. This coordinated response indicates a potential bidirectional relationship, where changes in metabolite concentrations, such as amino acids, can influence or contribute to the modulation of protein expression levels, and conversely, alterations in protein expression can, in turn, impact the metabolic pathways involved, establishing a dynamic proteomic-to-metabolic-to-proteomic relationship.

3. Integrated pathway analysis

The joint pathway analysis using MetaboAnalyst 5.0, integrated with the KEGG pathway library, was conducted with the identified responsive metabolites and proteins. The analysis aimed to assess the impact of Cu and Mo treatments on metabolic pathways, considering both metabolomic and proteomic data. The threshold for impact value, determined through pathway topology analysis (Relative-betweenness Centrality), was established at 0.1, the cutoff point for identifying perturbed pathways based on their significance and relevance within the dataset.11 Perturbed pathways resulting from the treatments are organized and presented in Table S4 for Cu treatments and Table S5 for Mo treatments. These tables specified the perturbations observed in different tissues, offering a detailed breakdown of how these treatments influenced specific metabolic pathways across various plant tissues. The responsive metabolites and proteins involved in the perturbed pathways are also

indicated in the tables, with root exposure exclusive (bold) or leaf exposure exclusive (underline) indicated.

The analysis identified a total of 23 perturbed pathways across all treatments, categorized into 6 metabolic categories: amino acid metabolism (10 pathways), biosynthesis of secondary metabolites (4 pathways), carbohydrate metabolism (5 pathways), lipid metabolism (2 pathways), nucleotide metabolism (1 pathway) and translation (1 pathway) (Table S4, S5). Further insights from the Venn diagram (Figure 7) revealed differential and overlapping pathway perturbations for Mo and Cu exposures through root and leaf routes. For Mo treatments, exposure through roots involved perturbations across all 23 identified pathways while exposure through leaves affected 15 out of the 23 pathways. For Cu exposure, root and leaf exposure perturbed 22 of the 23 pathways, with 14 pathways shared and 4 pathways exclusively through either root or leaf exposure. Ten pathways were consistently perturbed across all four treatments: 8 related to amino acid metabolism (alanine, aspartate and glutamate metabolism, arginine biosynthesis, tryptophan metabolism, cysteine and methionine metabolism, phenylalanine metabolism, glycine, serine and threonine metabolism, arginine and proline metabolism, tyrosine metabolism), 1 associated with the biosynthesis of secondary metabolites (stilbenoid, diarylheptanoid and gingerol biosynthesis), and 1 in carbohydrate metabolism (glyoxylate and dicarboxylate metabolism). Purine metabolism, a nucleotide metabolism pathway, was perturbed only by Mo exposure (both root and leaf routes). Additionally, 3 carbohydrate metabolism related pathways (pyruvate metabolism, citrate cycle (TCA cycle), and glycolysis/gluconeogenesis) and 1 amino acid metabolism pathway (valine, leucine and isoleucine biosynthesis) were perturbed only through root exposure, either with Cu or Mo. These findings highlight the complexity

and specificity of the metabolic responses to different treatments. The shared perturbed pathways between Mo and Cu exposure methods suggest commonalities in their effects on metabolic pathways, while specific pathway perturbations indicate distinct impacts of each treatment method on the plant's metabolic networks. In addition, the tissue-specific analysis revealed a noteworthy observation regarding the perturbed pathways in response to Mo exposure through the roots (Figure 7d). For plants subjected to this treatment, 12 pathways showed perturbations consistently across all tissues, which were driven by the responsive metabolites identified. The consistent perturbations across various plant tissues indicates uniformity in the tissue-specific distribution of responsive metabolites under this treatment, which might serve as a driving factor behind the synchronized perturbations observed in those pathways.

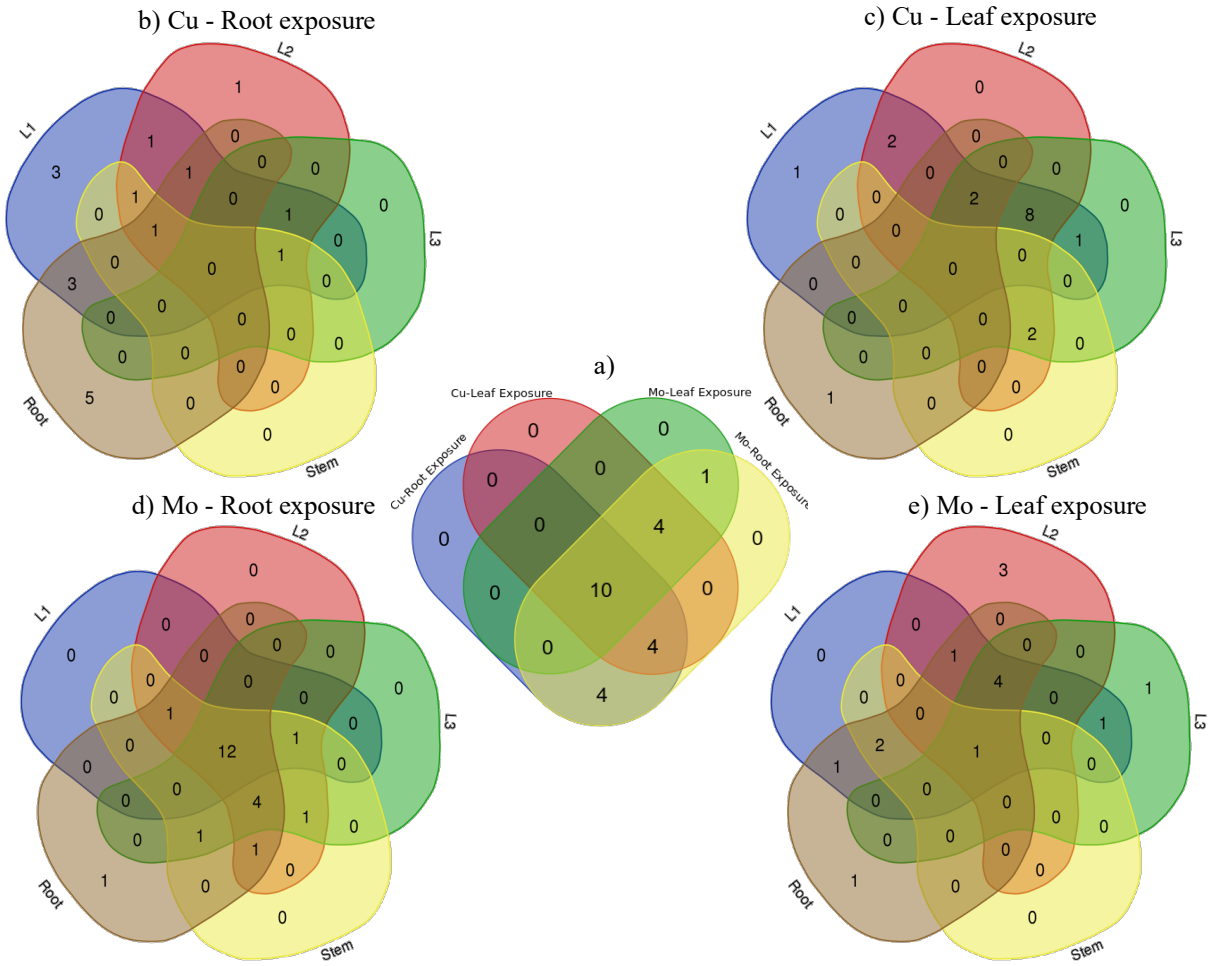

Figure 7. Venn diagrams of a) perturbed pathways with Cu and Mo exposure through root and leaf; b) tissue specific distribution of perturbed pathways with Cu exposure through root; c) tissue specific distribution of responsive metabolites with Cu exposure through leaf; d) tissue specific distribution of perturbed pathways with Mo exposure through root; e) tissue specific distribution of perturbed pathways with Mo exposure through leaf.

Finally, pathway mapping was visualized based on KEGG pathway templates, indicating responsive metabolites and proteins on perturbed pathways across all treatments (Figure 8). The map integrates responsive metabolites and proteins to illustrate their involvement in various metabolic pathways and processes affected by the treatments. While some responsive proteins weren't directly associated with the perturbed pathways identified through joint pathway analysis, they were labeled in green on the map, including 6 proteins actively

involved in photosynthesis and energy metabolism. Amino acid metabolism related pathways were most significantly perturbed, especially considering their involvement in various other crucial metabolic processes, such as the TCA cycle and the electron transport chain. For example, amino acids can be converted into intermediates of the TCA cycle, such as pyruvate and oxaloacetate.[107] This allows them to contribute to energy production through oxidative phosphorylation. The TCA cycle also provides intermediates for amino acid biosynthesis, demonstrating a two-way interaction between these pathways. In addition, through amino acid catabolism, NADH can donate electrons to the electron transport chain, and ultimately generates ATP, the primary energy currency of the cell. In turn, the electron transport chain also plays a crucial role in maintaining cellular redox balance, which is essential for proper amino acid metabolism.[107] This highlights the crucial role amino acids play in maintaining overall cellular function and metabolism. In addition, the observed upregulation of responsive proteins primarily associated with amino acid metabolism could indeed offer an explanation for the active alterations in amino acid levels within the tissues. This interconnectedness between proteins and metabolites in amino acid metabolism highlights their intricate regulatory roles in shaping cellular metabolism and energy production, emphasizing their significance in the plant's adaptive responses to different treatments.

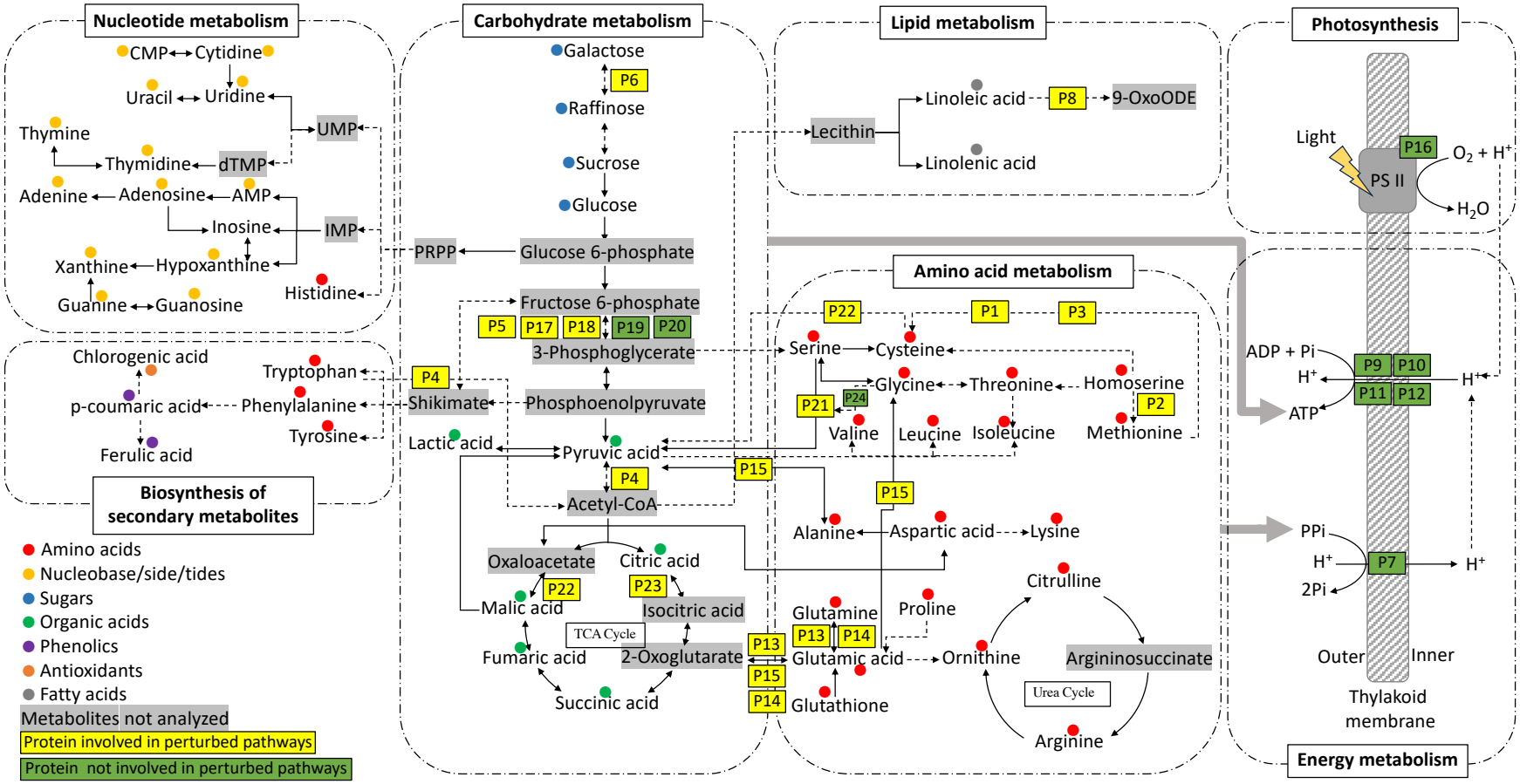

Figure 8. Pathway mapping of responsive metabolites and proteins based on KEGG.

4. Dose specific regulation

Due to the reported yellowing and stunted growth caused by excess intake of Mo through root exposure at 6.25 mg/plant dose, an additional lower dose (0.6 mg/plant) that more closely represents the field dose recommendation was added to our experiment for targeted metabolomics and proteomics analysis.[95] The PLS-DA analysis (Figure S7) indicated clear separations in metabolite concentrations within plant tissues exposed to high and low doses of Mo through root intake. This separation suggests distinct metabolic responses induced by different doses of Mo exposure. Although there was a significant overlap in responsive metabolites for Mo exposure through roots at high and low doses (66 responsive metabolites overlapped) (Figure S8B), the regulation patterns differed significantly between the two doses. For instance, at the low dose, compared to the control group where no Mo was introduced during plant growing, there was a prevalence of downregulation for amino acids (Figure S9A), especially isoleucine ($0.03 \leq FC \leq 0.08$), proline ($0.04 \leq FC \leq 0.72$), citrulline ($0.27 \leq FC \leq 0.43$), arginine ($0.30 \leq FC \leq 0.47$), and lysine ($0.23 \leq FC \leq 0.52$), in contrast to the upregulation observed at the high Mo dose. In addition, organic acids (low Mo dose: upregulation $FC \leq 27.91$, down regulation $FC \geq 0.04$; high Mo dose: upregulation $FC \leq 13.97$, down regulation $FC \geq 0.25$), antioxidants (low Mo dose: upregulation $FC \leq 17.33$, down regulation $FC \geq 0.15$; high Mo dose: upregulation $FC \leq 7.61$, down regulation $FC \geq 0.08$), and sugars (low Mo dose: upregulation $FC \leq 41.22$, down regulation $FC \geq 0.34$; high Mo dose: upregulation $FC \leq 10.20$, down regulation $FC \geq 0.09$) groups exhibited more pronounced regulations with the low dose (Figure S9A) compared to the high dose (Figure 5). These findings highlight the dose-dependent variations in the plant's metabolic response to Mo exposure through the roots. Similar to responsive metabolites, the responsive proteins

were mainly overlapped as well (23 out of 24), with an exception of aminotransferases peroxisomal (P 15) which was solely responsive to high dose. The overlapped responsive proteins induced differential regulation patterns with different dose. For example, glutamate dehydrogenase (P13) showcased downregulations ($0.13 \leq FC \leq 0.54$) with low dose while upregulations ($1.38 \leq FC \leq 1.63$) with high dose (Figure S9B). This provides a striking example of how different doses can elicit opposite regulatory responses in this enzyme. This contrasting regulation of P13 likely leads to distinct changes in its catalytic activity and, subsequently, influences the conversion of glutamate.[108] The magnitude of upregulation for glutamine (a product from glutamate) observed between high dose ($7.67 \leq FC \leq 39.60$) and low dose ($1.50 \leq FC \leq 1.95$) treatments could be attributed to these divergent expression patterns of glutamate dehydrogenase. These differences in pathway regulation provide a potential explanation for the varied growth response of plants subjected to different dose treatments of Mo.

D. Conclusions

The multi-omics investigation into the effects of Mo and Cu based ENMs exposure on plant metabolomics and proteomics with targeted analysis approaches presented a multi-layered understanding of the intricate responses within different tissues, doses, and exposure routes. The joint pathway analysis unveiled 23 perturbed pathways across all treatments. Notably, Mo exposure through roots impacted all identified pathways, with 12 pathways consistently perturbed across all tissues. In contrast, Mo exposure through leaves influenced 15 pathways, with only one pathway shared across all tissues. This underscores the significant influence of the exposure route and highlights the tissue-specific inducement of metabolic and proteomic responses in the plant's reaction. In addition, pathway mapping

visualized the involvement of responsive metabolites and proteins in perturbed pathways across all treatments, emphasizing the significance of amino acid metabolism. The observed upregulation of proteins associated with amino acid metabolism explained alterations in amino acid levels, highlighted a dynamic proteomic-to-metabolic-to-proteomic relationship, suggested an intricate interplay between metabolomic and proteomic responses. Metabolites also showcased distinct tissue preferences, with organic acids and fatty acids more prevalent in stem or root tissues, while sugars and amino acids were abundant in leaves, emphasizing their roles in energy storage, structural integrity, photosynthesis, and protein synthesis. Notably, the contrasting expression changes of key enzymes, exemplified by the case of glutamate dehydrogenase (P13), between different doses of Mo through root exposure highlighted dose-dependent regulatory patterns in enzymes and metabolites.

In summary, this extensive multiomics analysis provides invaluable insights into the intricate and interconnected mechanisms governing plant responses to Mo and Cu based ENMs exposure. The tissue-specificity, exposure methods and dose dependencies, and pathway perturbations uncovered here contribute significantly to understanding plant metabolism under various stress conditions, offering crucial guidance for agricultural practices, environmental safety, and further research on nanomaterial impacts on plants.

E. Acknowledgements

This work was supported by the National Science Foundation (NSF) under cooperative agreement number NSF-1901515. Arturo A. Keller would like to give special thanks to Agilent Technologies for their Agilent Thought Leader Award. Any findings and conclusions from this work belong to the authors and do not necessarily reflect the view of NSF.

F. Appendix

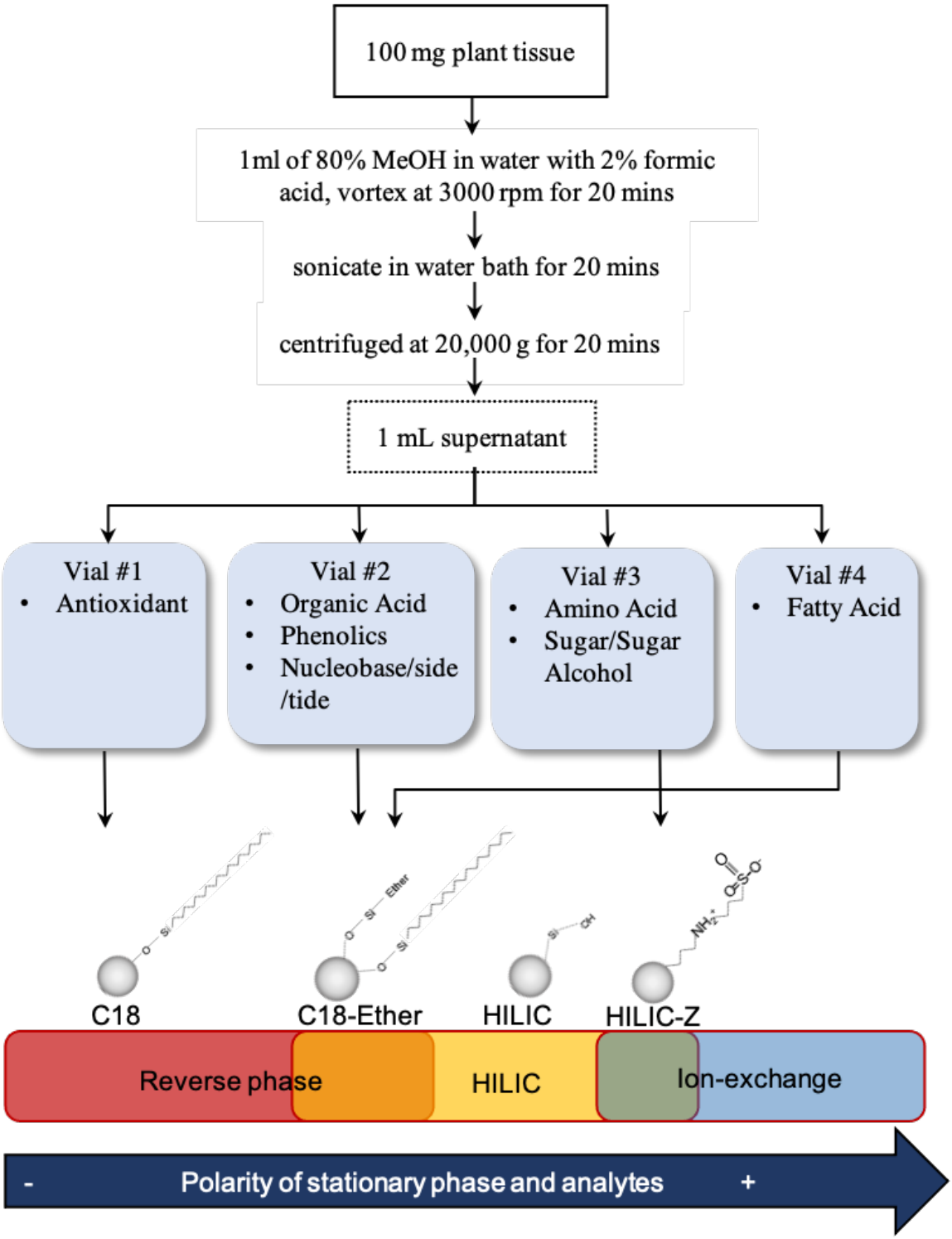

Figure S1. Flowchart of sample preparation for targeted metabolomics analysis.

Chromatogram –Antioxidant

HPLC Conditions	
Column	Agilent ZORBAX StableBond 80 ÅC18 4.6 mm × 50 mm, 3.5 µm (p/n: 835975-902)
Mobile phase A	0.1% formic acid with 5 mM ammonium formate in water
Mobile phase B	Methanol
Flow rate	0.50 mL/min
Column temp.	30 °C
Injection volume	10 µL
Total run time	13.5 minutes
Gradient	Time (min) %B 0 2 1.0 2 6.0 100 9.0 100 10.0 2 13.5 2
MS Conditions	
Ionization mode	ESI Positive/Negative
Gas temp.	230 °C
Gas flow	10.0 L/min
Nebulizer	20 psi
Sheath gas temp.	400 °C
Sheath gas flow	10 L/min
Capillary voltage	5,000 V Positive; 2,500 V Negative
Nozzle voltage	1,300 V Positive; 0 V Negative

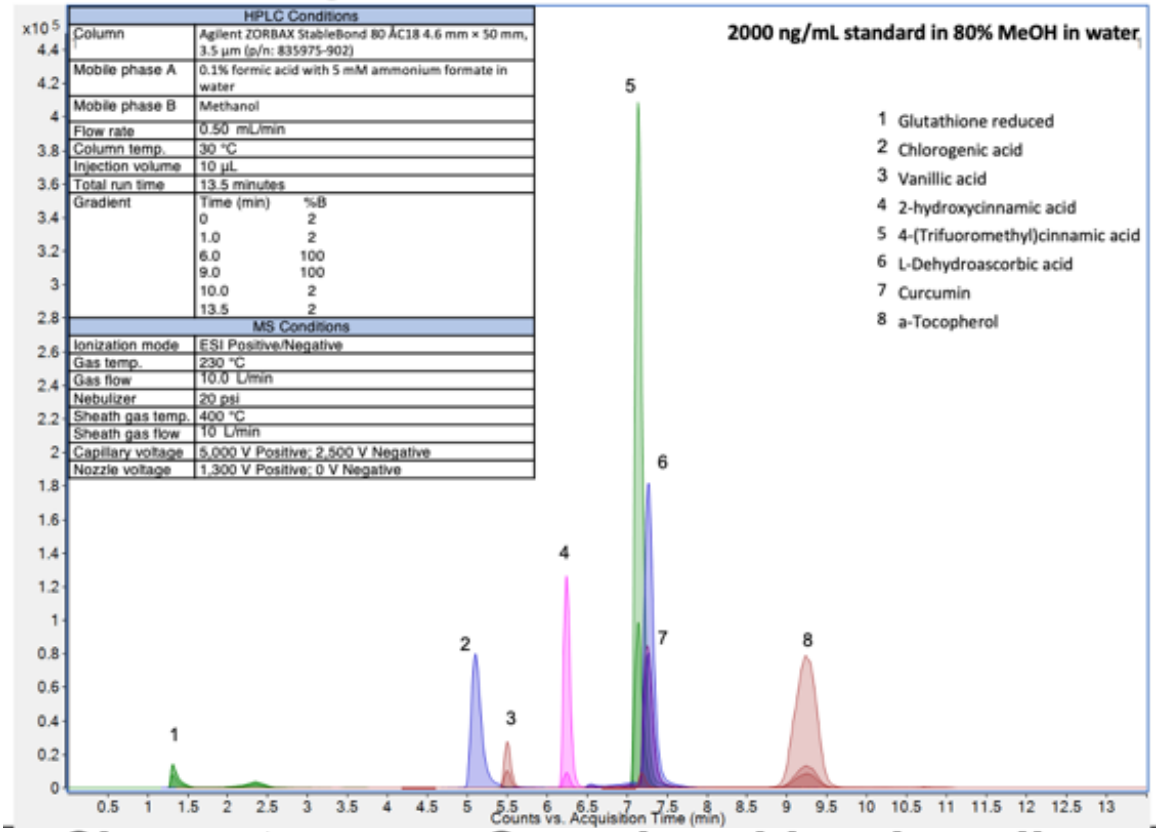

Chromatogram - Organic acids, phenolics

HPLC Conditions	
Column	Agilent Polaris 3 C18-Ether 150x3.0mm (p/n:A2021150X030)
Mobile phase A	Water + 0.1% formic acid
Mobile phase B	Methanol + 0.1% formic acid
Flow rate	0.40 mL/min
Column temp.	30 °C
Injection volume	2 µL
Total run time	12 minutes
Gradient	Time (min) %B 0 30 0.5 80 5.0 80 5.01 30
MS Conditions	
Ionization mode	ESI Negative
Gas temp.	230 °C
Gas flow	10.0 L/min
Nebulizer	40 psi
Sheath gas temp.	400 °C
Sheath gas flow	10 L/min
Capillary voltage	2,500 V
Nozzle voltage	0 V

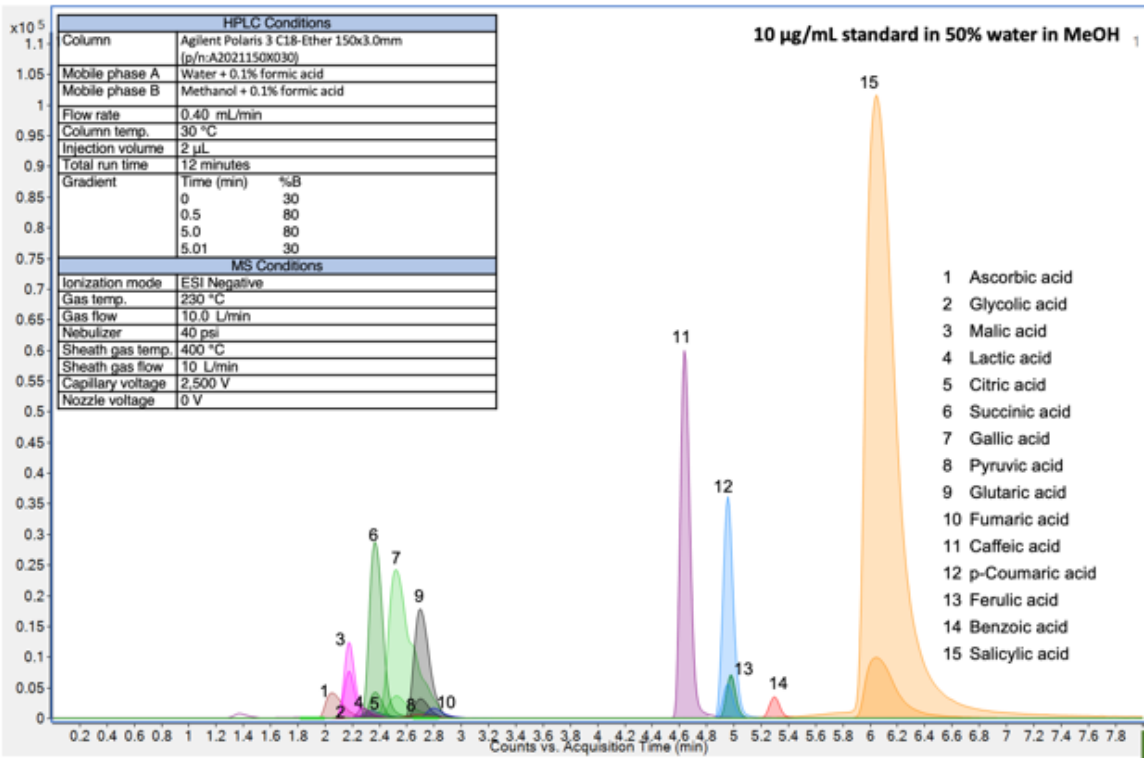

Chromatogram – Nucleobase/side/tide

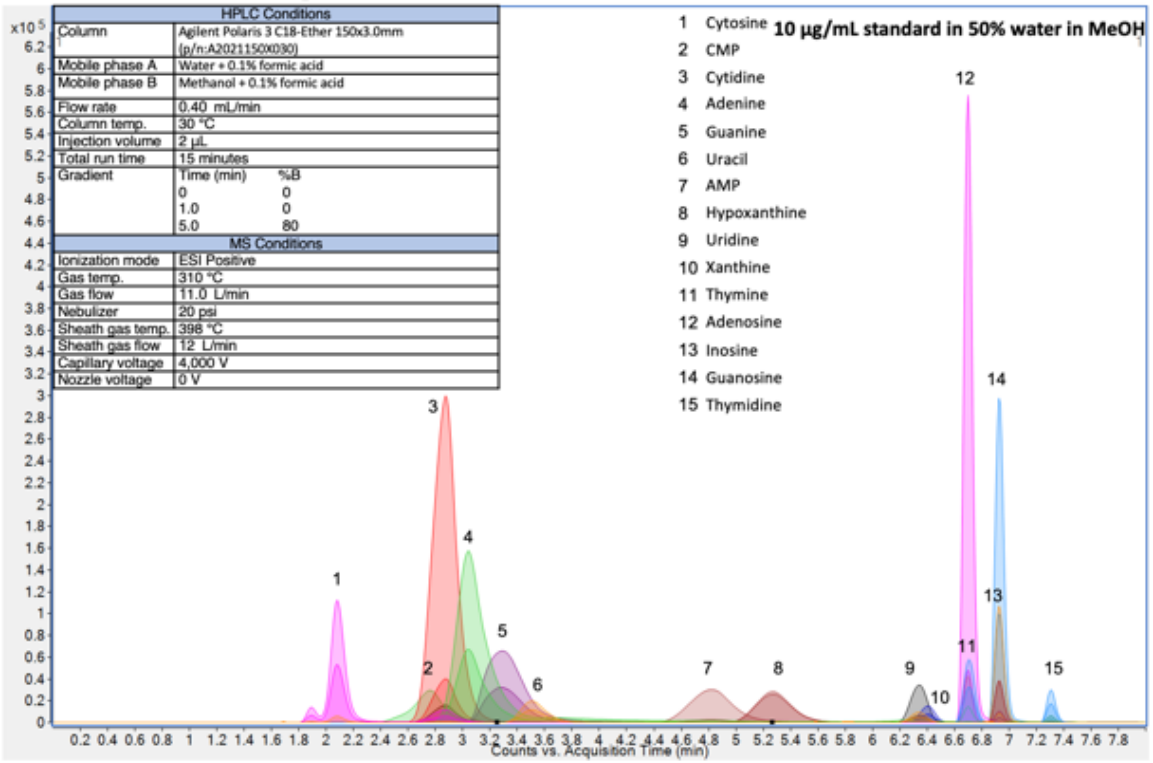

Chromatogram – Sugar, sugar alcohol

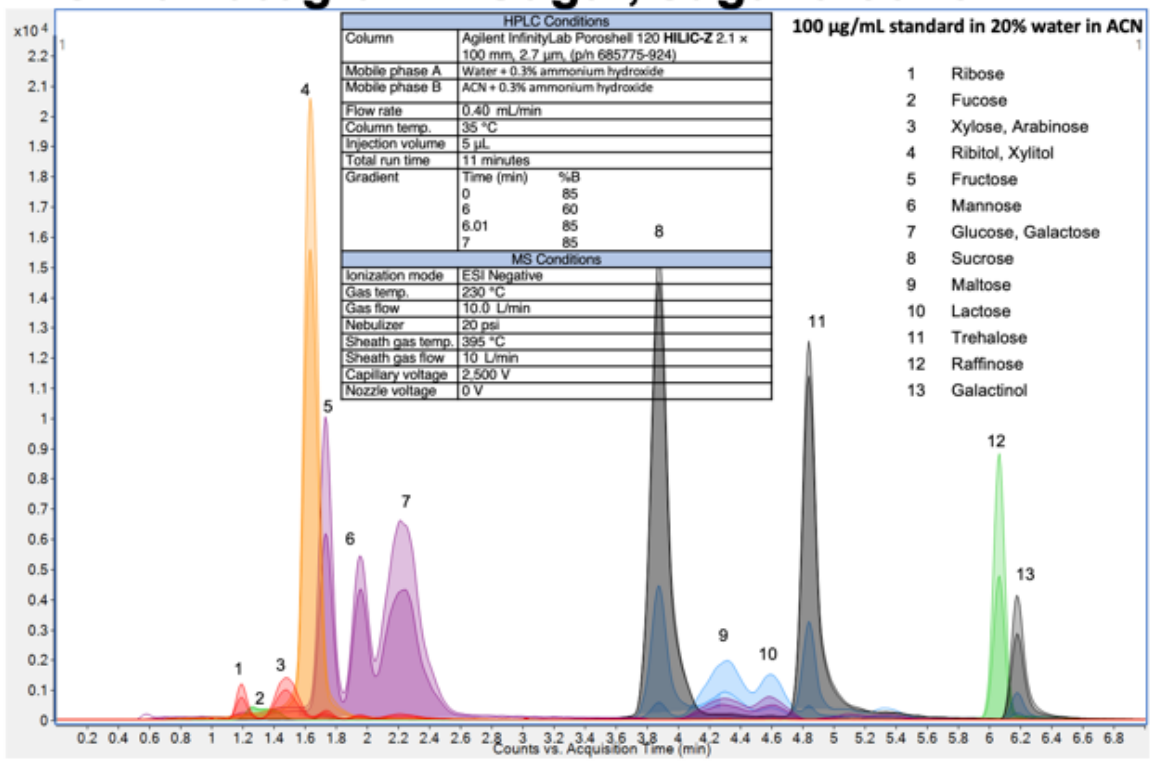

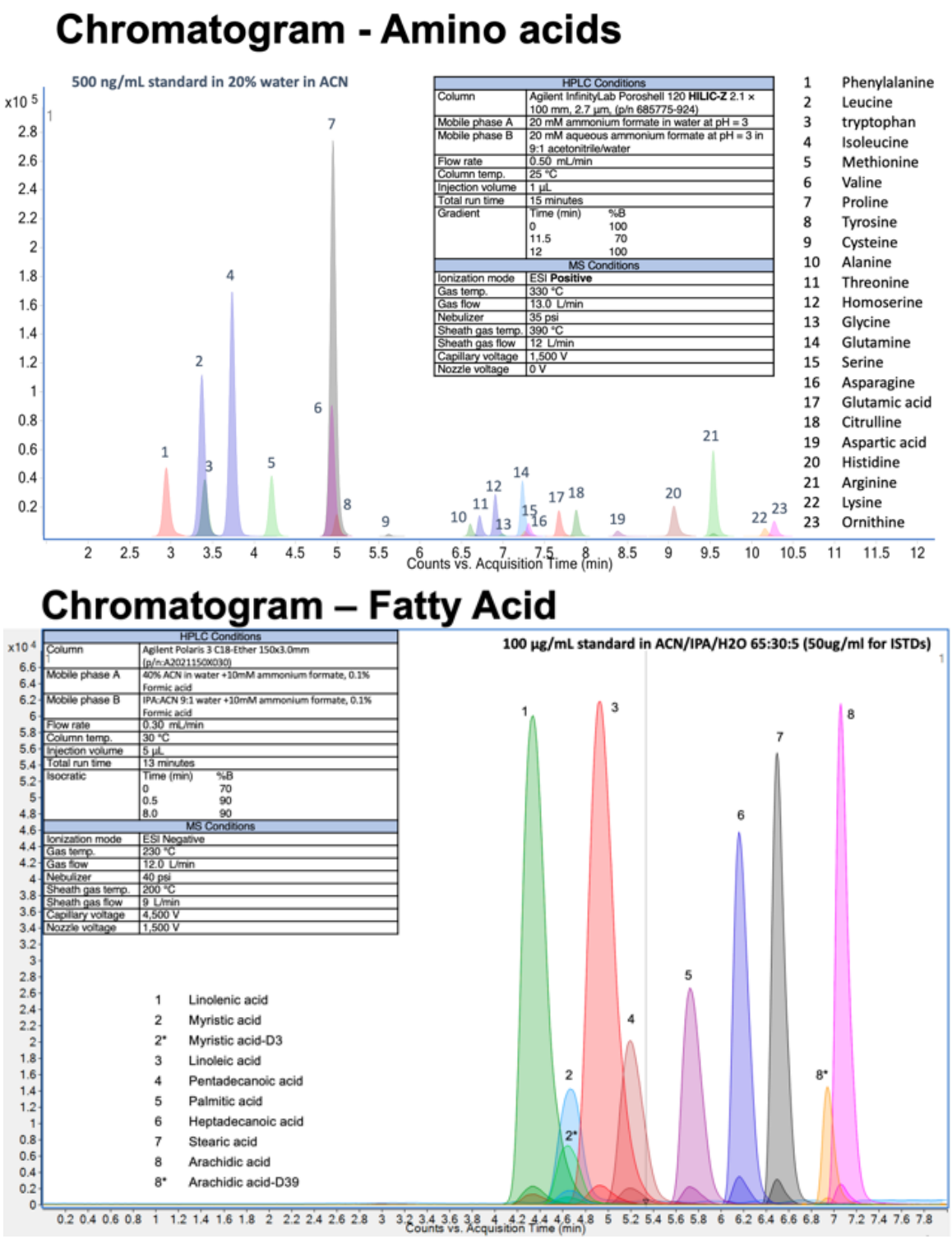

Figure S2. LC-MS/MS chromatograph of 6 groups of metabolites.

Table S1. Metabolite analytes grouped in vials with reconstitution solvent and LCMS column/mobile phase information.

Vial #	Analytes	Sample solvent	LCMS column	Mobile phase A	Mobile phase B	LOD	MDL
1	**Antioxidants**					**(ng/mL)**	**(ng/g)**
	Glutathione reduced					0.05	0.5
	Chlorogenic acid					0.005	0.05
	Vanillic acid	80% MeOH in water	Agilent ZORBAX StableBond 80 ÅC18 4.6 mm × 50 mm, 3.5 µm	0.1% formic acid with 5 mM ammonium formate in water	Methanol	0.6	6
	2-hydroxycinnamic acid					0.005	0.05
	4-(Trifuoromethyl)cinnamic acid					0.001	0.01
	L-Dehydroascorbic acid					0.01	0.1
	Curcumin					0.004	0.04
	a-Tocopherol					500	5000
2	**Organic Acid**					**(ug/mL)**	**(ug/g)**
	glycolic acid					4.60	46.02
	malic acid					0.52	5.16
	Citric acid					3.39	33.94
	lactic acid					6.39	63.92
	succinic acid	50% MeOH in water	Agilent Polaris 3 C18-Ether 150x3.0mm	0.1% formic acid in water	0.1% formic acid in MeOH	0.38	3.82
	Pyruvic acid					6.79	67.85
	Glutaric acid					2.85	28.46
	fumaric acid					0.35	3.52
	ascorbic acid					6.79	67.93
	Caffeic acid					0.58	5.79
	ferulic acid					0.34	3.40
	benzoic acid					0.81	8.10
2	**Phenolics**					**(ug/mL)**	**(ug/g)**
	Gallic acid	50% MeOH in water	Agilent Polaris 3 C18-Ether 150x3.0mm	0.1% formic acid in water	0.1% formic acid in MeOH	1.61	16.10
	p-Coumaric acid					0.342	3.42
	Salicylic acid					0.346	3.46
2	**Nucleobase/side/tide**					**(ug/mL)**	**(ug/g)**
	Cytosine					0.87	8.72
	CMP					0.32	3.22
	Cytidine					2.90	29.00
	Adenine					0.70	6.98
	Guanine					0.64	6.43
	uracil					0.66	6.56
	AMP	50% MeOH in water	Agilent Polaris 3 C18-Ether 150x3.0mm	0.1% formic acid in water	0.1% formic acid in MeOH	0.33	3.26
	Hypoxanthine					0.23	2.27
	Uridine					0.90	8.99
	Xanthine					0.26	2.62
	Adenosine					2.50	25.04
	Thymine					1.55	15.50
	Guanosine					2.79	27.92
	Inosine					0.58	5.78
	Thymidine					0.41	4.10
3	**Amino Acids**					**(ng/mL)**	**(ng/g)**
	Phenylalanine					0.50	5.00
	Leucine					0.01	0.05
	tryptophan	80% ACN in water	Agilent InfinityLab Poroshell 120 HILIC-Z 2.1 × 100 mm, 2.7 µm	water +10% stock (Stock: 200 mM ammonium formate in water	ACN+ 10% stock	0.01	0.05
	Isoleucine					0.01	0.05
	Methionine					0.05	0.50
	Valine					0.40	4.00
	Proline					1.00	10.00
	Tyrosine					0.15	1.50

	Cysteine			with formic acids adjusted pH = 3		5.00	50.00
	Alanine					0.01	0.05
	Threonine					0.40	4.00
	Homoserine					0.15	1.50
	Glycine					15.00	150.00
	Glutamine					0.50	5.00
	Serine					10.00	100.00
	Asparagine					1.00	10.00
	Glutamic acid					0.01	0.05
	Citrulline					0.15	1.50
	Aspartic acid					0.01	0.05
	Histidine					0.25	2.50
	Arginine					0.01	0.10
	Lysine					0.01	0.05
	Ornithine					0.01	0.10
3	**Sugar/Sugar Alcohols**					**(ug/mL)**	**(ug/g)**
	Ribose	80% ACN in water	Agilent InfinityLab Poroshell 120 HILIC-Z 2.1 × 100 mm, 2.7 µm	0.3% ammonium hydroxide in water	0.3% ammonium hydroxide in ACN	3.95	39.51
	Fucose					3.91	39.10
	Xylose, Arabinose					3.20	32.01
	Ribitol, Xylitol					0.65	6.46
	Fructose					2.60	25.95
	Mannose					2.05	20.46
	Glucose, Galactose					3.07	30.72
	Sucrose					1.08	10.76
	Maltose					2.23	22.27
	Lactose					22.94	229.42
	Trehalose					0.65	6.47
	Raffinose					1.26	12.56
	Galactinol					4.36	43.60
4	**Fatty Acid**					**(ug/mL)**	**(ug/g)**
	Linolenic acid	ACN/IPA/H2O =65:30:5	Agilent Polaris 3 C18-Ether 150x3.0mm	40% ACN in water +10mM ammonium formate, 0.1% Formic acid	IPA:ACN = 9:1 +10mM aqueous ammonium formate, 0.1% Formic acid	3.35	33.51
	myristic acid					3.74	37.40
	Linoleic acid					2.45	24.48
	Pentadecanoic acid					2.66	26.63
	Palmitic acid					13.63	136.33
	Heptadecanoic acid					10.91	109.07
	Stearic acid					12.91	129.10
	Arachidic acid					7.86	78.56

Table S2. The LC-MS/MS analysis parameters for metabolomics analysis

Compound	Retention time (min)	Precursor ion (m/z)	Product ions				
			Quant ion (m/z)	Collision energy (V)	Qual ion (m/z)	Collision energy (V)	Fragmentor (V)
Antioxidants							
Glutathione reduced	1.31	308.1	179	12	162	16	91
Chlorogenic acid	5.10	353.1	191.1	16	-	-	102
Vanillic acid	5.50	367.1	217.1	8	149.1	16	112
2-hydroxycinnamic acid	6.24	167	152.1	12	108	20	82
4-(Trifuoromethyl)cinnamic acid	7.14	163	119.1	12	117.1	28	81
L-Dehydroascorbic acid	7.25	173	158.1	12	-	-	174
Curcumin	7.27	215	171.1	12	151.1	20	87
a-Tocopherol	9.24	431.4	165.1	24	69.1	40	142
Organic Acids/Phenolics							
glycolic acid	2.04	75	47	8	72.9	8	46
malic acid	2.07	133	114.9	8	71	16	76
Citric acid	2.17	191	110.8	12	86.9	16	82
lactic acid	2.23	89.1	43.1	4	-	-	66
succinic acid	2.31	117	72.9	12	98.9	8	66
Pyruvic acid	2.36	87	43.1	4	-	-	66
Gallic acid	2.49	169	125.1	12	79	24	92
Glutaric acid	2.62	131	86.9	12	112.9	8	71
fumaric acid	2.67	115	70.9	4	-	-	56
ascorbic acid	2.67	175	114.9	12	-	-	87
Caffeic acid	4.58	179	135.1	16	-	-	94
p-coumaric acid	4.87	163	119.1	16	93.1	36	87
ferulic acid	5.09	193.1	134.1	16	178.1	12	87
benzoic acid	5.21	121	77.1	12	-	-	77
Salicyllic acid	5.96	137	93	20	65.1	36	82
Nucleobase/side/tide							
Cytosine	1.94	112.1	95	20	40.1	20	84
CMP	2.76	324.1	112	16	95	40	84
Cytidine	2.90	244.1	112	12	95	40	84
Adenine	3.08	136.1	119	24	92	32	84
Guanine	3.34	152.1	135	20	110	24	84
uracil	3.52	113	70	10	96	20	84
AMP	4.84	348.1	136	20	97	32	84
Hypoxanthine	5.28	137	110	24	55.1	36	148
Uridine	6.33	245.1	113	8	70	40	84
Xanthine	6.40	153	110	20	55.1	36	84
Adenosine	6.67	268.1	136	20	119	40	84
Thymine	6.71	127.1	110	16	54.1	28	84
Guanosine	6.91	284.1	152	12	135	40	84
Inosine	6.91	269.1	137	16	110	40	84
Thymidine	7.28	243.1	127	8	117	8	84
Amino acids							
Phenylalanine	2.95	166.1	120.1	13	103	29	80
Leucine	3.38	132.1	86.1	9	30.2	17	75
Tryptophan	3.41	205.1	188	8	146	20	80
Isoleucine	3.75	132.1	86.1	9	44.2	25	75
Methionine	4.22	150.1	104	9	56.1	17	75
Valine	4.95	118.1	72.1	9	55.1	25	70
Proline	4.96	116.1	70.1	17	43.2	37	75
Tyrosine	5.01	182.1	136.1	13	91.1	33	85
Cysteine	5.63	122	59.1	29	76	13	65
Alanine	6.61	90.1	44.2	9	45.3	40	40

Threonine	6.72	120.1	74.1	9	56.1	17	75
Homoserine	6.91	120.1	74.1	9	56.1	21	70
Glycine	7.00	76	30.3	12	-	-	35
Glutamine	7.23	147.1	84.1	17	130.1	9	80
Serine	7.26	106.1	88.1	8	42.2	24	67
Asparagine	7.31	133.1	87.1	5	74	17	75
Glutamic acid	7.68	148.1	84.1	17	130	5	75
Citrulline	7.89	176.1	159.1	9	70.1	25	80
Aspartic acid	8.38	134	88.1	9	74	13	70
Histidine	9.06	156.1	110.1	13	83.1	29	90
Arginine	9.54	175.1	70.1	24	60.1	12	100
Lysine	10.16	147.1	84.1	17	130.1	9	75
Ornithine	10.28	133.1	116	8	70	20	76
Sugar and Sugar Alcohol							
Ribose	1.18	149	89	4	-	-	76
L-fucose	1.35	163.1	89	0	59.1	12	76
Xylose/Arabinose*	1.43	149	89	4	-	-	76
Ribitol/Xylitol*	1.61	151.1	89	8	71.1	16	97
Fructose	1.72	179.1	89	4	-	-	71
Mannose	1.93	179.1	89	16	-	-	71
Glucose/Galactose*	2.19	179.1	89	16	-	-	71
Sucrose	3.81	341.1	179	20	-	-	148
Maltose	4.26	341.1	161.1	4	-	-	123
Lactose	4.57	341.1	161.1	4	-	-	123
Trehalose	4.79	341.1	179	12	-	-	154
Raffinose	6.03	503.2	179	20	221	32	174
Galactinol	6.17	341.1	179	12	-	-	133
Fatty Acids							
Linolenic acid	4.33	323.2	277.1	4	45.1	40	87
myristic acid	4.64	273.2	227.2	4	45.1	8	56
Linoleic acid	4.91	325.2	279.1	4	45.1	28	87
Pentadecanoic acid	5.17	287.2	241.2	4	45.1	16	71
Palmitic acid	5.70	301.2	255.2	4	45.1	20	36
Heptadecanoic acid	6.14	315.3	269.2	4	45.2	28	76
Stearic acid	6.49	329.3	283.2	4	45.1	32	72
Arachidic acid	7.05	357.3	311.3	4	45.1	32	82

Table S3. List of selected 24 targeted proteins with related pathways

Pathway ID	Pathway	Protein ID	Protein	Accession Number
A	Amino acid metabolism	P1	AA degradation methionine	AT3G23810
		P2	AA synthesis methionine	AT5G17920
		P3	S-adenosylmethionine synthase	AT1G0250
B	Fermentation	P4	aldehyde dehydrogenase	AT1G23800
C	Glycolysis	P5	glycolysis cytosolic branch UGPase	AT2G36460
		P6	glycolysis cytosolic branch aldolase	AT5G17310
D	H+ transporting	P7	transport H+ transporting pyrophosphatase	AT1G15690
E	Hormone metabolism	P8	lipoxygenase	AT1G55020
F	Mitochondrial electron transport / ATP synthesis	P9	transport p- and v-ATPase	AT1G78900
		P10	ATP synthase delta chain	AT4G09650
		P11	ATP synthase beta subunit	AT5G08670
		P12	ATP synthase F1-ATPase	AT2G07698
G	Nitrogen-metabolism	P13	glutamate dehydrogenase	AT5G07440
		P14	glutamate synthase ferredoxin dependent	AT5G04140
H	Photorespiratory pathway	P15	aminotransferases peroxisomal	AT1G70580
		P16	photosystem II stability/assembly factor	AT5G23120
I	Photosynthesis / Calvin Cycle	P17	calvin cycle aldolase	AT2G21330
		P18	calvin cycle FBPase	AT3G54050
		P19	fructose-bisphosphate aldolase	AT2G36460
		P20	calvin cycle GAP	AT3G26650
J	Redox	P21	catalase	AT1G20620
K	TCA / org transformation	P22	malate dehydrogenase	AT5G43330
		P23	TCA aconitase	AT4G35830
L	Tetrapyrrole biosynthesis	P24	tetrapyrrole synthesis prophobilinogen	AT5G08280

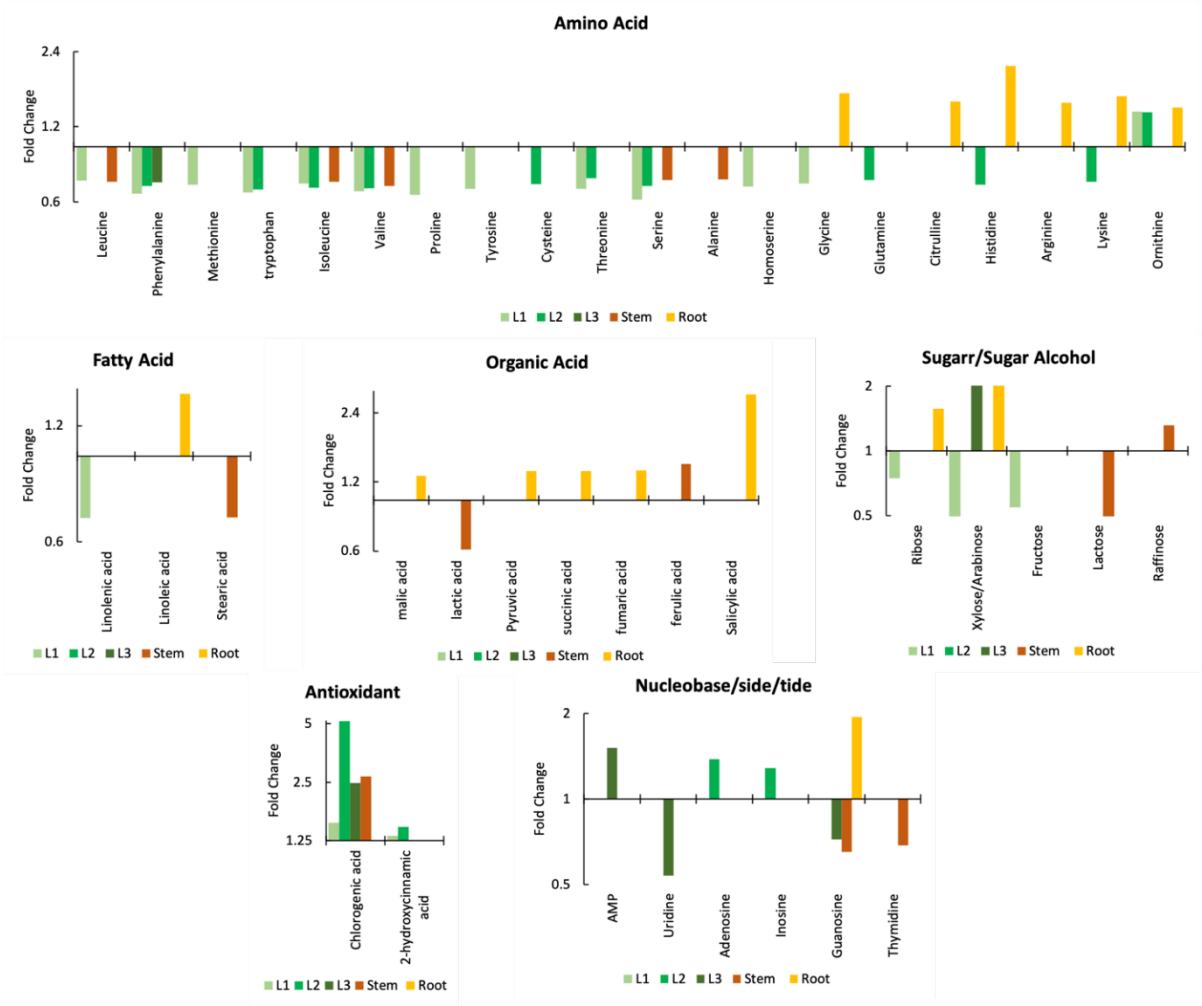

Figure S3. Fold change bar plots of 43 responsive metabolites in different plant tissues with Cu exposure through root.

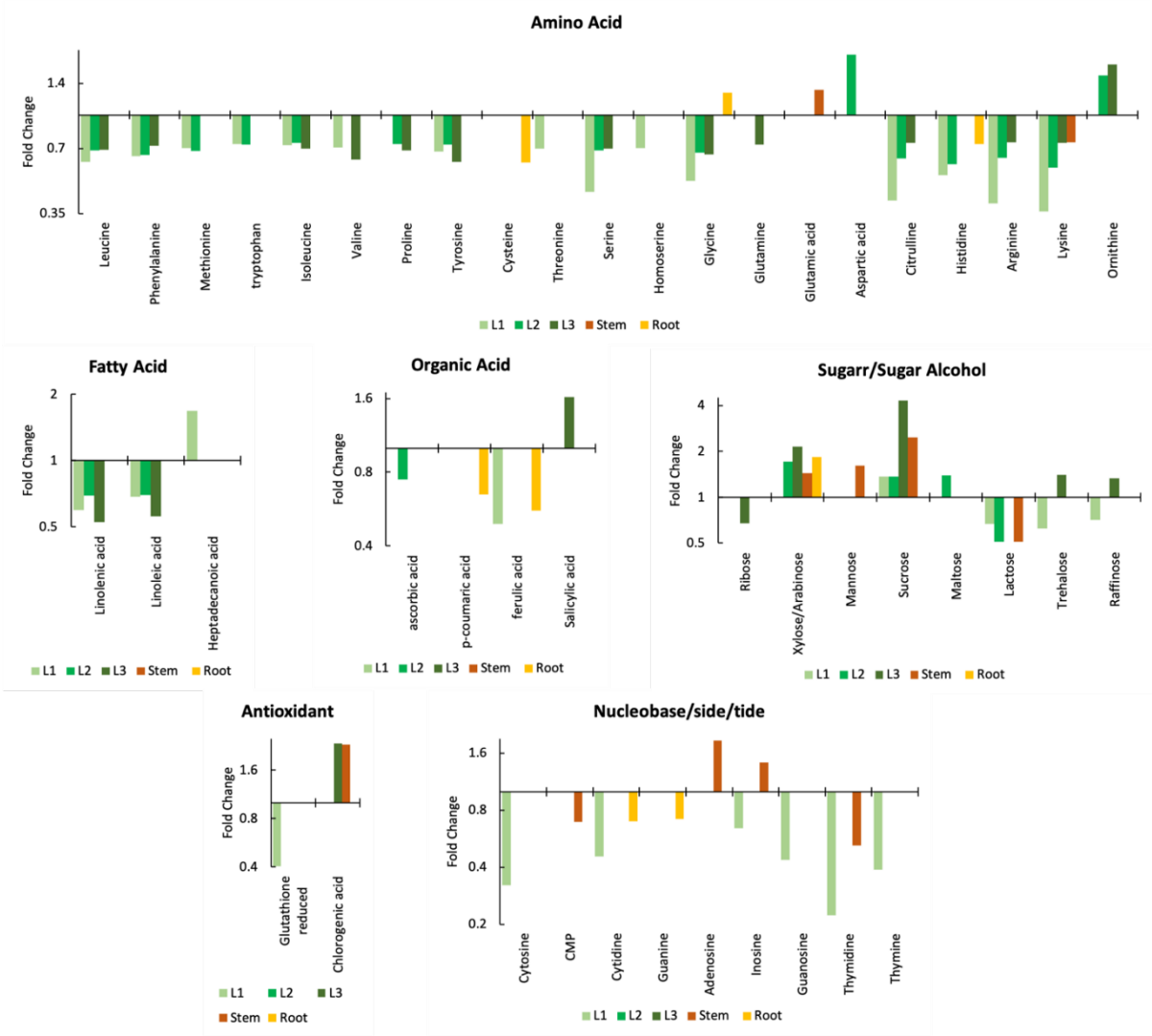

Figure S4. Fold change bar plots of 47 responsive metabolites in different plant tissues with Cu exposure through leaf.

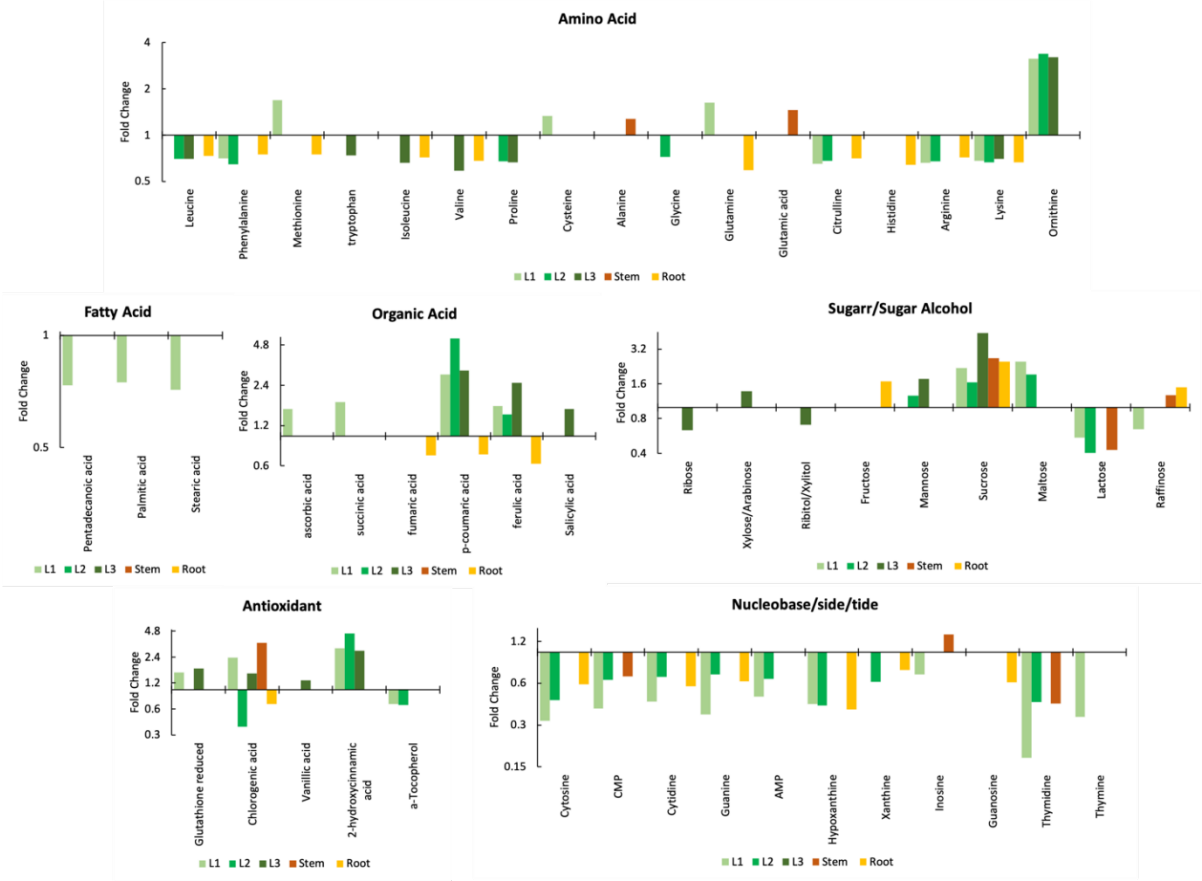

Figure S5. Fold change bar plots of 51 responsive metabolites in different plant tissues with Mo exposure through leaf.

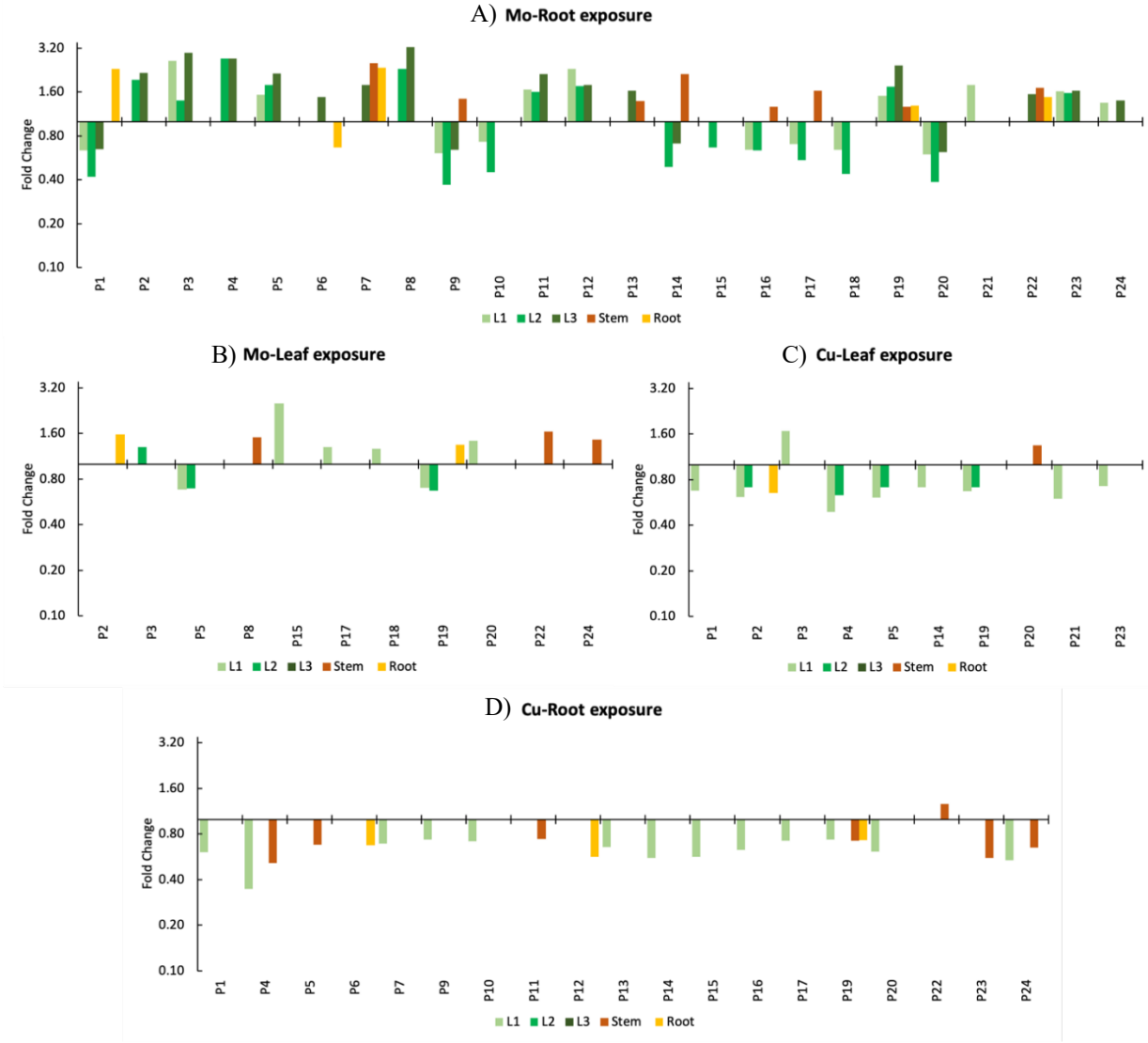

Figure S6. Fold change bar plots of A) 24 responsive proteins in different plant tissues with Mo exposure (6.25 mg/plant) through Root; B) 11 responsive proteins in different plant tissues with Mo exposure through leaf; C) 10 responsive proteins in different plant tissues with Cu exposure through leaf; and D) 19 responsive proteins in different plant tissues with Cu exposure through root. P1: AA degradation methionine; P2: AA synthesis methionine; P3: S-adenosylmethionine synthase; P4: aldehyde dehydrogenase; P5: glycolysis cytosolic branch UGPase; P6: glycolysis cytosolic branch aldolase; P7: transport H+ transporting pyrophosphatase; P8: lipoxygenase; P9: transport p- and v-ATPase; P10: ATP synthase delta chain; P11: ATP synthase beta subunit; P12: ATP synthase F1-ATPase; P13: glutamate dehydrogenase; P14: glutamate synthase ferredoxin dependent; P15: aminotransferases peroxisomal; P16: photosystem II stability/assembly factor HCF136; P17: calvin cycle aldolase; P18: calvin cycle FBPase; P19: fructose bisphosphate aldolase; P20: calvin cycle GAP; P21: catalase; P22: malate dehydrogenase P23: TCA aconitase; P24: tetrapyrrole synthesis prophobilinogen deaminase.

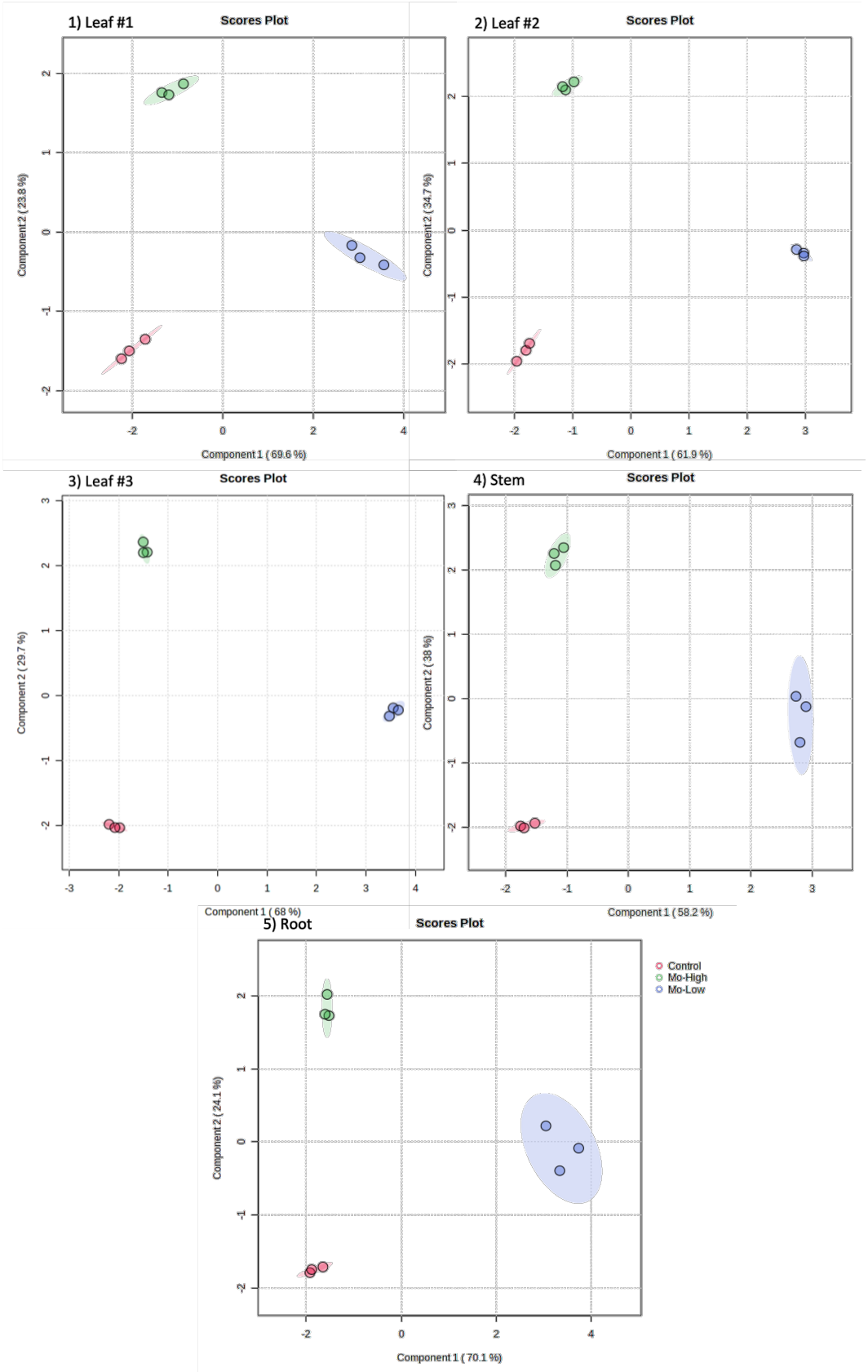

Figure S7. Partial Least Squares Discriminant Analysis (PLS-DA) of metabolite

concentrations in each plant tissues with Mo exposure through root at high dose vs. low dose.

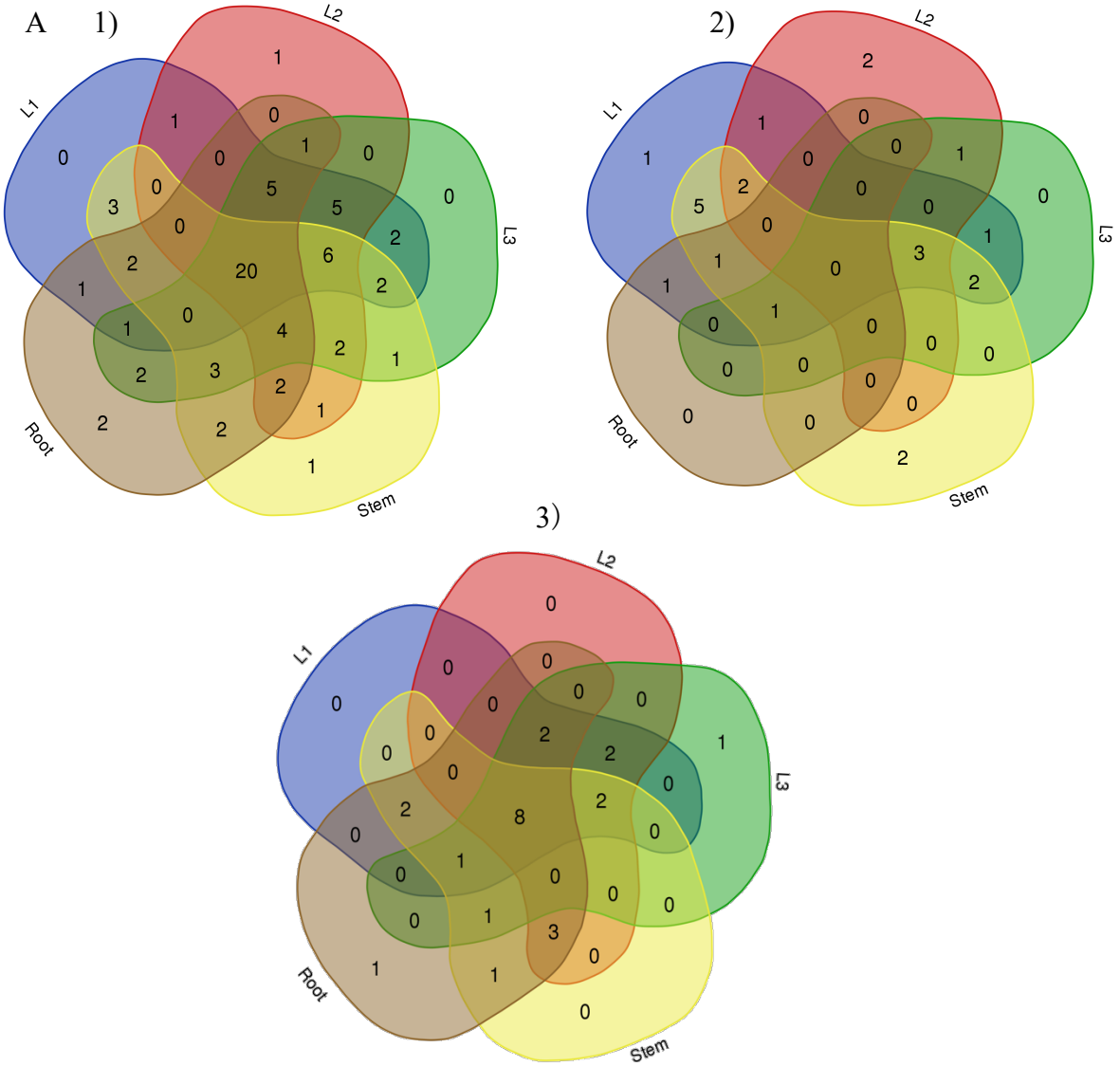

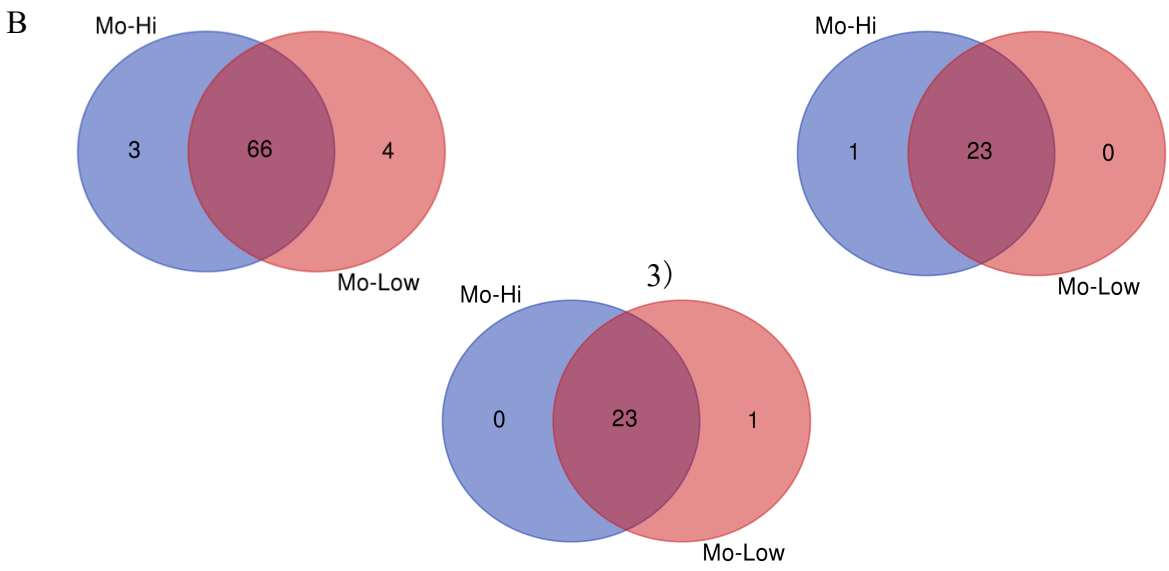

Figure S8. Venn diagram of A) tissue specific distribution for 1)70 responsive metabolites, 2) 23 responsive proteins and 3) 24 perturbed pathways in wheat with low Mo exposure through root; B) 1) responsive metabolites, 2) responsive proteins and 3) perturbed pathways in wheat with high Mo vs. low Mo exposure through root

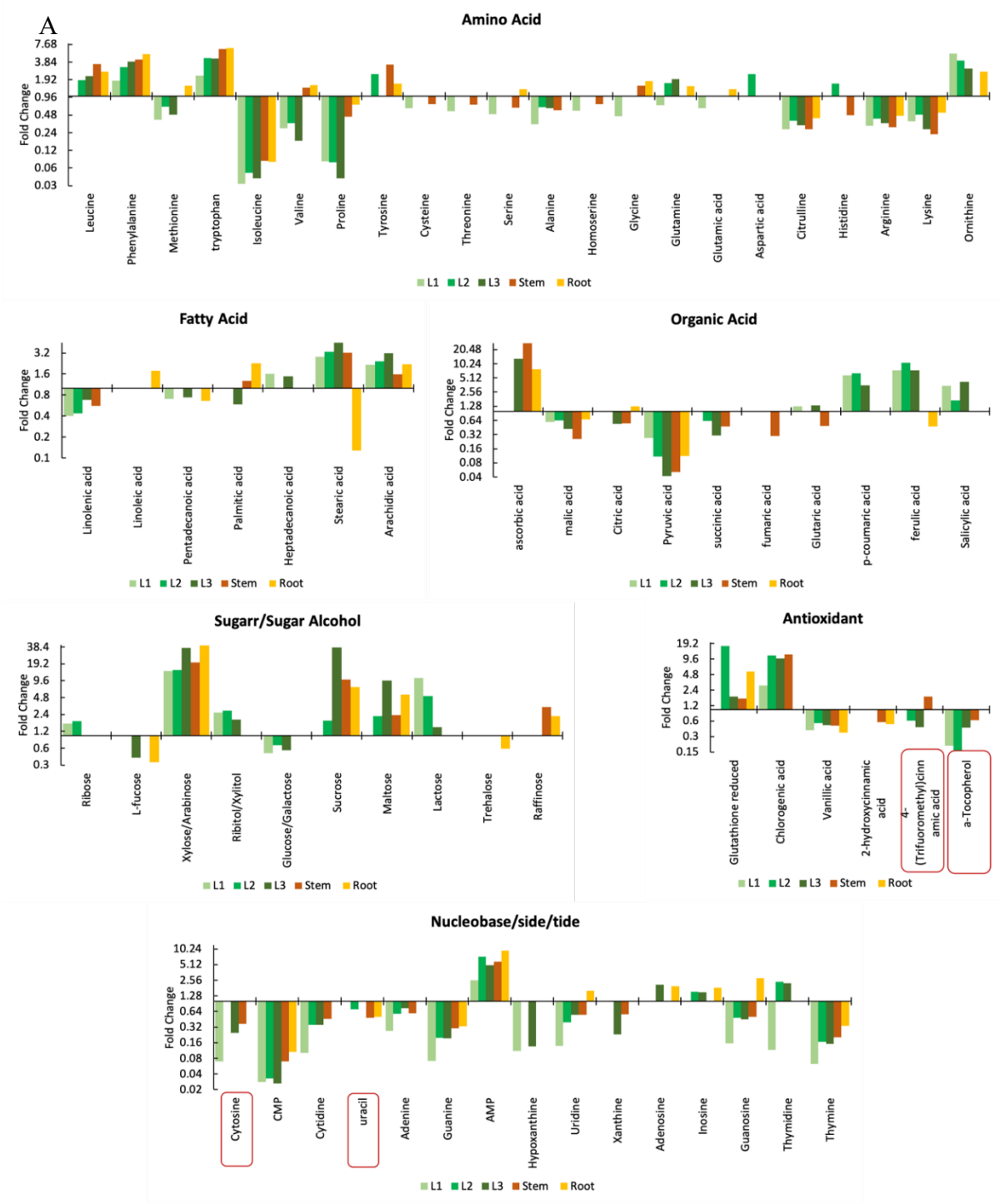
A
Amino Acid
Fold Change
7.68
3.84
1.92
0.96
0.48
0.24
0.12
0.06
0.03
Leucine
Phenylalanine
Methionine
tryptophan
Isoleucine
Valine
Proline
Tyrosine
Cysteine
Threonine
Serine
Alanine
Homoserine
Glycine
Glutamine
Glutamic acid
Aspartic acid
Citrulline
Histidine
Arginine
Lysine
Ornithine
L1 L2 L3 Stem Root
Fatty Acid
Fold Change
3.2
1.6
0.8
0.4
0.2
0.1
Linolenic acid
Linoleic acid
Pentadecanoic acid
Palmitic acid
Heptadecanoic acid
Stearic acid
Arachidic acid
L1 L2 L3 Stem Root
Organic Acid
Fold Change
20.48
10.24
5.12
2.56
1.28
0.64
0.32
0.16
0.08
0.04
ascorbic acid
malic acid
Citric acid
Pyruvic acid
succinic acid
fumaric acid
Glutaric acid
p-coumaric acid
ferulic acid
Salicylic acid
L1 L2 L3 Stem Root
Sugarr/Sugar Alcohol
Fold Change
38.4
19.2
9.6
4.8
2.4
1.2
0.6
0.3
Ribose
L-fucose
Xylose/Arabinose
Ribitol/Xylitol
Glucose/Galactose
Sucrose
Maltose
Lactose
Trehalose
Raffinose
L1 L2 L3 Stem Root
Antioxidant
Fold Change
19.2
9.6
4.8
2.4
1.2
0.6
0.3
0.15
Glutathione reduced
Chlorogenic acid
Vanillic acid
2-hydroxycinnamic acid
4-(Trifuoromethyl)cinnamic acid
a-Tocopherol
L1 L2 L3 Stem Root
Nucleobase/side/tide
Fold Change
10.24
5.12
2.56
1.28
0.64
0.32
0.16
0.08
0.04
0.02
Cytosine
CMP
Cytidine
uracil
Adenine
Guanine
AMP
Hypoxanthine
Uridine
Xanthine
Adenosine
Inosine
Guanosine
Thymidine
Thymine
L1 L2 L3 Stem Root

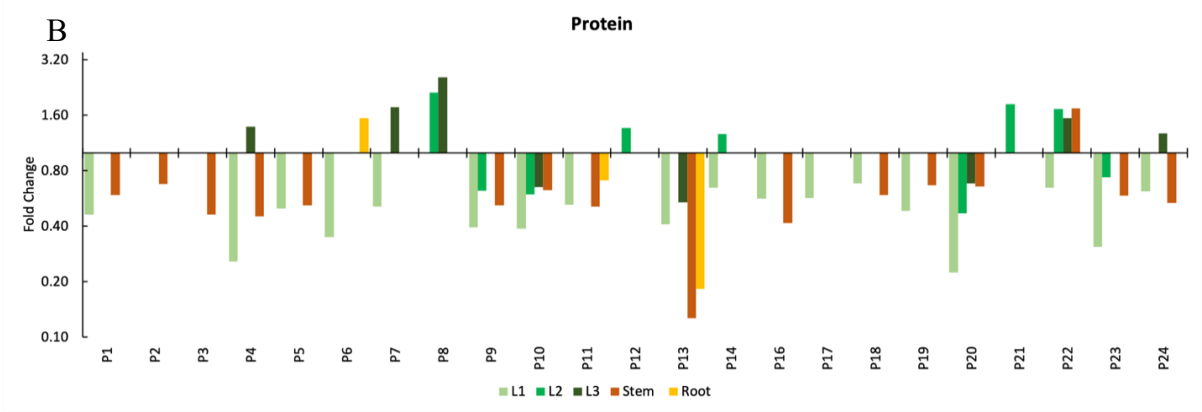

Figure S9. Fold change bar plots of a) 70 responsive metabolites (grouped by metabolite classes) and B) 23 responsive proteins in different plant tissues with Mo exposure at low concentration through Root.

Table S4. Joint-pathway analysis results for Cu exposure. Total is the total number of metabolites in the pathway; hit is the actually matched number of responsive metabolites; bold font means metabolite or protein only involved in perturbed pathways through root exposure; underline font means metabolite or protein only involved in perturbed pathways through leaf exposure.

Pathways	Pathway Class	Total	Cu Exposure							
			Root exposure			Leaf exposure			Metabolites	Proteins
			Hit	Impact	Tissue	Hit	Impact	Tissue		
Alanine, aspartate and glutamate metabolism	Amino acid metabolism	22	5	0.20	L2	3	0.64	L2, L3, S	**Alanine**; Aspartic acid; Glutamine; Glutamic acid; **Fumaric acid**; **Pyruvic acid**; **Succinic acid**	**P13**; **P15**
Arginine and proline metabolism	Amino acid metabolism	34	3	0.27	L1, R	4	0.34	L1, L2, L3	Arginine; Proline; Glutamic acid; Ornithine	P4
Arginine biosynthesis	Amino acid metabolism	18	5	0.31	L1, L2, R	6	0.40	L1, L2, L3	Arginine; Aspartic acid; Citrulline; Ornithine; **Fumaric acid**; Glutamine; Glutamic acid	**P13**; **P15**
Cysteine and methionine metabolism	Amino acid metabolism	46	5	0.19	L1	5	0.18	L1, L2	Aspartic acid; Serine; Methionine; Cysteine; Homoserine; **Pyruvic acid**	P1; P2; P3; **P22**
Glutathione metabolism	Amino acid metabolism	26	-	-	-	4	0.48	L1	Glutathione; Glycine; Glutamic acid; Cysteine	-
Glycine, serine and threonine metabolism	Amino acid metabolism	33	6	0.58	L1, L2, S, R	6	0.58	L1, L2, L3, R	Aspartic acid; Serine; Glycine; Threonine; Homoserine; **Pyruvic acid**; Tryptophan	**P15**
Phenylalanine metabolism	Amino acid metabolism	11	1	0.47	L1, L2, L3	1	0.47	L1, L2, L3	Phenylalanine	-
Tryptophan metabolism	Amino acid metabolism	28	1	0.12	L1, L2	1	0.12	L1, L2	Tryptophan	P4; P21
Tyrosine metabolism	Amino acid metabolism	16	3	0.22	L1, R	1	0.11	L1, L2, L3	Tyrosine; **Fumaric acid**; **Pyruvic acid**	-
Valine, leucine and isoleucine biosynthesis	Amino acid metabolism	22	5	0.11	R	-	-	-	**Threonine; Leucine; Pyruvic acid; Isoleucine; Valine**	-
Biosynthesis of secondary metabolites - unclassified	Biosynthesis of secondary metabolites	5	-	-	-	1	1.00	R	p-coumaric acid	-
Isoquinoline alkaloid biosynthesis	Biosynthesis of secondary metabolites	6	1	0.50	L1	1	0.50	L1, L2, L3	Tyrosine	-
Phenylpropanoid biosynthesis	Biosynthesis of secondary metabolites	46	-	-	-	4	0.10	-	Ferulic acid; Chlorogenic acid; Phenylalanine; p-coumaric acid	-
Stilbenoid, diarylheptanoid and gingerol biosynthesis	Biosynthesis of secondary metabolites	8	1	0.13	L1, L2, L3, S	1	0.13	L3, S	Chlorogenic acid	-
Citrate cycle (TCA cycle)	Carbohydrate metabolism	20	4	0.22	R	-	-	-	**Malic acid**; **Succinic acid**; **Pyruvic acid**; **Fumaric acid**	**P22**; P23
Galactose metabolism	Carbohydrate metabolism	27	-	-	-	2	0.12	L1, L3	Raffinose; Sucrose	**P6**
Glycolysis / Gluconeogenesis	Carbohydrate metabolism	26	2	0.12	R	-	-	-	**Pyruvic acid**; **Lactic acid**	P4; P5; **P17**
Glyoxylate and dicarboxylate metabolism	Carbohydrate metabolism	29	5	0.18	L1, R	4	0.17	L1, L2, L3, R	Serine; **Malic acid**; Glycine; Glutamine; **Succinic acid**; Glutamic acid	P14; **P15**; P21; **P22**; P23
Pyruvate metabolism	Carbohydrate metabolism	22	4	0.32	R	-	-	-	**Malic acid**; **Pyruvic acid**; **Lactic acid**; **Fumaric acid**	P4; **P22**
alpha-Linolenic acid metabolism	Lipid metabolism	28	1	0.11	L1	1	0.11	L1, L2, L3	Linolenic acid	-
Linoleic acid metabolism	Lipid metabolism	4	1	1.00	R	1	1.00	L1, L2, L3	Linoleic acid	-
Purine metabolism	Nucleotide metabolism	63	-	-	-	-	-	-	-	-
Aminoacyl-tRNA biosynthesis	Translation	46	17	0.11	L1, L2, S	18	0.11	L1, L2, L3	Aspartic acid; Histidine; Phenylalanine; Arginine; Glutamine; Cysteine; Glycine; Serine; Methionine; Valine; **Alanine**; Lysine; Isoleucine; Leucine; Threonine; Tryptophan; Tyrosine; Proline; Glutamic acid	-

Table S5. Joint-pathway analysis results for Mo exposure. Total is the total number of metabolites in the pathway; hit is the actually matched number of responsive metabolites; bold font means metabolite or protein only involved in perturbed pathways through root exposure; underline font means metabolite or protein only involved in perturbed pathways through leaf exposure.

Pathways	Pathway Class	Total	Mo Exposure							
			Root exposure			Leaf exposure			Metabolites	Proteins
			Hit	Impact	Tissue	Hit	Impact	Tissue		
Alanine, aspartate and glutamate metabolism	Amino acid metabolism	22	7	0.65	L1, L2, L3, S, R	5	0.52	L1, S, R	**Aspartic acid**; Alanine; Glutamine; Glutamic acid; Fumaric acid; **Pyruvic acid**; Succinic acid	**P13**; P15
Arginine and proline metabolism	Amino acid metabolism	34	4	0.34	L1, L2, L3, S, R	4	0.34	L1, L2, L3, R	Arginine; Proline; Glutamic acid; Ornithine;	**P4**
Arginine biosynthesis	Amino acid metabolism	18	7	0.40	L1, L2, L3, S, R	6	0.40	L1, L2, L3, R	Glutamic acid; Arginine; Citrulline; **Aspartic acid**; Ornithine; Fumaric acid; Glutamine	**P13**; P15
Cysteine and methionine metabolism	Amino acid metabolism	46	6	0.19	L1, L2, L3, S, R	2	0.18	L1, R	**Serine**; Methionine; Cysteine; **Homoserine**; **Aspartic acid**; **Pyruvic acid**	**P1**; P2; P3; P22
Glutathione metabolism	Amino acid metabolism	26	4	0.48	L3, S, R	4	0.48	L1, L3	Glutathione; Glycine; Glutamic acid; Cysteine;	-
Glycine, serine and threonine metabolism	Amino acid metabolism	33	7	0.58	L1, L2, L3, S, R	2	0.21	L2	**Serine**; Glycine; **Aspartic acid**; **Threonine**; **Homoserine**; **Pyruvic acid**; Tryptophan	P15
Phenylalanine metabolism	Amino acid metabolism	11	1	0.47	L1, L2, L3, S, R	1	0.47	L1, L2, R	Phenylalanine	-
Tryptophan metabolism	Amino acid metabolism	28	1	0.12	L1, L2, L3, S, R	1	0.12	L3	Tryptophan	**P4**; **P21**
Tyrosine metabolism	Amino acid metabolism	16	3	0.22	L1, L2, L3, S, R	1	0.11	R	**Tyrosine**; Fumaric acid; **Pyruvic acid**	-
Valine, leucine and isoleucine biosynthesis	Amino acid metabolism	22	5	0.11	L2, S, R	-	-	-	**Threonine**; Leucine; **Pyruvic acid**; Isoleucine; Valine	-
Biosynthesis of secondary metabolites - unclassified	Biosynthesis of secondary metabolites	5	1	1.00	L1, L2, L3, S, R	1	1.00	L1, L2, L3, R	p-coumaric acid	-
Isoquinoline alkaloid biosynthesis	Biosynthesis of secondary metabolites	6	1	0.50	L2, L3, S, R	-	-	-	**Tyrosine**	-
Phenylpropanoid biosynthesis	Biosynthesis of secondary metabolites	46	4	0.10	L2, L3, S, R	4	0.10	L1, L2, L3, R	Ferulic acid; Chlorogenic acid; Phenylalanine; p-coumaric acid;	-
Stilbenoid, diarylheptanoid and gingerol biosynthesis	Biosynthesis of secondary metabolites	8	1	0.13	L2, L3, S, R	1	0.13	L1, L2, L3, S, R	Chlorogenic acid	-
Citrate cycle (TCA cycle)	Carbohydrate metabolism	20	5	0.22	L1, L2, L3, S	-	-	-	**Malic acid**; Succinic acid; **Citric acid**; **Pyruvic acid**; Fumaric acid	P22; **P23**
Galactose metabolism	Carbohydrate metabolism	27	3	0.12	L2, L3, S	2	0.12	L1,S, R	Raffinose; Sucrose; **Galactose**	**P6**
Glycolysis / Gluconeogenesis	Carbohydrate metabolism	26	3	0.12	L1, L2, S, R	-	-	-	**Pyruvic acid**; **Lactic acid**; **Glucose**	**P4**; P5; P17; P18
Glyoxylate and dicarboxylate metabolism	Carbohydrate metabolism	29	7	0.24	L2, L3, S, R	4	0.15	L2	**Serine**; **Malic acid**; **Citric acid**; Glycine; Glutamic acid; Glutamine; Succinic acid	**P14**; P15; **P21**; P22; **P23**
Pyruvate metabolism	Carbohydrate metabolism	22	4	0.32	L1, L2, L3, S, R	-	-	-	**Malic acid**; **Pyruvic acid**; **Lactic acid**; Fumaric acid	**P4**; P22
alpha-Linolenic acid metabolism	Lipid metabolism	28	1	0.11	R	-	-	-	**Linolenic acid**	-
Linoleic acid metabolism	Lipid metabolism	4	1	1.00	L1, L2, L3, S, R	-	-	-	**Linoleic acid**	P8
Purine metabolism	Nucleotide metabolism	63	9	0.11	-	7	0.10	L2	Xanthine; Glutamine; AMP; **Adenosine**; Hypoxanthine; Guanine; **Adenine**; inosine; Guanosine	-
Aminoacyl-tRNA biosynthesis	Translation	46	19	0.11	L1, L2, L3, S, R	-	-	-	Histidine; Phenylalanine; Arginine; Glutamine; Cysteine; Glycine; **Aspartic acid**; **Serine**; Methionine; Valine; Alanine; Lysine; Isoleucine; Leucine; **Threonine**; Tryptophan; **Tyrosine**; Proline; Glutamic acid	-

Table S6. Joint-pathway analysis results for Mo exposure with high vs. low dose. (Bold means only involved in pathways with high exposure; Underline means only involved in pathways with low dose exposure.

Pathways	Pathway Class	Total	Mo Exposure through root							
			High Dose			Low Dose			Metabolites	Proteins
			Hit	Impact	Tissue	Hit	Impact	Tissue		
Alanine, aspartate and glutamate metabolism	Amino acid metabolism	22	7	0.65	L1, L2, L3, S, R	7	0.65	L1, L2, L3, R	Aspartic acid; Alanine; Glutamine; Glutamic acid; Fumaric acid; Pyruvic acid; Succinic acid	P13; **P15**
Arginine and proline metabolism	Amino acid metabolism	34	4	0.34	L1, L2, L3, S, R	4	0.34	L1, L2, L3, S, R	Arginine; Proline; Glutamic acid; Ornithine;	P4
Arginine biosynthesis	Amino acid metabolism	18	7	0.40	L1, L2, L3, S, R	7	0.40	L1, L2, L3, S, R	Glutamic acid; Arginine; Citrulline; Aspartic acid; Ornithine; Fumaric acid; Glutamine	P13; **P15**
Cysteine and methionine metabolism	Amino acid metabolism	46	6	0.19	L1, L2, L3, S, R	6	0.19	L1, L2, L3, R	Serine; Methionine; Cysteine; Homoserine; Aspartic acid; Pyruvic acid;	P1; P2; P3; P22
Glutathione metabolism	Amino acid metabolism	26	4	0.48	L3, S, R	4	0.48	L1, L2, L3, S, R	Glutathione; Glycine; Glutamic acid; Cysteine;	-
Glycine, serine and threonine metabolism	Amino acid metabolism	33	7	0.58	L1, L2, L3, S, R	7	0.58	L1, S, R	Serine; Glycine; Aspartic acid; Threonine; Homoserine; Pyruvic acid; Tryptophan	**P15**
Phenylalanine metabolism	Amino acid metabolism	11	1	0.47	L1, L2, L3, S, R	1	0.47	L1, L2, L3, S, R	Phenylalanine	-
Tryptophan metabolism	Amino acid metabolism	28	1	0.12	L1, L2, L3, S, R	1	0.12	L1, L2, L3, S, R	Tryptophan	P4; P21
Tyrosine metabolism	Amino acid metabolism	16	3	0.22	L1, L2, L3, S, R	3	0.22	L2, S, R	Tyrosine; Fumaric acid; Pyruvic acid	-
Valine, leucine and isoleucine biosynthesis	Amino acid metabolism	22	5	0.11	L2, S, R	5	0.11	L1, L2, L3, S, R	Threonine; Leucine; Pyruvic acid; Isoleucine; Valine;	-
Biosynthesis of secondary metabolites - unclassified	Biosynthesis of secondary metabolites	5	1	1.00	L1, L2, L3, S, R	1	1.00	L1, L2, L3	p-coumaric acid	-
Isoquinoline alkaloid biosynthesis	Biosynthesis of secondary metabolites	6	1	0.50	L2, L3, S, R	1	0.50	L2, S, R	Tyrosine	-
Phenylpropanoid biosynthesis	Biosynthesis of secondary metabolites	46	4	0.10	L2, L3, S, R	4	0.10	L1, L2, L3	Ferulic acid; Chlorogenic acid; Phenylalanine; p-coumaric acid;	-
Stilbenoid, diarylheptanoid and gingerol biosynthesis	Biosynthesis of secondary metabolites	8	1	0.13	L2, L3, S, R	1	0.13	L1, L2, L3, S	Chlorogenic acid	-
Citrate cycle (TCA cycle)	Carbohydrate metabolism	20	5	0.22	L1, L2, L3, S	5	0.22	L3, S, R	Malic acid; Succinic acid; Citric acid; Pyruvic acid; Fumaric acid;	P22; P23
Galactose metabolism	Carbohydrate metabolism	27	3	0.12	L2, L3, S	3	0.12	S, R	Raffinose; Sucrose; Galactose	P6
Glycolysis / Gluconeogenesis	Carbohydrate metabolism	26	3	0.12	L1, L2, S, R	2	0.12	L1, L2, L3, S, R	Pyruvic acid; **Lactic acid**; Glucose	P4; P5; P17; P18
Glyoxylate and dicarboxylate metabolism	Carbohydrate metabolism	29	7	0.24	L2, L3, S, R	7	0.24	L1, S, R	Serine; Malic acid; Citric acid; Glycine; Glutamic acid; Glutamine; Succinic acid	P14; **P15**; P21; P22; P23
Pyruvate metabolism	Carbohydrate metabolism	22	4	0.32	L1, L2, L3, S, R	3	0.32	L1, L2, L3, S, R	Malic acid; Pyruvic acid; **Lactic acid**; Fumaric acid	P4; P22
alpha-Linolenic acid metabolism	Lipid metabolism	28	1	0.11	R	1	0.11	L1, L2, L3, S	Linolenic acid	-
Linoleic acid metabolism	Lipid metabolism	4	1	1.00	L1, L2, L3, S, R	1	1.00	R	Linoleic acid	P8
Purine metabolism	Nucleotide metabolism	63	9	0.11	-	9	0.11	L3	Xanthine; Glutamine; AMP; Adenosine; Hypoxanthine; Guanine; Adenine; inosine; Guanosine	-
Pyrimidine metabolism	Nucleotide metabolism	38	-	-	-	7	0.13	L2, S, R	Glutamine; Uridine; CMP; Cytidine; Thymidine; Thymine; Uracil	-
Aminoacyl-tRNA biosynthesis	Translation	46	19	0.11	L1, L2, L3, S, R	19	0.11	L1, S, R	Histidine; Phenylalanine; Arginine; Glutamine; Cysteine; Glycine; Aspartic acid; Serine; Methionine; Valine; Alanine; Lysine; Isoleucine; Leucine; Threonine; Tryptophan; Tyrosine; Proline; Glutamic acid	-

V. Summary

The work presented here provides an improved method of analysis for targeted proteomics in plants (and specifically, for studying the impact of engineered nanomaterials (ENMs) on wheat (*Triticum aestivum*) plant growth using targeted proteomics and metabolomics. Chapter II describes the optimization of the proteomics method, starting with signature peptide selection, LC-MS/MS analytical method development and sample preparation optimization.[63] The results indicated that phenol extraction using fresh plant tissue, coupled with trypsin digestion, is the most effective sample preparation method. The optimized approach yielded higher total peptide concentration and improved detection of signature peptides, providing a valuable workflow for future targeted proteomics studies.

Chapter III investigated the effects of Mo based nano-fertilizer and Cu based nano-pesticide exposure on wheat using a multi-faceted approach.[95] Physiological measurements, metal uptake analysis, and the targeted proteomics method described in Chapter II were employed to understand the molecular and physiological responses. Mo exposure, particularly through root uptake, induced significant upregulation of proteins associated with metabolic pathways. Dose-dependent responses highlighted the delicate balance between nutrient stimulation and toxicity. Cu exposure exhibited tissue-specific effects, with pronounced downregulation, especially in the first leaf tissues. The study provided insights into optimizing nutrient management practices in crop production and advancing sustainable agriculture.

Chapter IV interrogated the metabolic and proteomic responses of wheat to Mo and Cu based ENMs exposure via root and leaf routes, allowing a more integrated view. Utilizing

LC-MS/MS analysis, the study assesses 82 metabolites and 24 proteins across different plant tissues. Joint pathway analysis revealed 23 perturbed pathways across all treatments. Particularly noteworthy was the effect of Mo exposure through roots, which affected all identified pathways, with 12 pathways consistently perturbed across all tissues. Pathway mapping visually depicts the involvement of responsive metabolites and proteins in perturbed pathways across all treatments, emphasizing the importance of amino acid metabolism. The observed upregulation of proteins associated with amino acid metabolism explained alterations in amino acid levels, revealing a dynamic relationship between proteomic and metabolic responses. Notably, the differing expression changes of key enzymes, exemplified by glutamate dehydrogenase (P13), between different doses of Mo through root exposure highlighted dose-dependent regulatory patterns in enzymes and metabolites. The findings contribute to a multi-dimensional understanding of plant responses, guiding agricultural practices and environmental safety protocols related to nanomaterial impacts on plant biology.

In summary, this study contributes to optimizing proteomic methodologies, unraveling the intricate effects of Mo and Cu exposure on wheat at molecular and physiological levels, and providing a multi-dimensional understanding of plant responses to ENMs. These findings not only advance our understanding of nanomaterial impacts on crop production but also hold significant implications for sustainable agriculture practices, nutrient management strategies, and environmental safety protocols. Moving forward, new research directions could focus on expanding this approach to encompass genomics, transcriptomics, alongside current proteomics and metabolomics, to enable the comprehensive measurement of the flow of molecular information from genes to metabolites. This integrated multi-omics approach

offers the potential to elucidate the intricate genetic and molecular mechanisms underlying plant responses to ENMs, allowing for a deeper understanding of how genotype influences phenotype in the context of ENMs exposure. By integrating multi-omics datasets, researchers can uncover regulatory networks, identify key molecular players, and decipher complex biological pathways involved in ENMs-induced responses. Moreover, the integration of advanced statistical modeling and machine learning techniques with multi-omics data holds promise for predictive modeling of ENMs-induced effects on plant physiology and ecosystem dynamics. These predictive models could facilitate the development of targeted interventions and precision agriculture strategies, ultimately enhancing the sustainability and safety of nanomaterial applications in agriculture.

VI. References

(1) Liu, Y.; Lu, S.; Liu, K.; Wang, S.; Huang, L.; Guo, L. Proteomics: A Powerful Tool to Study Plant Responses to Biotic Stress. *Plant Methods* **2019**, *15* (1), 135. https://doi.org/10.1186/s13007-019-0515-8.

(2) Meyer, J. G. Qualitative and Quantitative Data Analysis from Data-Dependent. In *Shotgun Proteomics*; Carrera, M., Mateos, J., Eds.; Methods in Molecular Biology; Springer US: New York, NY, 2021; Vol. 2259, pp 297–308. https://doi.org/10.1007/978-1-0716-1178-4_19.

(3) Hart-Smith, G.; Reis, R. S.; Waterhouse, P. M.; Wilkins, M. R. Improved Quantitative Plant Proteomics via the Combination of Targeted and Untargeted Data Acquisition. *Front. Plant Sci.* **2017**, *8*. https://doi.org/10.3389/fpls.2017.01669.

(4) Sinha, A.; Mann, M. A Beginner's Guide to Mass Spectrometry–Based Proteomics. *The Biochemist* **2020**, *42*. https://doi.org/10.1042/BIO20200057.

(5) Borràs, E.; Sabidó, E. What Is Targeted Proteomics? A Concise Revision of Targeted Acquisition and Targeted Data Analysis in Mass Spectrometry. *Proteomics* **2017**, *17* (17–18), 1700180. https://doi.org/10.1002/pmic.201700180.

(6) Lin, T.-T.; Zhang, T.; Kitata, R. B.; Liu, T.; Smith, R. D.; Qian, W.-J.; Shi, T. Mass Spectrometry-Based Targeted Proteomics for Analysis of Protein Mutations. *Mass Spectrometry Reviews* **2023**, *42* (2), e21741. https://doi.org/10.1002/mas.21741.

(7) Method of the Year 2012. *Nat Methods* **2013**, *10* (1), 1–1. https://doi.org/10.1038/nmeth.2329.

(8) Houston, N. L.; Lee, D.-G.; Stevenson, S. E.; Ladics, G. S.; Bannon, G. A.; McClain, S.; Privalle, L.; Stagg, N.; Herouet-Guicheney, C.; MacIntosh, S. C.; Thelen, J. J. Quantitation of Soybean Allergens Using Tandem Mass Spectrometry. *J. Proteome Res.* **2011**, *10* (2), 763–773. https://doi.org/10.1021/pr100913w.

(9) Ansari, P.; Stoppacher, N.; Baumgartner, S. Marker Peptide Selection for the Determination of Hazelnut by LC–MS/MS and Occurrence in Other Nuts. *Anal Bioanal Chem* **2012**, *402* (8), 2607–2615. https://doi.org/10.1007/s00216-011-5218-6.

(10) Rogniaux, H.; Pavlovic, M.; Lupi, R.; Lollier, V.; Joint, M.; Mameri, H.; Denery, S.; Larré, C. Allergen Relative Abundance in Several Wheat Varieties as Revealed via a Targeted Quantitative Approach Using MS. *PROTEOMICS* **2015**, *15* (10), 1736–1745. https://doi.org/10.1002/pmic.201400416.

(11) Stevenson, S. E.; McClain, S.; Thelen, J. J. Development of an Isoform-Specific Tandem Mass Spectrometry Assay for Absolute Quantitation of Maize Lipid Transfer

Proteins. *J. Agric. Food Chem.* **2015**, *63* (3), 821–828. https://doi.org/10.1021/jf504708u.

(12) Stecker, K. E.; Minkoff, B. B.; Sussman, M. R. Phosphoproteomic Analyses Reveal Early Signaling Events in the Osmotic Stress Response. *Plant Physiology* **2014**, *165* (3), 1171–1187. https://doi.org/10.1104/pp.114.238816.

(13) Humbal, A.; Pathak, B. Application of Nanotechnology in Plant Growth and Diseases Management: Tool for Sustainable Agriculture. In *Agricultural and Environmental Nanotechnology: Novel Technologies and their Ecological Impact*; Fernandez-Luqueno, F., Patra, J. K., Eds.; Interdisciplinary Biotechnological Advances; Springer Nature: Singapore, 2023; pp 145–168. https://doi.org/10.1007/978-981-19-5454-2_6.

(14) Şahin, E. Ç.; Aydın, Y.; Utkan, G.; Uncuoğlu, A. A. Chapter 22 - Nanotechnology in Agriculture for Plant Control and as Biofertilizer. In *Synthesis of Bionanomaterials for Biomedical Applications*; Ozturk, M., Roy, A., Bhat, R. A., Vardar-Sukan, F., Policarpo Tonelli, F. M., Eds.; Micro and Nano Technologies; Elsevier, 2023; pp 469–492. https://doi.org/10.1016/B978-0-323-91195-5.00025-8.

(15) Chaud, M.; Souto, E. B.; Zielinska, A.; Severino, P.; Batain, F.; Oliveira-Junior, J.; Alves, T. Nanopesticides in Agriculture: Benefits and Challenge in Agricultural Productivity, Toxicological Risks to Human Health and Environment. *Toxics* **2021**, *9* (6), 131. https://doi.org/10.3390/toxics9060131.

(16) Yadav, A.; Yadav, K.; Abd-Elsalam, K. A. Nanofertilizers: Types, Delivery and Advantages in Agricultural Sustainability. *Agrochemicals* **2023**, *2* (2), 296–336. https://doi.org/10.3390/agrochemicals2020019.

(17) Chen, Y.; Liu, L. Targeted Proteomics. In *Functional Proteomics*; Wang, X., Kuruc, M., Eds.; Methods in Molecular Biology; Springer New York: New York, NY, 2019; Vol. 1871, pp 265–277. https://doi.org/10.1007/978-1-4939-8814-3_17.

(18) Mosa, K. A.; Ismail, A.; Helmy, M. Omics and System Biology Approaches in Plant Stress Research. In *Plant Stress Tolerance: An Integrated Omics Approach*; Mosa, K. A., Ismail, A., Helmy, M., Eds.; SpringerBriefs in Systems Biology; Springer International Publishing: Cham, 2017; pp 21–34. https://doi.org/10.1007/978-3-319-59379-1_2.

(19) Hur, M.; Campbell, A. A.; Almeida-de-Macedo, M.; Li, L.; Ransom, N.; Jose, A.; Crispin, M.; Nikolau, B. J.; Wurtele, E. S. A Global Approach to Analysis and Interpretation of Metabolic Data for Plant Natural Product Discovery. *Nat Prod Rep* **2013**, *30* (4), 565–583. https://doi.org/10.1039/c3np20111b.

(20) Jamil, I. N.; Remali, J.; Azizan, K. A.; Nor Muhammad, N. A.; Arita, M.; Goh, H.-H.; Aizat, W. M. Systematic Multi-Omics Integration (MOI) Approach in Plant Systems Biology. *Frontiers in Plant Science* **2020**, *11*.

(21) Han, W.; Ward, J. L.; Kong, Y.; Li, X. Editorial: Targeted and Untargeted Metabolomics for the Evaluation of Plant Metabolites in Response to the Environment. *Frontiers in Plant Science* **2023**, *14*.

(22) Allwood, J. W.; Williams, A.; Uthe, H.; van Dam, N. M.; Mur, L. A. J.; Grant, M. R.; Pétriacq, P. Unravelling Plant Responses to Stress—The Importance of Targeted and Untargeted Metabolomics. *Metabolites* **2021**, *11* (8), 558. https://doi.org/10.3390/metabo11080558.

(23) Hart-Smith, G. Combining Targeted and Untargeted Data Acquisition to Enhance Quantitative Plant Proteomics Experiments. In *Plant Proteomics: Methods and Protocols*; Jorrin-Novo, J. V., Valledor, L., Castillejo, M. A., Rey, M.-D., Eds.; Methods in Molecular Biology; Springer US: New York, NY, 2020; pp 169–178. https://doi.org/10.1007/978-1-0716-0528-8_13.

(24) McCord, J. P.; Groff, L. C.; Sobus, J. R. Quantitative Non-Targeted Analysis: Bridging the Gap between Contaminant Discovery and Risk Characterization. *Environment International* **2022**, *158*, 107011. https://doi.org/10.1016/j.envint.2021.107011.

(25) Majumdar, S.; Keller, A. A. Omics to Address the Opportunities and Challenges of Nanotechnology in Agriculture. *Critical Reviews in Environmental Science and Technology* **2020**, 1–42. https://doi.org/10.1080/10643389.2020.1785264.

(26) Picotti, P.; Bodenmiller, B.; Aebersold, R. Proteomics Meets the Scientific Method. *Nat Methods* **2013**, *10* (1), 24–27. https://doi.org/10.1038/nmeth.2291.

(27) Chawade, A.; Alexandersson, E.; Bengtsson, T.; Andreasson, E.; Levander, F. Targeted Proteomics Approach for Precision Plant Breeding. *J. Proteome Res.* **2016**, *15* (2), 638–646. https://doi.org/10.1021/acs.jproteome.5b01061.

(28) Mirzajani, F.; Askari, H.; Hamzelou, S.; Schober, Y.; Römpp, A.; Ghassempour, A.; Spengler, B. Proteomics Study of Silver Nanoparticles Toxicity on Oryza Sativa L. *Ecotoxicology and Environmental Safety* **2014**, *108*, 335–339. https://doi.org/10.1016/j.ecoenv.2014.07.013.

(29) Vannini, C.; Domingo, G.; Onelli, E.; De Mattia, F.; Bruni, I.; Marsoni, M.; Bracale, M. Phytotoxic and Genotoxic Effects of Silver Nanoparticles Exposure on Germinating Wheat Seedlings. *Journal of Plant Physiology* **2014**, *171* (13), 1142–1148. https://doi.org/10.1016/j.jplph.2014.05.002.

(30) Hossain, Z.; Mustafa, G.; Sakata, K.; Komatsu, S. Insights into the Proteomic Response of Soybean towards Al_2O_3, ZnO, and Ag Nanoparticles Stress. *Journal of Hazardous Materials* **2016**, *304*, 291–305. https://doi.org/10.1016/j.jhazmat.2015.10.071.

(31) Majumdar, S.; Almeida, I. C.; Arigi, E. A.; Choi, H.; VerBerkmoes, N. C.; Trujillo-Reyes, J.; Flores-Margez, J. P.; White, J. C.; Peralta-Videa, J. R.; Gardea-Torresdey, J. L. Environmental Effects of Nanoceria on Seed Production of Common Bean (*Phaseolus Vulgaris*): A Proteomic Analysis. *Environ. Sci. Technol.* **2015**, *49* (22), 13283–13293. https://doi.org/10.1021/acs.est.5b03452.

(32) Salehi, H.; Chehregani, A.; Lucini, L.; Majd, A.; Gholami, M. Morphological, Proteomic and Metabolomic Insight into the Effect of Cerium Dioxide Nanoparticles to Phaseolus Vulgaris L. under Soil or Foliar Application. *Science of The Total Environment* **2018**, *616–617*, 1540–1551. https://doi.org/10.1016/j.scitotenv.2017.10.159.

(33) Nguyen, N. H. A.; Falagan-Lotsch, P. Mechanistic Insights into the Biological Effects of Engineered Nanomaterials: A Focus on Gold Nanoparticles. *International Journal of Molecular Sciences* **2023**, *24* (4), 4109. https://doi.org/10.3390/ijms24044109.

(34) Knott, C. A. AGR-224: Identifying Wheat Growth Stages. 8.

(35) Huang, X.; Cervantes-Avilés, P.; Li, W.; Keller, A. A. Drilling into the Metabolomics to Enhance Insight on Corn and Wheat Responses to Molybdenum Trioxide Nanoparticles. *Environ. Sci. Technol.* **2021**, acs.est.1c00803. https://doi.org/10.1021/acs.est.1c00803.

(36) Jiang, L.; He, L.; Fountoulakis, M. Comparison of Protein Precipitation Methods for Sample Preparation Prior to Proteomic Analysis. *Journal of Chromatography A* **2004**, *1023* (2), 317–320. https://doi.org/10.1016/j.chroma.2003.10.029.

(37) Méchin, V.; Damerval, C.; Zivy, M. Total Protein Extraction with TCA-Acetone. In *Plant Proteomics*; Humana Press: New Jersey, 2006; Vol. 355, pp 1–8. https://doi.org/10.1385/1-59745-227-0:1.

(38) Faurobert, M.; Pelpoir, E.; Chaïb, J. Phenol Extraction of Proteins for Proteomic Studies of Recalcitrant Plant Tissues. In *Plant Proteomics: Methods and Protocols*; Thiellement, H., Zivy, M., Damerval, C., Méchin, V., Eds.; Methods in Molecular Biology; Humana Press: Totowa, NJ, 2007; pp 9–14. https://doi.org/10.1385/1-59745-227-0:9.

(39) Wang, W.; Scali, M.; Vignani, R.; Spadafora, A.; Sensi, E.; Mazzuca, S.; Cresti, M. Protein Extraction for Two-Dimensional Electrophoresis from Olive Leaf, a Plant Tissue Containing High Levels of Interfering Compounds. *Electrophoresis* **2003**, *24* (14), 2369–2375. https://doi.org/10.1002/elps.200305500.

(40) Hoofnagle, A. N.; Whiteaker, J. R.; Carr, S. A.; Kuhn, E.; Liu, T.; Massoni, S. A.; Thomas, S. N.; Townsend, R. R.; Zimmerman, L. J.; Boja, E.; Chen, J.; Crimmins, D. L.; Davies, S. R.; Gao, Y.; Hiltke, T. R.; Ketchum, K. A.; Kinsinger, C. R.; Mesri, M.; Meyer, M. R.; Qian, W.-J.; Schoenherr, R. M.; Scott, M. G.; Shi, T.; Whiteley, G. R.;

Wrobel, J. A.; Wu, C.; Ackermann, B. L.; Aebersold, R.; Barnidge, D. R.; Bunk, D. M.; Clarke, N.; Fishman, J. B.; Grant, R. P.; Kusebauch, U.; Kushnir, M. M.; Lowenthal, M. S.; Moritz, R. L.; Neubert, H.; Patterson, S. D.; Rockwood, A. L.; Rogers, J.; Singh, R. J.; Van Eyk, J.; Wong, S.; Zhang, S.; Chan, D. W.; Chen, X.; Ellis, M. J.; Liebler, D. C.; Rodland, K. D.; Rodriguez, H.; Smith, R. D.; Zhang, Z.; Zhang, H.; Paulovich, A. G. Recommendations for the Generation, Quantification, Storage and Handling of Peptides Used for Mass Spectrometry-Based Assays. *Clin Chem* **2016**, *62* (1), 48–69. https://doi.org/10.1373/clinchem.2015.250563.

(41) Hahne, H.; Pachl, F.; Ruprecht, B.; Maier, S. K.; Klaeger, S.; Helm, D.; Médard, G.; Wilm, M.; Lemeer, S.; Kuster, B. DMSO Enhances Electrospray Response, Boosting Sensitivity of Proteomic Experiments. *Nature Methods* **2013**, *10* (10), 989–991. https://doi.org/10.1038/nmeth.2610.

(42) Bian, Y.; Zheng, R.; Bayer, F. P.; Wong, C.; Chang, Y.-C.; Meng, C.; Zolg, D. P.; Reinecke, M.; Zecha, J.; Wiechmann, S.; Heinzlmeir, S.; Scherr, J.; Hemmer, B.; Baynham, M.; Gingras, A.-C.; Boychenko, O.; Kuster, B. Robust, Reproducible and Quantitative Analysis of Thousands of Proteomes by Micro-Flow LC–MS/MS. *Nature Communications* **2020**, *11* (1), 157. https://doi.org/10.1038/s41467-019-13973-x.

(43) Mitulovic, G.; Stingl, C.; Steinmacher, I.; Hudecz, O.; Hutchins, J. R. A.; Peters, J.-M.; Mechtler, K. Preventing Carryover of Peptides and Proteins in Nano LC-MS Separations. *Anal. Chem.* **2009**, *81*, 5955–5960.

(44) Damerval, C.; Vienne, D. D.; Zivy, M.; Thiellement, H. Technical Improvements in Two-Dimensional Electrophoresis Increase the Level of Genetic Variation Detected in Wheat-Seedling Proteins. *ELECTROPHORESIS* **1986**, *7* (1), 52–54. https://doi.org/10.1002/elps.1150070108.

(45) Wu, X.; Gong, F.; Wang, W. Protein Extraction from Plant Tissues for 2DE and Its Application in Proteomic Analysis. *Proteomics* **2014**, *14* (6), 645–658. https://doi.org/10.1002/pmic.201300239.

(46) Isaacson, T.; Damasceno, C. M. B.; Saravanan, R. S.; He, Y.; Catalá, C.; Saladié, M.; Rose, J. K. C. Sample Extraction Techniques for Enhanced Proteomic Analysis of Plant Tissues. *Nat Protoc* **2006**, *1* (2), 769–774. https://doi.org/10.1038/nprot.2006.102.

(47) Maldonado, A. M.; Echevarría-Zomeño, S.; Jean-Baptiste, S.; Hernández, M.; Jorrín-Novo, J. V. Evaluation of Three Different Protocols of Protein Extraction for Arabidopsis Thaliana Leaf Proteome Analysis by Two-Dimensional Electrophoresis. *J Proteomics* **2008**, *71* (4), 461–472. https://doi.org/10.1016/j.jprot.2008.06.012.

(48) Wu, X.; Xiong, E.; Wang, W.; Scali, M.; Cresti, M. Universal Sample Preparation Method Integrating Trichloroacetic Acid/Acetone Precipitation with Phenol Extraction

for Crop Proteomic Analysis. *Nat Protoc* **2014**, *9* (2), 362–374. https://doi.org/10.1038/nprot.2014.022.

(49) Laskay, Ü. A.; Lobas, A. A.; Srzentić, K.; Gorshkov, M. V.; Tsybin, Y. O. Proteome Digestion Specificity Analysis for Rational Design of Extended Bottom-up and Middle-down Proteomics Experiments. *J. Proteome Res.* **2013**, *12* (12), 5558–5569. https://doi.org/10.1021/pr400522h.

(50) Patole, C.; Bindschedler, L. V. Plant Proteomics. In *Advances in Biological Science Research*; Elsevier, 2019; pp 45–67. https://doi.org/10.1016/B978-0-12-817497-5.00004-5.

(51) Gingras, A.-C.; Aebersold, R.; Raught, B. Advances in Protein Complex Analysis Using Mass Spectrometry. *The Journal of Physiology* **2005**, *563* (1), 11–21. https://doi.org/10.1113/jphysiol.2004.080440.

(52) Majumdar, S.; Pagano, L.; Wohlschlegel, J. A.; Villani, M.; Zappettini, A.; White, J. C.; Keller, A. A. Proteomic, Gene and Metabolite Characterization Reveal the Uptake and Toxicity Mechanisms of Cadmium Sulfide Quantum Dots in Soybean Plants. *Environ. Sci.: Nano* **2019**, *6* (10), 3010–3026. https://doi.org/10.1039/C9EN00599D.

(53) Mikołajczak, B.; Fornal, E.; Montowska, M. LC–Q–TOF–MS/MS Identification of Specific Non-Meat Proteins and Peptides in Beef Burgers. *Molecules* **2018**, *24* (1), 18. https://doi.org/10.3390/molecules24010018.

(54) Duncan, O.; Trösch, J.; Fenske, R.; Taylor, N. L.; Millar, A. H. Resource: Mapping the *Triticum Aestivum* Proteome. *Plant J* **2017**, *89* (3), 601–616. https://doi.org/10.1111/tpj.13402.

(55) Ren, D.; Pipes, G. D.; Liu, D.; Shih, L.-Y.; Nichols, A. C.; Treuheit, M. J.; Brems, D. N.; Bondarenko, P. V. An Improved Trypsin Digestion Method Minimizes Digestion-Induced Modifications on Proteins. *Analytical Biochemistry* **2009**, *392* (1), 12–21. https://doi.org/10.1016/j.ab.2009.05.018.

(56) León, I. R.; Schwämmle, V.; Jensen, O. N.; Sprenger, R. R. Quantitative Assessment of In-Solution Digestion Efficiency Identifies Optimal Protocols for Unbiased Protein Analysis. *Mol Cell Proteomics* **2013**, *12* (10), 2992–3005. https://doi.org/10.1074/mcp.M112.025585.

(57) Suliman, M.; Chateigner-Boutin, A.-L.; Francin-Allami, M.; Partier, A.; Bouchet, B.; Salse, J.; Pont, C.; Marion, J.; Rogniaux, H.; Tessier, D.; Guillon, F.; Larré, C. Identification of Glycosyltransferases Involved in Cell Wall Synthesis of Wheat Endosperm. *Journal of Proteomics* **2013**, *78*, 508–521. https://doi.org/10.1016/j.jprot.2012.10.021.

(58) Nelson, C. J.; Alexova, R.; Jacoby, R. P.; Millar, A. H. Proteins with High Turnover Rate in Barley Leaves Estimated by Proteome Analysis Combined with in Planta Isotope Labeling. *Plant Physiology* **2014**, *166* (1), 91–108. https://doi.org/10.1104/pp.114.243014.

(59) Fiorino, G. M.; Fresch, M.; Brümmer, I.; Losito, I.; Arlorio, M.; Brockmeyer, J.; Monaci, L. Mass Spectrometry-Based Untargeted Proteomics for the Assessment of Food Authenticity: The Case of Farmed Versus Wild-Type Salmon. *J AOAC Int* **2019**, *102* (5), 1339–1345. https://doi.org/10.5740/jaoacint.19-0062.

(60) Maia, T. M.; Staes, A.; Plasman, K.; Pauwels, J.; Boucher, K.; Argentini, A.; Martens, L.; Montoye, T.; Gevaert, K.; Impens, F. *A Simple Approach for Accurate Peptide Quantification in MS-Based Proteomics*; preprint; Biochemistry, 2019. https://doi.org/10.1101/703397.

(61) Ruotolo, R.; Maestri, E.; Pagano, L.; Marmiroli, M.; White, J. C.; Marmiroli, N. Plant Response to Metal-Containing Engineered Nanomaterials: An Omics-Based Perspective. *Environ. Sci. Technol.* **2018**, *52* (5), 2451–2467. https://doi.org/10.1021/acs.est.7b04121.

(62) Hart-Smith, G.; Reis, R. S.; Waterhouse, P. M.; Wilkins, M. R. Improved Quantitative Plant Proteomics via the Combination of Targeted and Untargeted Data Acquisition. *Front. Plant Sci.* **2017**, *8*. https://doi.org/10.3389/fpls.2017.01669.

(63) Li, W.; Keller, A. A. Optimization of Targeted Plant Proteomics Using Liquid Chromatography with Tandem Mass Spectrometry (LC-MS/MS). *ACS Agric. Sci. Technol.* **2023**, *3* (5), 421–431. https://doi.org/10.1021/acsagscitech.3c00017.

(64) Ze, Y.; Liu, C.; Wang, L.; Hong, M.; Hong, F. The Regulation of TiO2 Nanoparticles on the Expression of Light-Harvesting Complex II and Photosynthesis of Chloroplasts of Arabidopsis Thaliana. *Biol Trace Elem Res* **2011**, *143* (2), 1131–1141. https://doi.org/10.1007/s12011-010-8901-0.

(65) Faizan, M.; Faraz, A.; Yusuf, M.; Khan, S. T.; Hayat, S. Zinc Oxide Nanoparticle-Mediated Changes in Photosynthetic Efficiency and Antioxidant System of Tomato Plants. *Photosynt.* **2018**, *56* (2), 678–686. https://doi.org/10.1007/s11099-017-0717-0.

(66) Servin, A. D.; Castillo-Michel, H.; Hernandez-Viezcas, J. A.; Diaz, B. C.; Peralta-Videa, J. R.; Gardea-Torresdey, J. L. Synchrotron Micro-XRF and Micro-XANES Confirmation of the Uptake and Translocation of TiO_2 Nanoparticles in Cucumber (*Cucumis Sativus*) Plants. *Environ. Sci. Technol.* **2012**, *46* (14), 7637–7643. https://doi.org/10.1021/es300955b.

(67) Ngo, Q. B.; Dao, T. H.; Nguyen, H. C.; Tran, X. T.; Nguyen, T. V.; Khuu, T. D.; Huynh, T. H. Effects of Nanocrystalline Powders (Fe, Co and Cu) on the Germination, Growth, Crop Yield and Product Quality of Soybean (Vietnamese Species DT-51).

Adv. Nat. Sci: Nanosci. Nanotechnol. **2014**, *5* (1), 015016. https://doi.org/10.1088/2043-6262/5/1/015016.

(68) Waqas, M. A.; Kaya, C.; Riaz, A.; Farooq, M.; Nawaz, I.; Wilkes, A.; Li, Y. Potential Mechanisms of Abiotic Stress Tolerance in Crop Plants Induced by Thiourea. *Frontiers in Plant Science* **2019**, *10*, 1336. https://doi.org/10.3389/fpls.2019.01336.

(69) Moreira, A.; Moraes, L. A. C.; Schroth, G. Copper Fertilization in Soybean–Wheat Intercropping under No–till Management. *Soil and Tillage Research* **2019**, *193*, 133–141. https://doi.org/10.1016/j.still.2019.06.001.

(70) Lung, I.; Opriș, O.; Soran, M.-L.; Culicov, O.; Ciorîță, A.; Stegarescu, A.; Zinicovscaia, I.; Yushin, N.; Vergel, K.; Kacso, I.; Borodi, G.; Pârvu, M. The Impact Assessment of CuO Nanoparticles on the Composition and Ultrastructure of Triticum Aestivum L. *Int J Environ Res Public Health* **2021**, *18* (13), 6739. https://doi.org/10.3390/ijerph18136739.

(71) Zhao, L.; Huang, Y.; Adeleye, A. S.; Keller, A. A. Metabolomics Reveals Cu(OH) $_2$ Nanopesticide-Activated Anti-Oxidative Pathways and Decreased Beneficial Antioxidants in Spinach Leaves. *Environ. Sci. Technol.* **2017**, *51* (17), 10184–10194. https://doi.org/10.1021/acs.est.7b02163.

(72) Zhao, L.; Huang, Y.; Paglia, K.; Vaniya, A.; Wancewicz, B.; Keller, A. A. Metabolomics Reveals the Molecular Mechanisms of Copper Induced Cucumber Leaf (*Cucumis Sativus*) Senescence. *Environ. Sci. Technol.* **2018**, *52* (12), 7092–7100. https://doi.org/10.1021/acs.est.8b00742.

(73) Majumdar, S.; Long, R. W.; Kirkwood, J. S.; Minakova, A. S.; Keller, A. A. Unraveling Metabolic and Proteomic Features in Soybean Plants in Response to Copper Hydroxide Nanowires Compared to a Commercial Fertilizer. *Environ. Sci. Technol.* **2021**, acs.est.1c00839. https://doi.org/10.1021/acs.est.1c00839.

(74) Huang, X.; Keller, A. A. Metabolomic Response of Early-Stage Wheat (Triticum Aestivum) to Surfactant-Aided Foliar Application of Copper Hydroxide and Molybdenum Trioxide Nanoparticles. *Nanomaterials* **2021**, *11* (11), 3073. https://doi.org/10.3390/nano11113073.

(75) Cervantes-Avilés, P.; Huang, X.; Keller, A. A. Dissolution and Aggregation of Metal Oxide Nanoparticles in Root Exudates and Soil Leachate: Implications for Nanoagrochemical Application. *Environ. Sci. Technol.* **2021**, *55* (20), 13443–13451. https://doi.org/10.1021/acs.est.1c00767.

(76) Ruiz-Perez, D.; Guan, H.; Madhivanan, P.; Mathee, K.; Narasimhan, G. So You Think You Can PLS-DA? *BMC Bioinformatics* **2020**, *21* (1), 2. https://doi.org/10.1186/s12859-019-3310-7.

(77) Padhi, P. P.; Mishra, A. P. The Role of Molybdenum in Crop Production.

(78) Kusiak, M.; Sierocka, M.; Świeca, M.; Pasieczna-Patkowska, S.; Sheteiwy, M.; Jośko, I. Unveiling of Interactions between Foliar-Applied Cu Nanoparticles and Barley Suffering from Cu Deficiency. *Environmental Pollution* **2023**, *320*, 121044. https://doi.org/10.1016/j.envpol.2023.121044.

(79) Kohatsu, M. Y.; Lange, C. N.; Pelegrino, M. T.; Pieretti, J. C.; Tortella, G.; Rubilar, O.; Batista, B. L.; Seabra, A. B.; Jesus, T. A. D. Foliar Spraying of Biogenic CuO Nanoparticles Protects the Defence System and Photosynthetic Pigments of Lettuce (*Lactuca Sativa*). *Journal of Cleaner Production* **2021**, *324*, 129264. https://doi.org/10.1016/j.jclepro.2021.129264.

(80) Nayyar, V. K.; Randhawa, N. S.; Pasricha, N. S. Effect of Interaction between Molybdenum and Copper on the Concentration of These Nutrients in Berseem and Its Yield. *Indian Journal of Agricultural Sciences* **1980**, *50* (5), 434–440.

(81) Pandey, M.; Shrestha, J.; Subedi, S.; Shah, K. K. ROLE OF NUTRIENTS IN WHEAT: A REVIEW. *Trop.agr.bio.* **2020**, *1* (1), 18–23. https://doi.org/10.26480/trab.01.2020.18.23.

(82) Caspi, V.; Droppa, M.; Horváth, G.; Malkin, S.; Marder, J. B.; Raskin, V. I. The Effect of Copper on Chlorophyll Organization during Greening of Barley Leaves. *Photosynthesis Research* **1999**, *62* (2), 165–174. https://doi.org/10.1023/A:1006397714430.

(83) Zakikhani, H.; Khanif, Y. M.; Anuar, A. R.; Radziah, O.; Soltangheisi, A. Effects of Different Levels of Molybdenum on Uptake of Nutrients in Rice Cultivars. *Asian Journal of Crop Science* **2014**, *6* (3), 236–244. https://doi.org/10.3923/ajcs.2014.236.244.

(84) Yamamoto, H.; Cheuk, A.; Shearman, J.; Nixon, P. J.; Meier, T.; Shikanai, T. Impact of Engineering the ATP Synthase Rotor Ring on Photosynthesis in Tobacco Chloroplasts. *Plant Physiol* **2023**, *192* (2), 1221–1233. https://doi.org/10.1093/plphys/kiad043.

(85) KAISER, B. N.; GRIDLEY, K. L.; NGAIRE BRADY, J.; PHILLIPS, T.; TYERMAN, S. D. The Role of Molybdenum in Agricultural Plant Production. *Ann Bot* **2005**, *96* (5), 745–754. https://doi.org/10.1093/aob/mci226.

(86) Li, M.; Zhang, P.; Guo, Z.; Cao, W.; Gao, L.; Li, Y.; Tian, C. F.; Chen, Q.; Shen, Y.; Ren, F.; Rui, Y.; White, J. C.; Lynch, I. Molybdenum Nanofertilizer Boosts Biological Nitrogen Fixation and Yield of Soybean through Delaying Nodule Senescence and Nutrition Enhancement. *ACS Nano* **2023**, *17* (15), 14761–14774. https://doi.org/10.1021/acsnano.3c02783.

(87) Khoudi, H.; Maatar, Y.; Gouiaa, S.; Masmoudi, K. Transgenic Tobacco Plants Expressing Ectopically Wheat H+-Pyrophosphatase (H+-PPase) Gene TaVP1 Show Enhanced Accumulation and Tolerance to Cadmium. *Journal of Plant Physiology* **2012**, *169* (1), 98–103. https://doi.org/10.1016/j.jplph.2011.07.016.

(88) Wang, J.; Moeen-ud-din, M.; Yin, R.; Yang, S. ROS Homeostasis Involved in Dose-Dependent Responses of Arabidopsis Seedlings to Copper Toxicity. *Genes* **2023**, *14* (1), 11. https://doi.org/10.3390/genes14010011.

(89) Mhamdi, A.; Queval, G.; Chaouch, S.; Vanderauwera, S.; Van Breusegem, F.; Noctor, G. Catalase Function in Plants: A Focus on Arabidopsis Mutants as Stress-Mimic Models. *J Exp Bot* **2010**, *61* (15), 4197–4220. https://doi.org/10.1093/jxb/erq282.

(90) Zhang, Y.; Zheng, L.; Yun, L.; Ji, L.; Li, G.; Ji, M.; Shi, Y.; Zheng, X. Catalase (CAT) Gene Family in Wheat (Triticum Aestivum L.): Evolution, Expression Pattern and Function Analysis. *Int J Mol Sci* **2022**, *23* (1), 542. https://doi.org/10.3390/ijms23010542.

(91) Lawson-Wood, K.; Jaafar, M.; Felipe-Sotelo, M.; Ward, N. I. Investigation of the Uptake of Molybdenum by Plants from Argentinean Groundwater. *Environ Sci Pollut Res* **2021**, *28* (35), 48929–48941. https://doi.org/10.1007/s11356-021-13902-w.

(92) Chen, J.; Wang, J.; Wang, R.; Xian, B.; Ren, C.; Liu, Q.; Wu, Q.; Pei, J. Integrated Metabolomics and Transcriptome Analysis on Flavonoid Biosynthesis in Safflower (Carthamus Tinctorius L.) under MeJA Treatment. *BMC Plant Biol* **2020**, *20* (1), 353. https://doi.org/10.1186/s12870-020-02554-6.

(93) Mesnage, R.; Agapito-Tenfen, S. Z.; Vilperte, V.; Renney, G.; Ward, M.; Séralini, G.-E.; Nodari, R. O.; Antoniou, M. N. An Integrated Multi-Omics Analysis of the NK603 Roundup-Tolerant GM Maize Reveals Metabolism Disturbances Caused by the Transformation Process. *Sci Rep* **2016**, *6* (1), 37855. https://doi.org/10.1038/srep37855.

(94) Sun, Y.; Zhu, G.; Zhao, W.; Jiang, Y.; Wang, Q.; Wang, Q.; Rui, Y.; Zhang, P.; Gao, L. Engineered Nanomaterials for Improving the Nutritional Quality of Agricultural Products: A Review. *Nanomaterials (Basel)* **2022**, *12* (23), 4219. https://doi.org/10.3390/nano12234219.

(95) Li, W.; Keller, A. A. Assessing the Impacts of Cu and Mo Engineered Nanomaterials on Crop Plant Growth Using a Targeted Proteomics Approach. *ACS Agric. Sci. Technol.* **2024**, *4* (1), 103–117. https://doi.org/10.1021/acsagscitech.3c00431.

(96) Huang, X.; Keller, A. A. Metabolomics Response of Wheat (*Triticum Aestivum*) to "Green" and Conventional Nonionic Surfactants at Different Application Stages. *ACS Agric. Sci. Technol.* **2022**, *2* (5), 1042–1051. https://doi.org/10.1021/acsagscitech.2c00176.

(97) Kumar, N.; Hoque, Md. A.; Sugimoto, M. Robust Volcano Plot: Identification of Differential Metabolites in the Presence of Outliers. *BMC Bioinformatics* **2018**, *19* (1), 128. https://doi.org/10.1186/s12859-018-2117-2.

(98) Kalinger, R. S.; Pulsifer, I. P.; Hepworth, S. R.; Rowland, O. Fatty Acyl Synthetases and Thioesterases in Plant Lipid Metabolism: Diverse Functions and Biotechnological Applications. *Lipids* **2020**, *55* (5), 435–455. https://doi.org/10.1002/lipd.12226.

(99) Igamberdiev, A. U.; Eprintsev, A. T. Organic Acids: The Pools of Fixed Carbon Involved in Redox Regulation and Energy Balance in Higher Plants. *Frontiers in Plant Science* **2016**, *7*.

(100) Skelton, R. Of Storage and Stems: Examining the Role of Stem Water Storage in Plant Water Balance. *Plant Physiol* **2019**, *179* (4), 1433–1434. https://doi.org/10.1104/pp.19.00057.

(101) Stirbet, A.; Lazár, D.; Guo, Y.; Govindjee, G. Photosynthesis: Basics, History and Modelling. *Ann Bot* **2019**, *126* (4), 511–537. https://doi.org/10.1093/aob/mcz171.

(102) Schimmel, P.; Alexander, R. W. Protein Synthesis. In *Encyclopedia of Physical Science and Technology (Third Edition)*; Meyers, R. A., Ed.; Academic Press: New York, 2003; pp 219–240. https://doi.org/10.1016/B0-12-227410-5/00617-7.

(103) Walker, M. C.; van der Donk, W. A. The Many Roles of Glutamate in Metabolism. *J Ind Microbiol Biotechnol* **2016**, *43* (0), 419–430. https://doi.org/10.1007/s10295-015-1665-y.

(104) Lee, K.-T.; Liao, H.-S.; Hsieh, M.-H. Glutamine Metabolism, Sensing, and Signaling in Plants. *Plant Cell Physiol* **2023**, pcad054. https://doi.org/10.1093/pcp/pcad054.

(105) Majumdar, R.; Minocha, R.; Minocha, S. C. Ornithine: At the Crossroads of Multiple Paths to Amino Acids and Polyamines. In *Amino acids in higher plants*; D'Mello, J. P. F., Ed.; CAB International: UK, 2015; pp 156–176. https://doi.org/10.1079/9781780642635.0156.

(106) Liebsch, D.; Juvany, M.; Li, Z.; Wang, H.-L.; Ziolkowska, A.; Chrobok, D.; Boussardon, C.; Wen, X.; Law, S. R.; Janečková, H.; Brouwer, B.; Lindén, P.; Delhomme, N.; Stenlund, H.; Moritz, T.; Gardeström, P.; Guo, H.; Keech, O. Metabolic Control of Arginine and Ornithine Levels Paces the Progression of Leaf Senescence. *Plant Physiology* **2022**, *189* (4), 1943–1960. https://doi.org/10.1093/plphys/kiac244.

(107) Chandel, N. S. Amino Acid Metabolism. *Cold Spring Harb Perspect Biol* **2021**, *13* (4), a040584. https://doi.org/10.1101/cshperspect.a040584.

(108) Plaitakis, A.; Kalef-Ezra, E.; Kotzamani, D.; Zaganas, I.; Spanaki, C. The Glutamate Dehydrogenase Pathway and Its Roles in Cell and Tissue Biology in Health and Disease. *Biology (Basel)* **2017**, *6* (1), 11. https://doi.org/10.3390/biology6010011.